UNIVERSITÀ DEGLI STUDI DI MILANO
DIPARTIMENTO DI BIOSCIENZE

DOTTORATO DI RICERCA
DBMC
IN BIOLOGIA MOLECOLARE E CELLULARE

UNIVERSITÀ DEGLI STUDI DI MILANO

Corso di Dottorato in Biologia Molecolare e Cellulare

XXXI Ciclo

From Protein Structure to Drug Design (Discovery)

Targeting the ion channel ASIC1 and a pathogenic variant of human Gelsolin

Amal Hassan

PhD Thesis

Scientific tutor: Prof. Martino Bolognesi,

Scientific co-tutors: Dr. Eloise Mastrangelo and Dr. Matteo De Rosa

Academic year: 2018-2019

SSD: BIO/10

Thesis performed at department of Bioscience, University of Milan, Italy.

The thesis work has been performed mainly at the University of Milan, within the structural biology unit (SBU), in the CNR- Biophysics Institute laboratories, and in part in two institutes: 1. The Weizmann institute of science, Rehovot, Israel 2. The membrane protein lab (MPL), Oxford, UK

The work on the membrane protein project, Acid-sensing ion channel 1, has been partly supported by the EU Program Instruct Integrating Biology (PID: 3912).

Table of content

Abstract (English)

Knowledge of the three-dimensional structure of therapeutically relevant proteins paves the way for novel strategies in pharmacological research (such as the structure-based drug design (SBDD) method) and establishes the foundations for structural bioinformatics.

In this context, during my PhD Thesis, two therapeutically relevant proteins have been studied. First, a membrane protein, Acid Sensing Ion Channel (ASIC) isoform 1, a validated target in neurodegenerative disorders, was selected. Previous studies showed that diminazene aceturate (DA) is a potent small-molecule inhibitor of ASIC channels. Here, several DA analogues were screened by molecular docking and the best binders were tested in cell-based assays to further assess their efficacy. In order to determine the inhibitory capability of the synthesized analogues *in vitro* on the purified protein, the expression of ASIC1 was undertaken, using different organisms of expression. The protein purification was performed in a high-throughput approach in order to recover enough protein for crystallization, with the final aim of studying the mechanism of action of DA analogs, and support the design of new, isoform-selective and brain-penetrant drugs.

Secondly, the soluble protein Gelsolin (GSN), responsible for a familial degenerative disease (AGel amyloidosis) was studied. Aim of this project was to understand the impact of the D187N mutation on GSN structure and its propensity to aberrant aggregation and/or degradation. D187N

GSN mutant was the first identified in man, but its crystal structure had until now eluded any characterization. Conversely, a nanobody (Nb11) was shown to protect GSN from aberrant proteolysis, but its mechanism of protection remained unclear. Here, the structure of the Nb11:D187N complex was solved at 1.9 Å resolution, enabling the characterization of the Nb11action mechanism. The structural data were complemented with biophysical and biochemical characterisations. These studies were then extended to two recently identified pathological variants of GSN (G167R and N184K).

Abstract (Italian)

La conoscenza della struttura tridimensionale di un potenziale target farmacologico apre la via a nuove strategie terapeutiche (ad esempio tramite structure-based drug design (SBDD)) ed è requisito fondamentale per la bioinformatica strutturale.

In questo contesto, durante la mia tesi di dottorato, sono state studiate due proteine di interesse biomedico. La prima è una proteina di membrana, l'isoforma 1 dell'Acid Sensing Ion Channel (ASIC), implicata in diverse malattie neurodegenerative. In studi precedenti il diminazene aceturato (DA) si era dimostrato un potente inibitore del canale. Diversi analoghi di DA sono stati progettati su base strutturale e la loro affinità per ASIC analizzata tramite docking molecolare. Le molecole migliori sono state testate in saggi cellulari per valutarne l'efficacia. Per caratterizzare la capacità inibitoria degli analoghi sintetizzati *in vitro*, è stato messo a punto un protocollo per la produzione della proteina ASIC1, utilizzando diversi sistemi di espressione eterologa. La purificazione della proteina è stata effettuata usando un approccio high-throughput per supportare successivamente la cristallizzazione della proteina, al fine di ottenere informazioni più dettagliate sul meccanismo d'azione degli analoghi del DA e, di conseguenza, disegnare nuovi farmaci, isoforma-selettivi e in grado di attraversare la barriera emato-encefalica.

In secondo luogo, ho studiato la proteina Gelsolin (GSN), responsabile di una malattia familiare degenerativa (detta amiloidosi AGel). Lo scopo di questo progetto era quello di investigare l'effetto della mutazione D187N

sulla struttura di GSN e la sua propensione ad aggregare e/o degradarsi in maniera anomala. Il D187N GSN è stato il primo mutante ad essere identificato, ma, ad oggi, non si avevano informazioni sulla sua struttura. In uno studio precedente, era stato identificato un nanobody (Nb11) in grado di proteggere la proteina dalla degradazione, ma il meccanismo di protezione non era stato chiarito. Nel mio lavoro ho risolto la struttura del complesso Nb11:D187N a 1.9 Å, permettendo la caratterizzazione molecolare del meccanismo di azione del Nb11. I dati strutturali ottenuti sono stati completati con una caratterizzazione biofisica e biochimica, estesa anche ad altre due varianti patologiche della GSN, recentemente identificate (G167R e N184K).

1 State of the art

1.1 Structure based design

Identification of promising lead compounds in the course of drug discovery approach is critical for accelerating the time required for rational design of potential hits as drugs. Structure-based drug design (SBDD) is an iterative, rational, and lead compound sculpting process on the chemical structure (usually fragments of a small molecule). It involves both the synthesis of new derivatives and the evaluation of their binding efficacy to the target structure, either through computational docking or by the elucidation of the structure as a complex with the lead compound, with the aim of identifying a suitable molecule for therapeutic approaches (Figure 1).

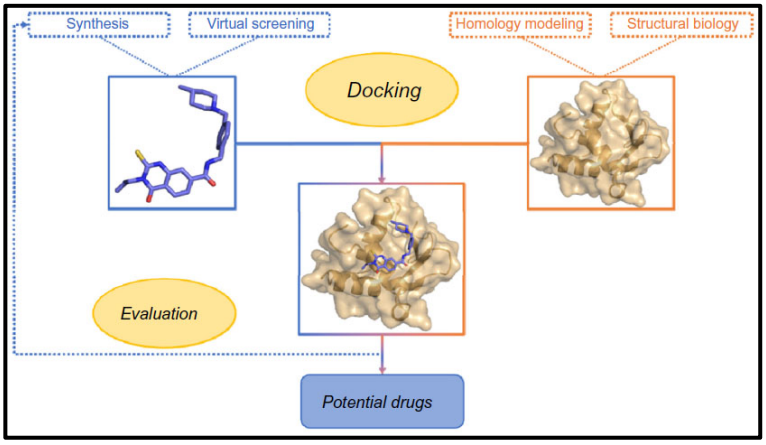

Figure 1: Illustration of the structure-based drug design (SBDD) approach

Structural biology methods have contributed in the achievement of high levels of selectivity and potency including the ability to achieve novel cell-permeant chemical probes (drugs). For example, these probes can be applied in genetic approaches (e.g. RNA interference and CRISPR) to identify suitable biological targets.

The idea to use protein structural information to guide in the design of novel therapeutic molecules stems from the 1950s-60s, when the first protein structure was determined using X-ray crystallography [1] [2]. The

drug discovery approach by SBDD covers different areas, including genome information, to determine novel biological targets, followed by exploration of chemical space using large libraries of compounds for screening based on knowledge of the protein structure (Figure 2) [3]. Following the first work describing this approach in 1976, SBDD has surmounted a number of hurdles but is nowadays an essential element of the drug discovery pipeline in pharmaceutical companies [4] [5].

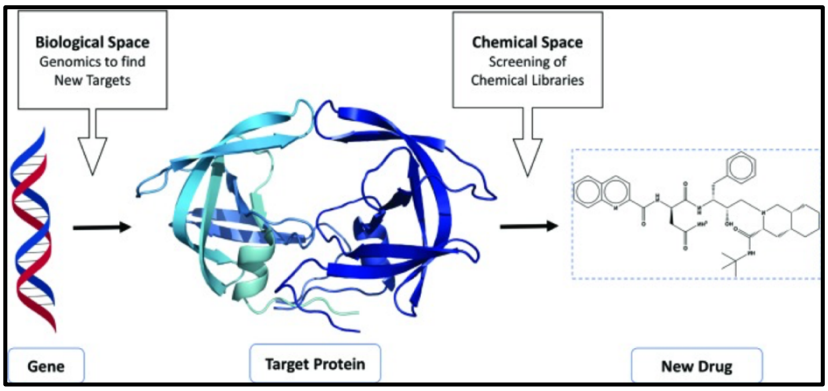

Figure 2: An overview of the drug discovery approach

The illustrated target protein is HIV-1 proteinase (PDB:3PHV) and its inhibitor drug (PDDB:9HVP). The HIV-1 protease plays a critical role in the life cycle of the HIV retrovirus that causes AIDS disease. Its structure was obtained in 1989 and has allowed the elucidation of some crucial structural information, which with the help of the SBDD approach permitted the development of the first HIV-protease inhibitors 6 (the Hoffman-La Roche Invirasse™), as well as the production of recent potent inhibitors (adapted from Thomas et al., 2017).

The choice of a drug target is based on biological and biochemical bases, usually linked to specific disease(s). One of the best examples of the SBDD approach is the development of the HIV-1 protease inhibitors (Figure 2) [6] [7].

The main limitation of the SBDD approach is that not all targets, such as membrane proteins or other complex macromolecular assemblies, are amenable to high-resolution structural studies, and that the target molecule should have a well-defined binding pocket to ensure the SBDD approach to be applied efficiently. This impedes the use of the SBDD approach and confines medicinal chemistry to experimental or ligand-based methods, in which an understanding of the structure-function relationship is only based on the (bio)chemical properties of known compounds. An alternative approach based on virtual or *in-silico* screening uses docking [8] and molecular dynamics simulations, to screen libraries of potential small molecules and predict the ligand-protein interactions [8] [9]. These methods are powerful tools at least as a first approach, due to their low cost and quick results for further optimisation of the compounds.

1.2 Membrane proteins

All cells and organelles are bound by a membrane, which permits compartmentalization and facilitate selective chemical information to be exchanged. Membrane proteins are embedded in the lipid bilayer and represent up to 30% of the proteome of most organisms [10]. They are of great pharmaceutical interest due to their location/function within the cell (Figure 3) as they regulate key processes such as signalling or transport of important biomolecules [11]. Due the importance of membrane protein (such as GPCRs and ion channels) in physio- and

pathological pathways, they are currently considered as interesting targets for drug discovery.

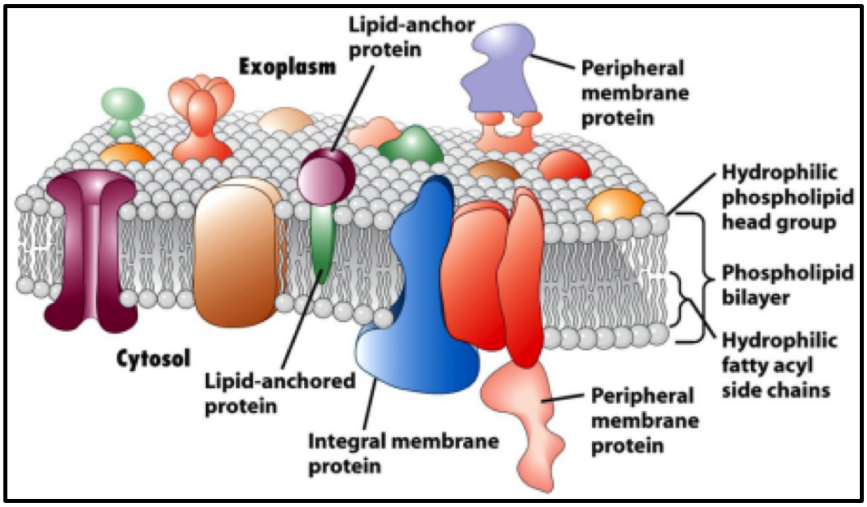

Figure 3: Membrane proteins on the cell membranes

These proteins such as transporters, receptors and ion channels are responsible for regulating the cellular function. Membrane proteins account for up to two thirds of known druggable targets, highlighting their critical pharmaceutical importance. Reproduced from https://www.creative-proteomics.com/services/membrane-proteomics.htm

1.2.1 Overexpression of membrane proteins in different host systems

Producing high-quality purified membrane proteins for drug discovery and biophysical studies is a significant challenge, mainly due to the levels of expression in prokaryotic and eukaryotic systems and difficulties in purification of membrane protein due to the presence of high concentrations of detergent that can induce changes in conformational and functional states of the protein. The major bottleneck in membrane protein studies is however their overexpression and the choice of the correct host system [12] (Figure 4).

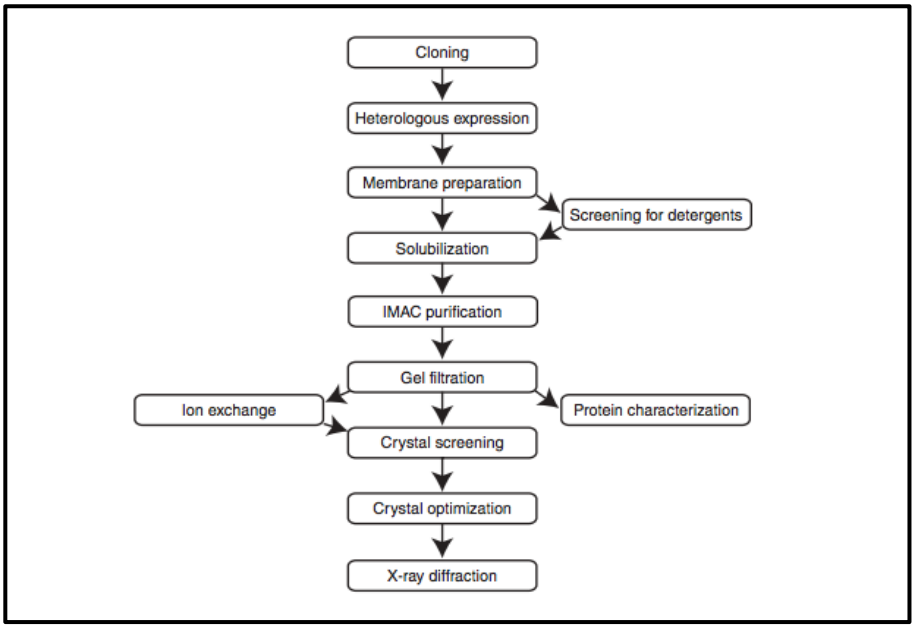

Figure 4: Schematic overview of the workflow for producing membrane proteins for X-ray crystallography.

Reproduced from Newby et al., 2009.

Membrane proteins have been expressed in *Escherichia coli (E. coli)* due to low costs and quick expression, leading to easily screen different constructs at the same time [13]. Unfortunately, membrane proteins expressed in *e. coli* are often unfolded and not suitable for biochemical assays or crystallisation [14] [15] [16]. Moreover, *E. coli* does not possess the cellular machinery to undergo post-translation modifications, including glycosylation, phosphorylation or palmitoylation, which are only performed in higher expression systems (such as insect cells or/and mammalian cell lines) [17].

Although no "universal" solution can be applied for the production of all types of eukaryotic proteins [18], alternative methods have been used,

including the baculovirus- infected insect cells system [19]. This system has become a common expression system adopted for crystallographic studies (e.g. the case of solved β-adrenergic G protein-coupled receptor [20]). Two main types of insect cells are used for this purpose, *Spodoptera frugiperda Sf*9 cells (Sf9) and Trichoplusia ni cell line BTI-TN5B1-4 (High Five ™), for which the protein expression level can significantly vary in different cell lines [21] [22].

Recently, the mammalian expression system has attracted interest since it guarantees native post-translational modifications [23]. Human Embryonic Kidney (HEK293) and Chinese hamster ovarian (CHO) cells are the most used cell lines for structural studies as well as for functional assays such as electrophysiology for ion channels. However, few membrane protein structures, stemming from these approaches, are available due to slow cell growth rate, higher costs of maintenance and medium [24]. Therefore, the choice of the most suitable host expression system depends, mainly, on the target protein, and a screening of different hosts is required before attempting large scale protein expression.

1.2.2 The use of detergents for efficient solubilisation and crystallisation

Once expression has been reached at the desired level, it is necessary to extract the protein from its membrane environment, and to do so amphipathic molecules, such as detergents, are used, forming mixed detergent-protein-lipid micelles (Figure 5). The choice of detergent is a crucial point in the purification protocol and often a number of detergents

are tested for their capacity to extracts proper amounts of functional and folded proteins.

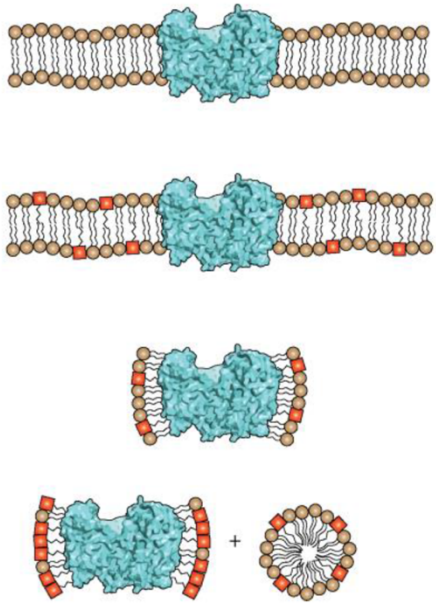

Figure 5: Illustration of the protein-lipid micelle formation

Extraction of membrane protein (coloured in cyan) from the lipid bilayer (brown) with detergent (in red squares). The concentration of detergent is increased, from top to bottom, up to a complete extraction of the protein. Detergents are, amphipathic molecules which facilitate the extraction of membrane protein by disrupting the lipid-lipid and lipid-protein interactions [85]. However, excess detergent can lead to protein inactivation, but lack of detergent can also lead to protein aggregation (adapted from Stetsenko et al.,2017)

However, it is still a difficult task to find the suitable detergent for solubilisation and purification steps (Figure 7). For example, non-ionic detergents are the most used class of detergents for membrane protein solubilisation, purification, crystallisation and for functional assays as they partially disrupt the interaction between the lipids present in the membrane and the protein. Dodecylmaltoside (DDM) molecule (Figure 6) is one of the most used detergents to extract membrane proteins due to its low cost and its high-efficiency in solubilising diverse membrane protein from different expression host systems [25].

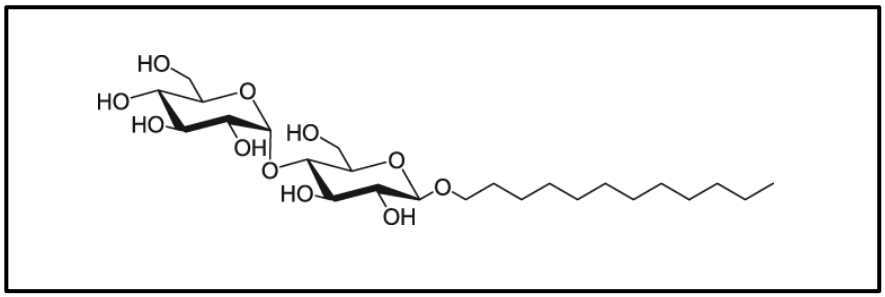

Figure 6: The chemical structure of the n-dodecyl-β-D-maltopyranoside (DDM) detergent.

The detergent concentration must be kept above the critical micellar concentration (CMC), which is the minimal detergent concentration at which micelles can be formed; the capacity of a particular detergent to extract and maintain the membrane protein solubility is connected to its aptitude to form micelles [26].

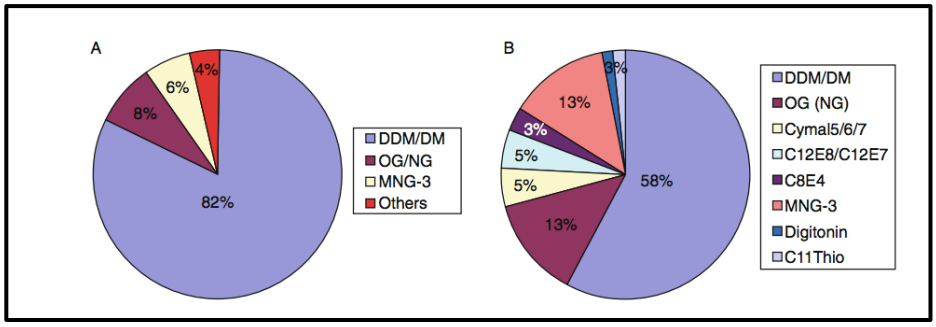

Figure 7: Detergents used for extraction and crystallization of eukaryotic membrane proteins

(A) percentage of the most used detergents for protein extraction and purification. DDM/DM are the most used for eukaryotic membrane proteins during the extraction step. (B) percentage of detergents used for protein crystallization; DDM/DM. Reproduced from He et al.,2014.

1.3 Acid-sensing ion channel: membrane protein target

The extracellular pH levels in the brain are maintained at pH 7.4 through various protons (H^+) transporting mechanisms involving ion channels, pumps and transporters. However, significant fluctuations in pH occurs as a result of high neural activity, inflammation states, neurodegenerative

disorders, hypoxia, energy consumption and metabolic demands [27] [28] [29]. Such acidosis states are a common feature in pathological conditions, such as multiple sclerosis (MS), stroke and epilepsy, which are characterized by massive cell loss, leading to deterioration in quality and function of tissues. Accordingly, neuron cells start to activate specific mechanisms to respond to these pH changes in order to compensate the sudden pH changes. Recent studies have shown that this significant reduction of the extracellular-pH can activate a family of ligand-gated cation channels [30] [31] including Acid-sensing ion channels (ASICs) which are able to detect significant changes in pH.

ASICs are expressed in neurons through the central (CNS) and peripheral nervous system (PNS) [32] and are involved in mediating a number of physiological processes such as depression, pain, sensory transduction, retinal function and memory [33] [34]. Moreover, the role of ASICs in mediating pathological pathways has been reported. In particular, the first isoform of this family, ASIC1, facilitates seizure termination by responding to brain acidosis produced by abnormally high neuronal activity [35] [36] [31]. Acidification arises from the release of protons from synaptic vesicles, which can be balanced by the activation of postsynaptic ASICs [37] [38]. Previous *in vivo* studies [39] [40], have demonstrated that inhibiting the activity of ASIC1a isoform can attenuate the neurological damage, and have shown the important role of acidosis-associated and ASICs in neuronal activity, indicating novel targets for drug discovery in neurodegenerative disorders.

Here, ASIC1 has been studied as a biological target for the design of, isoform-selective and brain-penetrant drugs [41] [42].

1.3.1 Overview about the channel structure

ASICs are displayed as a chalice-like shape, comprising short intracellular N- and C- termini, two hydrophobic transmembrane domains (TM1 and TM2), and a large cysteine-rich extracellular domain (ECD) (Figure 8).

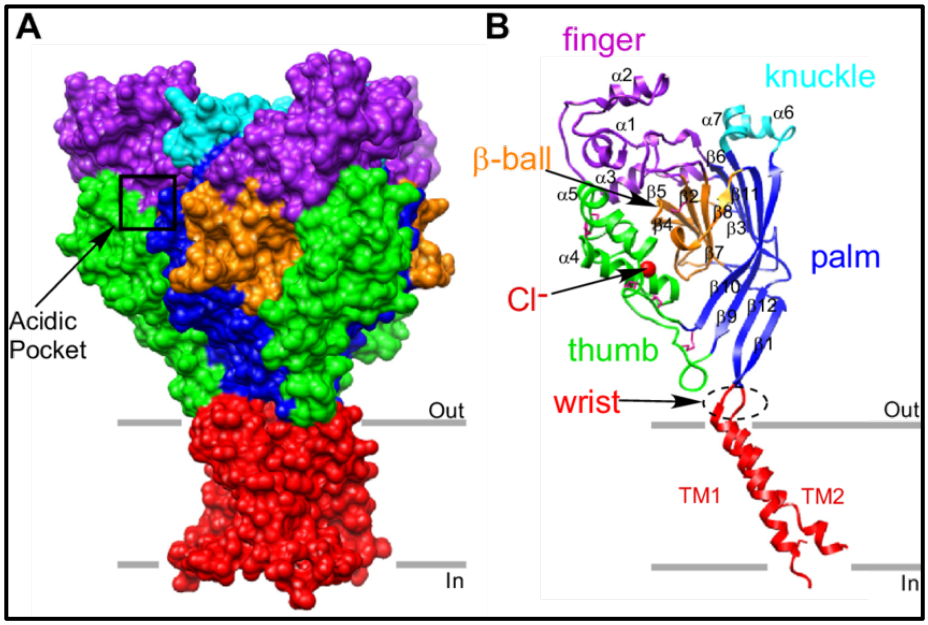

Figure 8: Acid-Sensing Ion Channel 1 (ASIC1) structure overview

(A) surface representation of the trimeric chicken ASIC1 (cASIC1- PDB code: 3HGC), where the coloration indicates the channel's domains (adapted from Gonzales et al., 2009).

To date, seven ASIC isoforms (ASIC1a, ASIC1b, ASIC2a, ASIC2b, ASIC3 and ASIC4, ASIC5) encoded by 5 genes (*ACCN1-5*) have been identified [43] [44]. Two alternate isoforms; a and b of ASIC1 and 2 have similar alternate splice site [45] and differ in the N-terminus part of the protein. The ASIC channel is composed of three individual subunits which can assemble in

functional homo- and heteromeric channels (previous work suggests a tetramer [46]). Based on the subunit composition, the current kinetics and gating mechanism of the channel can heavily vary [47] [48] [49], which is relevant from a pharmacological point of view. Once activated by protons, the channel becomes permeable to Na^+ [46] and it has also been demonstrated recently that ASIC1a and other ASIC channels possess high Ca^{2+} permeability, implying an important role in the increase of the intracellular concentration of calcium [39]. It also implies that these channels play an important role in membrane excitability and intracellular signalling in neurons [50] [51] (Figure 9)

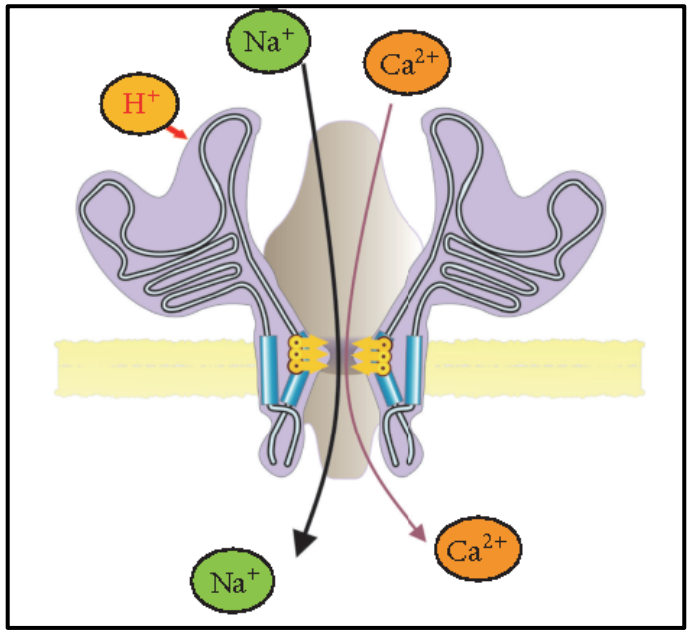

Figure 9: Schematic view of ASIC structure (represented here as a trimer)

The activation of the channel by H^+, mediates a Na^+ and Ca^{2+} (in lower proportion) influx in neuron cells. The increase in intracellular concentrations of these two ions is believed to activate a number of intracellular messengers (adapted from Ortega-Ramírez et al., 2017).

To date, only the homotrimeric crystal structure of the chicken ASIC1a (cASIC1a) [52] in different states is available (PDB: 2QTS and 3HGC). Both structures were obtained at low pH and represented similar structure with some significant differences at the transmembrane domain [53]. The ECD of each individual subunit resembles a clenched hand, and the sub-regions within the ECD include the wrist, palm, finger, knuckle, thumb and beta-ball domains (Figure 8). The palm domain, which is considered as the central element of each subunit, is composed of four large beta-strands that extend along the ECD. The TM1 and TM2 regions are connected with the "hand" area by the "wrist" domain. The crystal structure of the chicken ASIC1 has been obtained in absence of the N- and C- termini, which seem to play an essential role in ion permeation and channel gating, and in modulating the channel activity by intramolecular contacts [54]. Within the ECD a number of intra-subunit contact sites are presented, the most notable one being the acidic pocket (commonly called "the pH sensor"). This pocket located distantly from the transmembrane domain [55], is a highly negatively charged cavity which is believed to play an essential role in the pH-dependent gating mechanism, being also a possible binding site for some ASIC's modulators [54]. Activation of ASICs rely on a significant increase in the extracellular proton concentration in a range of extracellular pH, from acidic (pH 4.0) to nearly alkaline conditions (up to pH 7.8) depending on their subunit's composition. For instance, the homotrimeric channels, ASIC3 and ASIC1b are known to be the most sensitive ones (activated at pH 6.4, and 6.1 respectively) and ASIC2a being the less sensitive one (pH 4.5) [49]. After proton-induced

activation of ASICs, the channel assumes a desensitization/inactivation state and produces a characteristic transient current. Indeed, at this induced steady-state desensitization state, the channel fails to respond to further decreases in the extracellular pH, and prevents acidosis- mediated neurons death.

The induction of desensitization/inactivation and response to extracellular modulators is produced via the ECD. Therefore, it is thought to play a critical role in the channel activation, as well as being a target for therapeutics to inhibit the ASICs activity [56] [56]. The ECD is composed by seven α- helices (α 1-7) and twelve β- sheets (β 1-12), two conserved glycosylation sites within β10

[57] [58], and N394 between α6 and α7, and is characterised by 14 disulphide bonds, which is common motif for the DEG/ENaC family. The glycosylation states can affect the proton sensitivity as wells as proper trafficking to the surface. Even though H^+ is the simplest ligand of ASICs, the structural and molecular mechanisms underpinning proton-induced activation of the channel has never been elucidated; some questions remain about how proton and/or other modulators bind the ECD and stimulate the channel activation and steady-state desensitization.

1.3.2 Pharmacologic characterisation of ASICs

Recent studies have shown that ASICs can be activated not only by a sudden pH change but also by the addition of modulators such as the snake venom toxin, MitTx [59], amiloride and other small molecules. Many inhibitors and modulators are known to affect the channel activity,

including zinc, peptide toxins, neuropeptide and small molecules that stabilise interactions within the extracellular domain [60].

The acidic pocket is known to play a prominent role in ASICs modulation and one of the most studied inhibitors of ASICs is psalmotoxin 1 (PcTx1), a peptidic venom composed of 40 amino acids which was isolated from a spider [61]. PcTx1 inhibits specifically and efficiently ASIC1a and ASIC1a/2b (nM affinity) [62] [63] by stimulating the steady-state desensitization. This modulator does not act as a "classic blocker", occluding the pore, but instead acts as a gating modifier of the channel shifting the pH dependence of the steady-state desensitization to neutral pH. Data from molecular docking of PcTx1 using the crystal structure of cASIC1, experiments using site-directed mutagenesis of the channel, and the recent crystal structure of ASIC1 in complex with PcTx1, suggest that the toxin binds within the acidic pocket of the channel.

Other peptide toxins isolated from snake venoms, known as Mambalgins, are able to specifically inhibit ASIC1a, ASIC1a/2a and ASIC1a/2b isoforms expressed in the CNS with inhibitory concentration range (IC_{50}) between 55 to 246 nM [64] [65] [66].

APETx2, a 42 amino acids peptide derived from the venom of the sea anemone *Anthopleura elegantissima* is known to inhibit selectively ASIC3 with IC_{50} between 63 nM and 2 µM (according to the subunit composition) [67] and interestingly it is not isoform selective. Its binding site on ASIC3 and

the mechanism of inhibition are not documented yet, but recent studies have shown that APETx2 can also inhibit the activity of other channels such as the voltage-dependant Na+ channel Nav1.8.

Amiloride, a potassium-sparing diuretic molecule, is the first reported blocker of ASICs [30] [68] able to inhibit the channel activity by occluding the pore [57]. Recent *in silico* studies have shown that amiloride interacts with several amino acid residues located near the desensitization gate [69]. However, amiloride and its derivatives are not selective nor potent inhibitors of ASICs (IC_{50} 5-100 µM) as they can inhibit other ion channels, such as those belonging to the epithelial sodium channel or calcium exchanger family [70].

A new class of antiparasitic diarylamidines including DAPI (IC_{50} 2.8 µM), diminazene (IC_{50} 0.3µM) and pentamidine (IC_{50} 38 µM) have shown *in vivo* (hippocampal neurons) to interact and inhibit the ability of ASICs to produce current [71]. In particular, diminazene aceturate (DA) is known to act as a reversible blocker of different ASIC isoforms [72]. *In-silico* docking of DA to cASIC1 crystal structure has suggested that this di-cationic compound is more likely to bind within the ECD of the channel in a groove-shaped region and not as a pore blocker as amiloride. This region is formed by the β-ball and palm domain that partly overlaps with the binding site of the PcTx1 toxin. This proposed binding site in the ECD is not yet experimentally verified since the underlying inhibition mechanism and interaction with specific ASIC isoform are still elusive, but DA, due its

inhibitory effects on ASICs [72], can be considered as an interesting lead compound for structure-based drug discovery strategy [73].

1.3.3 ASIC 1 and neurodegenerative disorders: state of-the- art

ASIC1 is highly expressed in mammalian CNS and unlike other ASICs, this isoform subunit is more permeable to calcium, a property linked to the critical role of ASIC1a in acidosis-induced neuronal injuries and inflammation states in the brain [72]. Increase evidences in the literature suggest that an abnormal expression and activation of ASIC1a in the brain lead to progressive neurodegenerative states. Recent data from autoimmune encephalomyelitis (EAE) experiments have shown that ASIC1a is upregulated in axons in a mouse model bearing multiple sclerosis (MS) [74]. Moreover, a correlation between the increased expression of ASIC1a and axon injury marker has been observed. ASIC1a plays a key role during stroke, where low amount of oxygen and nutrients are delivered to the brain, causing cells to die and tissue acidosis. It has been demonstrated that the injection of PcTx1 (ASIC1 blocker) in animal models bearing ischemia disease lead to a reduction in the infarct volume (up to 60%). Furthermore, *ASIC1* gene knockout in mice model has led to significant neuroprotection and decreased ASIC1a expression levels. Hence, ASIC1a is thought to play an essential role in acidosis-mediated neuronal injury [75] [76] [77]. Lastly, electrophysiological and *in-vivo* experiments suggest that ASICs are associated with inflammation states and may be modulated by a number of inflammatory mediators [78] [59] released during the process. Indeed, tissue acidosis is a dominant feature in inflammation conditions after ischemia, at which the expressing levels

of ASICs (such as ASIC1a and ASIC3) are significantly increased. More studies are surely needed to delineate the role of ASIC1 isoform in neurogenerative disorders (Table 1). However, ASIC1a isoform is considered as a potential therapeutic target to intervene in these disorders. Literature data on ASICs has highlighted the potential role of their activation during local pH changes in mouse and human brains, but despite considerable efforts and progresses in the field to understand the molecular mechanisms of such disorders, an effective therapeutic approach has yet not emerged.

Disease	Role of ASICs
Parkinson's disease	Lactic acidosis occurs in the brains of patients with PD.
	Amiloride helps to protect against substantia nigra neuronal degeneration, inhibiting apoptosis.
	Parkin gene mutations result in abnormal ASIC currents.
Huntington's disease	ASIC1 inhibition enhances ubiquitin-proteasome system activity and reduces Huntington-polyglutamine accumulation.
Pain	ASIC3 is involved in: 1) primary afferent gastrointestinal visceral pain, 2) chemical nociception of the upper gastrointestinal system, and 3) mechanical nociception of the colon.
	Blocking neuronal ASIC1a expression in dorsal root ganglia may confer analgesia.
	NSAIDs inhibit sensory neuronal ASIC expression.
Cerebral ischemia	Neuronal ASIC2 expression in the hypothalamus is upregulated after ischemia.
	Blockade of ASIC1a exerts a neuroprotective effect in a middle cerebral artery occlusion model.
Multiple sclerosis	ASIC1a is upregulated in oligodendrocytes and in axons of an acute autoimmune encephalomyelitis mouse model, as well as in brain tissue from patients with multiple sclerosis. Blockade of ASIC1a may attenuate myelin and neuronal damage in multiple sclerosis.
Multiple sclerosis Seizure	Intraventricular injection of PcTX-1 increases the frequency of tonic-chronic seizures.
Seizure Malignant glioma	Low-pH stimulation increases ASIC1a inhibitory neuronal currents.
	ASIC1a is widely expressed in malignant glial cells.
Malignant glioma	PcTx1 or ASIC1a knock-down inhibits cell migration and cell-cycle progression in gliomas.
	Amiloride analogue benzamil also produces cell-cycle arrest in glioblastoma.

Table 1: The role of Acid-Sensing Ion channels (ASICs) in neurologic disorders (adapted from [44])

1.4 Gelsolin amyloidosis: soluble target

1.4.1 Gelsolin physiopathology

Gelsolin (GSN) is a key protein in regulating the oligomeric state of actin, by means of its severing, capping and nucleating activities (Figure 10) [79] [80]. Cytosolic GSN is important for the remodeling of the cytoskeletal structure [81]. Whereas, extracellular GSN, which is 24-residue longer than the cytosolic isoform, and stabilized by a disulfide bond, is secreted into the blood [82] [83] [84] [85]. Both GSN isoforms consist of roughly 750 amino acid residue (approximately 85 kDa) and are organized into six homologous domains (named G1–G6).

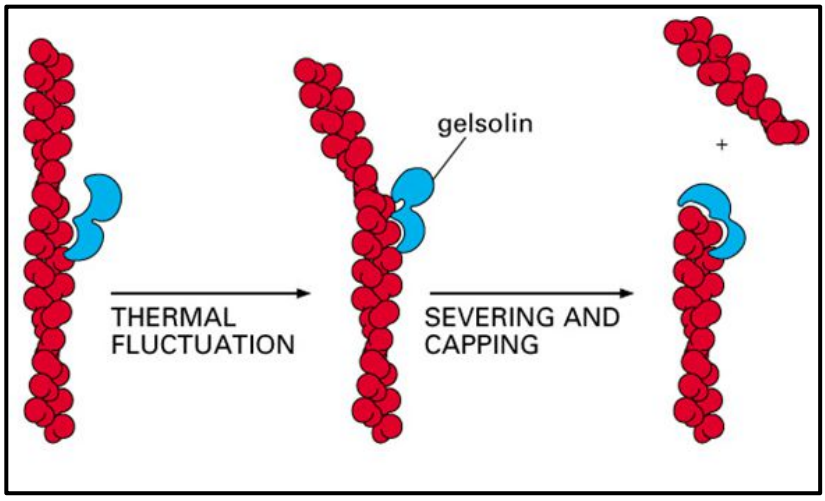

Figure 10: Actin filament (in red), severing and capping by gelsolin protein (in blue)

All GSN domains share a typical gelsolin-like fold [86] [87]. Each module hosts at least one binding site for Ca^{2+}. Binding of Ca^{2+} induces both subtle local and large global conformational changes [88] [89] [90] (Figure 11).

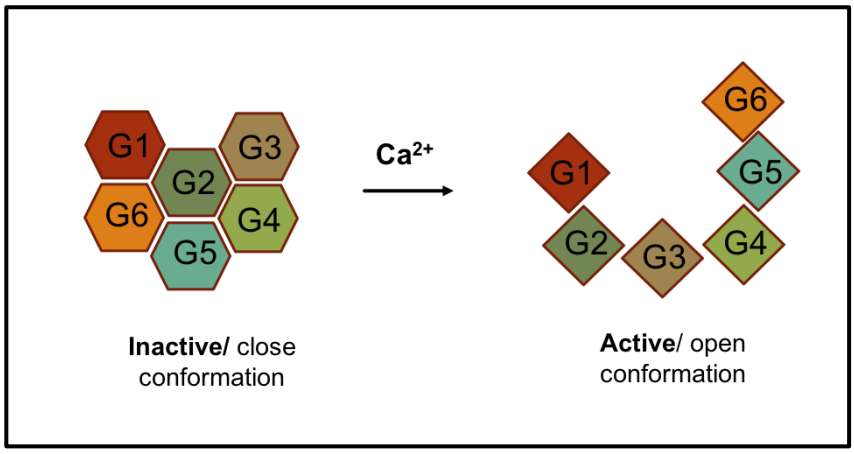

Figure 11: Schematic illustration of the structural conformational change of the full-length gelsolin (GSN) upon calcium ions binding

The left-hand side shows the six domains of GSN in a calcium-free conformation (compact/packed inactive conformation). On the right-hand side, the calcium bound-conformation of GSN is presented (open/release conformation)

Gelsolin exists in two functional conformational states. In the absence of Ca^{2+} (Figure 11, left), the protein adopts a closed and compact conformation, hampering the binding to actin filaments (inactive form). Upon increase of Ca^{2+} concentration, the GSN structure unwinds, exposes the actin binding surfaces and adopts an active conformation (Figure 11, right) [91]. The active conformation is highly dynamic, mainly due to the loss of interdomain contacts which are mediated by flexible stretches of the polypeptide chain [92]. Therefore, no high resolution three-dimensional structure of calcium-activated gelsolin is available, and most of the structural analysis of GSN relies on the study of the isolated domains of the protein [86 88]. Studies on the isolated domains show that Ca^{2+} ions play a structural role for the gelsolin-like fold, i.e. thermodynamic stability of the domain is higher in the presence of the ion. This observation is

somehow in contrast to the effect of Ca^{2+} observed on the full-length protein [89 93].

Owing to the pivotal physiological activities of GSN, both in the cytosolic and extracellular form, and its ubiquitous nature, GSN plays a major role in a plethora of physiological activities, such as cell motility and division, organelle trafficking and muscle contraction [94]. As a consequence, a large body of evidence suggests a GSN role in a variety of pathological processes (which are thoroughly reviewed in [87 95] (Figure 12). GSN has also some neuroprotective effects, and it could be exploited for the development of therapeutic interventions in neurological disorders, comprising ischemic stroke [96], Alzheimer's disease and multiple sclerosis [97 98].

Recent evidence suggests that the cytosolic GSN exerts an important role in cell metabolism and signaling through an actin-independent mechanism [99]. However, a clear relationship between the gelsolin levels and its effect in countering or inducing these pathological conditions remains to be elucidated. Contrary, mutations in gelsolin are directly responsible for a rare form of amyloidosis, referred as Gelsolin Amyloidosis (AGel, OMIM reference number 105120).

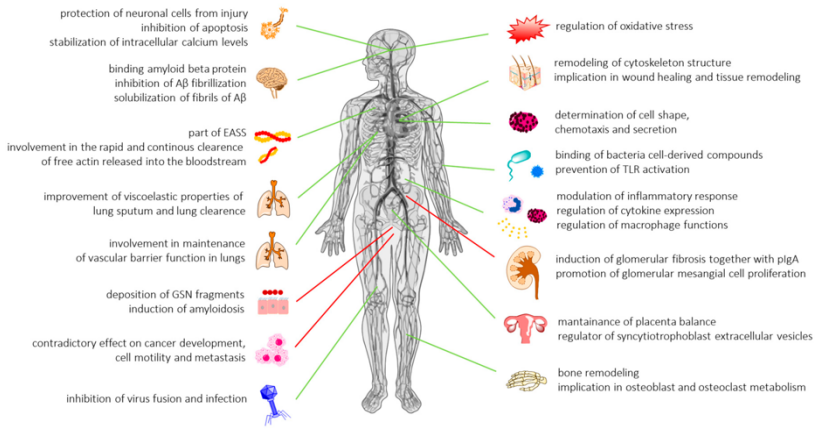

Figure 12: Schematic view of the physiological and pathological processes in which gelsolin is involved

Green arrows indicate the beneficial effect of gelsolin in the maintenance of health and physiological balance; red arrows indicate disadvantageous gelsolin-mediated events (image taken from Piktel et al.,2018)

1.4.2 Gelsolin amyloidosis (AGel)

Amyloidosis-related diseases are degenerative in nature, with pathogenicity stemming from the misfolding of the precursor protein. This process leads to the accumulation of insoluble protein aggregates, known as amyloids, in various organs and tissues. More than 20 amyloidogenic diseases, including central and systemic forms, have been identified. These amyloidoses can be either hereditary, owing to mutation(s) or deletion(s) in the etiological protein, or sporadic, (e.g. associated with external factors).

The first genetic form of gelsolin amyloidosis, which was until very recently the only one described, was identified in the 1969 and named Meretoja's syndrome or familial amyloidosis Finnish-type (FAF) [100]. FAF is

caused by the substitution of residue D187 to either N or Y (numbering according to the mature plasma protein) [101] [102]. This AGel form is essentially a systemic amyloidosis, characterized by a prototypical symptomatic triad caused by the accumulation of GSN fibrillar aggregates in the eyes, skin, peripheral and central nerves. Thanks to the broader use of genetic tests and an increase awareness, AGel cases have been described in many other countries, suggesting that this disease is often undiagnosed or misdiagnosed [103].

Recently, two novel pathological variants of gelsolin have been described, associated with a renal-localized amyloidosis. This novel form of AGel is caused by the following mutations: N184 to K and G167 to R [104] [105]. Moreover, a sporadic form of AGel with marked wild-type GSN deposits surrounding a sellar glioma of the hypophysis has been also described [106]. Therefore, AGel can be classified into three different type (systemic, kidney-localized, sporadic), based on the nature of the protein (mutated or wild-type) and the organ(s) where gelsolin fibrils are deposited. All AGel types share the lack of proper pharmacological therapies that cure the disease targeting the source of toxicity. Only palliative or symptomatic treatments are available.

The molecular mechanisms underlying the kidney amyloidosis, caused by the N184K [107] as well as the G167R variant, [108] have been partially investigated in our lab and are still under investigations. Conversely, the systemic amyloidosis variants (D187N/Y) have been extensively characterized by biochemical and biophysical studies. *In vitro* and *in vivo*

experiments led to a final consensus on the pathological mechanism underlying the Finnish AGel type [109]. D187 is present in a cluster of residues that chelate Ca^{2+} in the G2 domain of GSN [110]. Its substitution to N/Y compromises the Ca^{2+} binding, decreasing the thermodynamic stability of the domain [111] [112]. This increased conformational flexibility makes the protein susceptible to aberrant proteolysis by furin, an endogenous protease in the Golgi [111], which mainly produces a C-terminal fragment, C68 (Figure 13). Once exported to the extracellular space, C68 becomes a substrate for other enzymes (e.g. metalloproteases). The proteolytic cascade (Figure 13) leads to the production of two amyloidogenic peptides of 5 and 8 kDa prone to aggregation. Only the exported isoform of the protein is responsible for the disease.

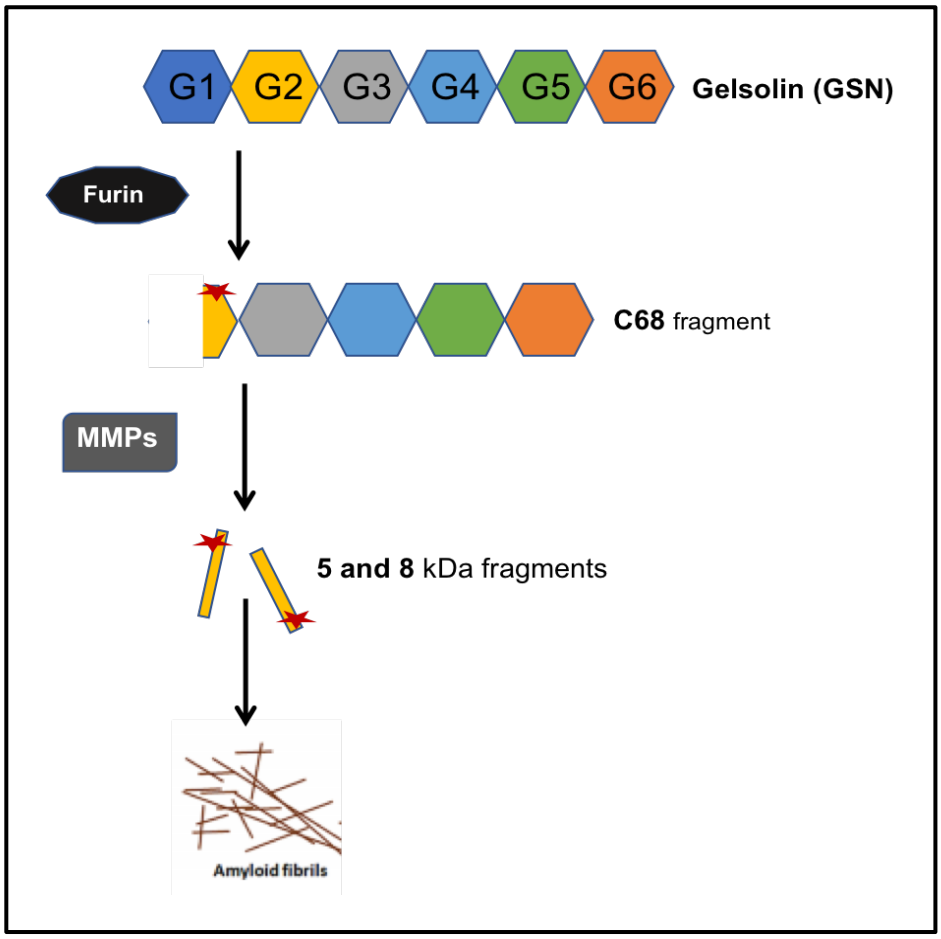

Figure 13: Schematic representation of the aberrant proteolytic pathway of the D187N/Y mutated gelsolin protein.

Gelsolin variants (carrying the mutation in G2) are aberrantly cleaved by furin protease (in the Golgi apparatus). The C68 fragment is exported to the extracellular environment and cleaved by the matrix metallo-proteases (MMPs) to produce 5−8 kDa fragments. These 5 and 8 kDa fragments readily aggregate and deposit as amyloid fibrils.

In contrast to the extensive biological and biochemical knowledge available for the GSN D187N mutant, its crystal structure is still unknown. The absence of high-resolution structural information, limited the understanding of the mechanisms of D187N GSN instability and aberrant proteolysis.

1.4.3 Nanobodies against gelsolin amyloidosis

Nanobodies (Nbs) are the variable fragment of Camelid heavy-chain antibodies [113] (Figure 14). Nbs can be easily produced in both prokaryotic and eukaryotic hosts [114], are characterized by small size (approximately 15 kDa) and better stability compared to conventional antibodies and derivatives (e.g. Fabs or scFvs) [115 116 117].

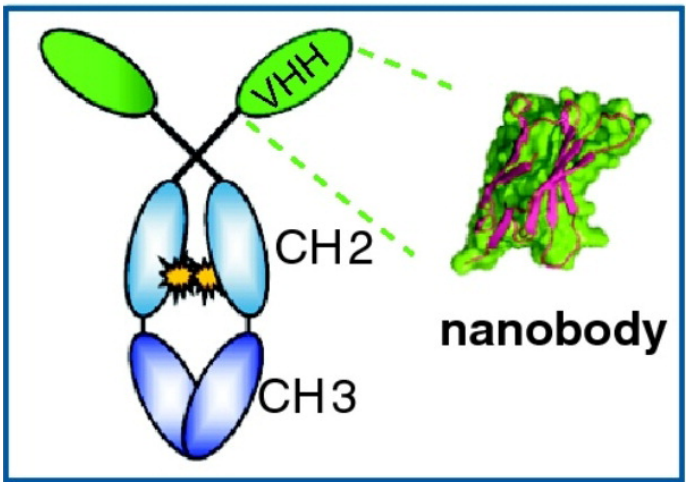

Figure 14: Nanobody structure

Adapted and modified image from Steyaert et al.,2011

Thanks to their unique compact prolate structure, Nbs expose a convex paratope and can access cavities and clefts on protein's surface [118 119], which are usually inaccessible to conventional antibodies due to their large size. These unique features promoted the application of Nbs in fundamental research, diagnostics and therapy [120 121 122], where Nbs are used as neutralizing agents, receptor-ligand antagonists or vehicles for targeted drug therapy [122 123]. In addition, Nbs can be used as molecular

chaperons during the expression or the purification of the target protein; or as an *additive* for protein crystallization [124].

A recently reported nanobody-based strategy showed great potential as alternative therapeutic approach for AGel [125] [126] [85]. Several Nbs, raised against WT GSN, bind the mutated protein and are able to detect or prevent its aggregation. Among them, Nb11 resulted the most efficient one. *In vitro* and *in vivo* studies show that Nb11 can block gelsolin degradation by indirectly inhibiting furin enzyme [85]. That is, Nb11 binds with high affinity the G2 domain of GSN and shields the mutated domain, preventing the first step of the aberrant proteolytic cascade.

2 Aims of the thesis

In this thesis, I aimed to show that structural biology can substantially contribute to the development of novel therapeutic strategies. It can be exploited to dissect the molecular basis of disease, to identify novel ligands or to characterize the mechanism of action and rationally optimize previously identified leads.

ASIC1a is considered a validated therapeutic target for neurodegenerative diseases. However, pharmacological blockade of ASIC1a can promote dysfunction in synaptic plasticity, hippocampal LTP and spatial memory. These effects can be related to the low potency and selectivity of known inhibitors. Thus, we aim at obtaining small molecules with higher selectivity for ASIC1a and good bioavailability, that could help to define a novel therapy for neurological diseases. To this aim I performed rational design based on *in silico* docking results, followed by chemical synthesis and pharmacological characterization of DA analogs. Final aim is obtaining 3D structural information of ASIC1a in presence of 1-2 modulators in order to characterize the overall binding mode of this new class of compounds, and to continuously provide structure-based feedback to medicinal chemistry efforts. Thus, the expression and purification of the ASIC protein have been explored in different host organisms, and the use of high-throughput methods have been performed to find the correct construct, expression and purification conditions required for crystallization.

Gelsolin amyloidosis (AGel) is a rare autosomal dominant disease, caused by mutations (D187N/Y, G167R or N184K) in the second domain (G2) of

gelsolin. D187N, the most common and studied mutation, impairs G2 stability and the protein becomes susceptible to aberrant proteolysis. The cleaved fragments aggregate and accumulate in the body causing the disease. This mutant is well characterised but its 3D structure has never been obtained. Conversely, G167R or N184K variants have been only recently discovered. A recently described nanobody (Nb11) has shown potential for the treatment of AGel. Nb11 binds D187N-mutated gelsolin, indirectly inhibits aberrant proteolysis and prevents its aggregation. This part of thesis aims at 1) understanding Nb11 mechanism of action; 2) testing the efficacy of Nb11 on the renal variants of the disease (G167R and N184K); 3) exploit the Nb to crystallize the elusive D187N gelsolin variant.

3 Main results and discussion

3.1.1 Acid sensing ion channel 1

ASIC1 is a major ASICs isoform, characterized by pH-mediated activity, sodium permeability and high expression levels in the neurons of the central nervous system (CNS).

This chapter focuses on the initial *in silico* structural studies of ASIC1, and describes the main results obtained through three years of extensive work, in home lab and abroad (via Instruct internships), to produce the protein.

3.1.2 Molecular dynamics simulation

Diminazene aceturate (DA), as other small molecules that belong to anti-protozoan diarylamidines family, has been reported to inhibit ASIC1a current in cultured hippocampal neurons with relatively high affinity, thus it was chosen, in this PhD project, as an interesting small molecule to be used as an initial template to perform SBDD.

DA is a symmetric molecule, where two arylamidines are connected by a 3-atom triazene linker (Figure 15). Novel/patentable variations either at its functional groups (R, AG), or at the connecting linker (CL) should increase the affinity for ASIC1a while improving their drug-like profile (solubility, bioavailability, brain permeability, metabolic stability among others).

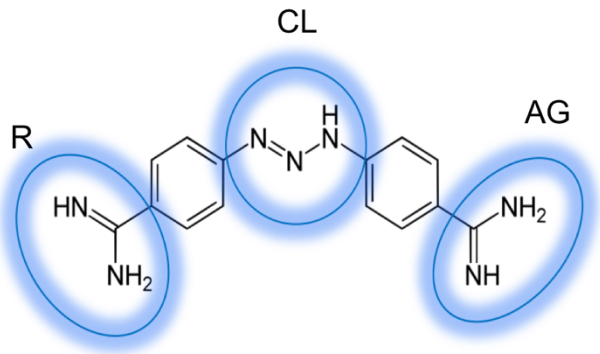

Figure 15: The chemical structure of Diminazene Aceturate (DA)

The highlighted groups were modified in order to optimise the molecular features of DA and enhance its capacity to bind ASIC1a. In particular to enhance its specificity and permeability to pass the Blood Brain Barrier (BBB), DA was functionalised by replacing the pattern in the second phenyl ring at either the AG or a more lipophilic substitution pattern.

As a first step, *in-silico* studies and molecular dynamics simulations have been proven to be important instruments to understand the interaction of ASIC1 with DA-related compounds and to rationally design DA analogues. Several crystal structures of chicken ASIC1 (cASIC1) have been reported so far [46 51 64 127 128 129] showing a tight trimeric assembly of the protein with a wide extracellular domain involved in pH-based channel gating. Chen et al. [59] analysing the monomer of cASIC1 by *in silico* docking with diarylamidine blockers of the channel, have speculated that diarylamidines, such as DA, could bind ASIC1 in a crevice close to the extracellular β-ball domain (Figure 16). Conversely, since DA is a positively charged molecule, the idea is that it could bind near to the pH sensor site located at the interface between two subunits of the trimeric assembly, and therefore not considered in the *in silico* structural analysis performed

in analogy with the docking sites of the spider or the snake toxins (Baconguis & Gouaux, [127] [130]).

To test this hypothesis, molecular dynamics (MD) simulations have been accomplished on the extracellular domain (ECD) of chicken ASIC1 trimer (PDB code: 4FZ0), in the presence of three DA molecules starting at two different locations (Figure 16) either in front of the pH sensor, or in front of the putative binding domain proposed by Chen et al. In both cases, after few nanoseconds of simulation some DA molecules migrate inside the pH sensor (named also acidic pocket), maintaining such location along the entire simulation (Figure 17) reports the MD simulation performed, showing the DA initial location (Figure 17 B yellow spheres) at ~35 Å from its final docking site, inside the pH sensor. The starting structure and the final structure of MD simulation are shown as cartoon in red and blue, respectively. Interestingly, the putative DA docking site overlaps with one of the binding sites for amiloride (a non-ASIC-specific marketed drug) as was observed in the crystal structure of chicken ASIC1 bounds to the snake toxin [130]. To start analysing the structural changes of the channel induced by different pH, a further MD simulation has been performed at pH 4 for 18 nanoseconds (Figure 17 A), showing that the pH sensor, e.g. the putative DA binding site, tends to maintain its initial conformation (Figure 17 A).

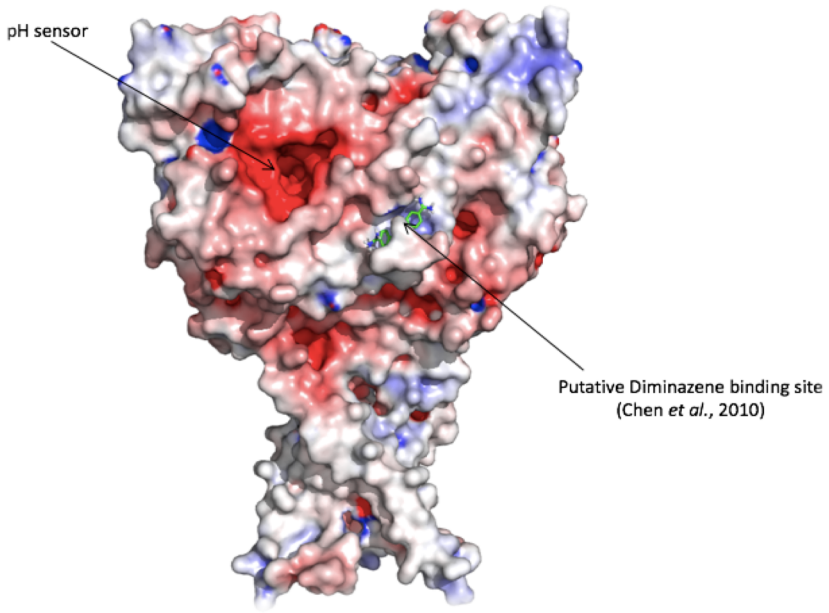

Figure 16: Docked Diminazene (DA) onto chicken ASIC1 crystal structure (PDB code: 4FZ0)

The data reported here was obtained from the work of Chen et al., 2010, displaying the predicted binding site of DA on the channel surface.

3.1.3 In-silico docking

Based on ASIC1 structural analysis and *in silico* modelling above mentioned, a class of DA-like molecules were designed with potent and specific affinity for ASIC1 isoform (in collaboration with the department of chemistry- Professor P. Seneci group). This class of DA-like compounds represents a novel class of ASIC blockers that might be useful for ASIC functional studies and be of therapeutic importance in future for intervention in ASIC1a-related neurodegenerative disorders. Briefly, DA was functionalised at AG or/and R or/and CL (Figure 15); replacing the charged amidine groups with aminoguanidines to ensure a significant proportion of non-ionized molecules at physiological pH and capacity to

penetrate through the Blood Brain Barrier (BBB). In order to enhance the affinity for ASIC1a, the second phenyl ring was substituted by inducing another AG (symmetrical and p-disubstituted aryl of AG). Therefore, the interaction affinity of the optimised molecules (whose chemical structure is not shown here for patent issues) was tested *in-silico* using AutoDock4 program [131] on the ECD-ASIC1 (PDB code: 3HGC), taking into account the results obtained by MD simulations (see material and methods for more details about the experimental run).

A molecular graphics package, such as PyMOL (https://pymol.org/), was also used to visualise the ligand's poses on the structure. In Figure 18, the binding mode of the best two ranked ligands (DG327, DG296) are shown as well as the orientation of DA. Preliminary data from the analysis on the amino acid residues that are involved in the interaction with these molecules have been drawn (not shown).

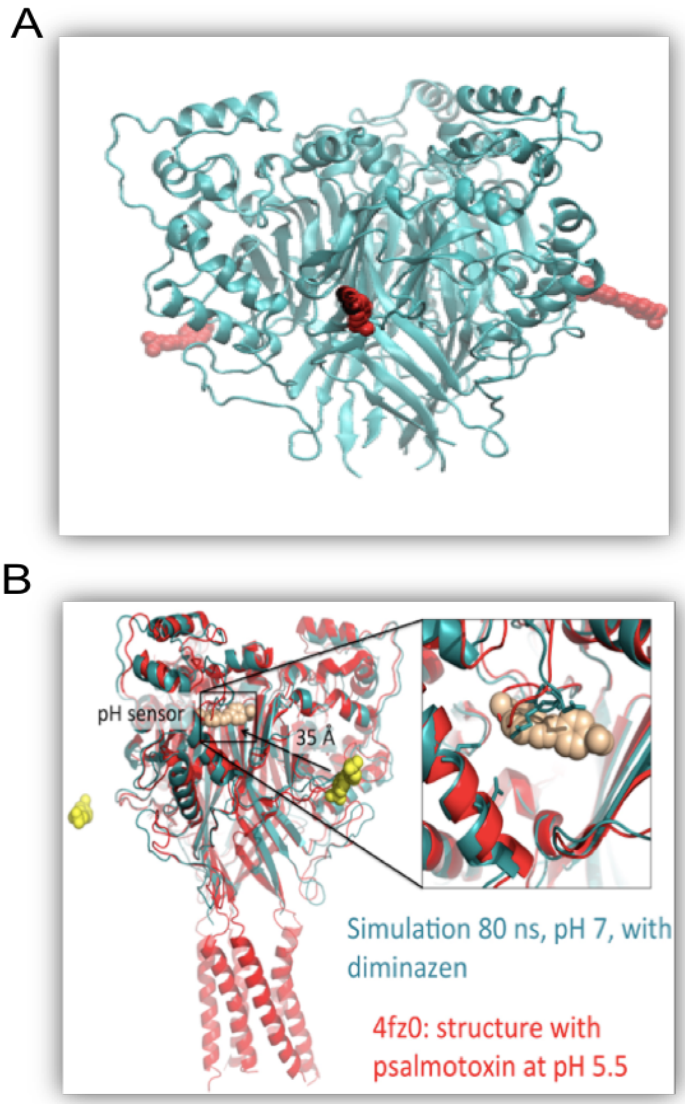

Figure 17: Molecular Dynamics Simulation (MDS) onto the extracellular domain of chicken ASIC1 (cASIC1) with DA at pH 7

A. the image is taken during the simulation, indicating the initial locations of three DA molecules (red spheres) on the extracellular domain of ASIC1. B. Final state result of DA's positions (light brown spheres) on the ASIC1 protein (light blue) after 80 ns of MD simulation in comparison with the initial locations of the DA molecules (yellow spheres). The structure of ASIC1 after the simulation has been superimposed on the structure of ASIC1 obtained at pH 5.5 (pdb=4fz0 in red) in complex with psalmotoxin, a small peptide known to be a potent inhibitor of ASIC1.

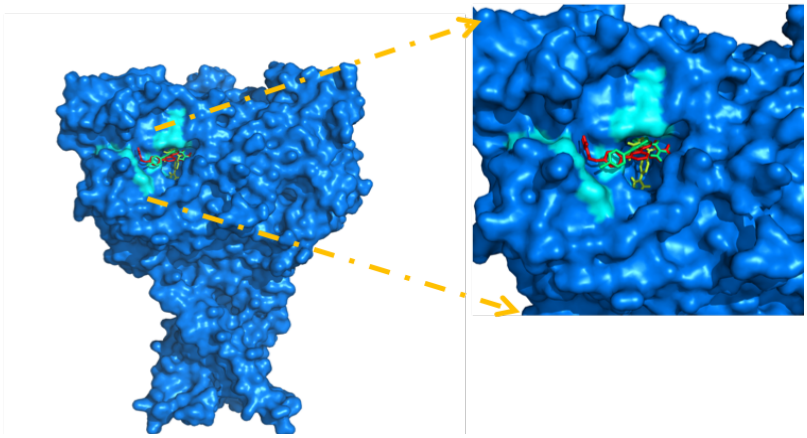

Figure 18: 3D presentation of the binding mode of compounds DA-like compounds on ASIC1

Surface representation of chicken ASIC1 (blue) (PDB 3HGC) displaying the results of binding interaction with DG296 (green sticks), DG327 (red) in stick presentation during the docking analysis compared to the DA (in yellow sticks). Although the three molecules overlap binding in the binding site (the acidic pocket of the extracellular domain), DA is orientated deeper in the pocket.

As a result, the 5 best compounds out of 60 were selected, according to their calculated free energy of binding (Table 2) and synthesized by Prof. Seneci.

Compound	Binding energy EB (Kcal/mol)	Inhibitor Concentration IC_{50} (μM)
DG327	-14	0.41
DG296	-13	1.40
SB038	-13	N. A
SB046	-12	N. A
DG324	-11	N. A
DA	-6	10

Table 2. List of docking results of the top- ranked 5 compounds (DA- like) and of the reference compound DA.

The compounds were ranked based on their interaction affinity with ASIC1 from in-silico analysis (left side) and their inhibitory effetct (IC_{50}) values from test in-cell based (right side). The free energy of binding (Eb) is represented by delta G (Kcal/mol) calculated by Autodock4. Some compounds are not yet tested (NA).

The synthesized compounds have been tested in cell-based assays using patch clamp electrophysiology [132] by our collaborators at the University of Naples "Federico II", department of Neuroscience- group of Prof. L. Annunziato (the IC_{50} values are reported in Table 2). Briefly the test was performed on human embryonic kidney 293 (HEK293) cells, functionally expressing ASIC1a isoform and the whole-cell patch-clamp assay was carried out at room temperature, holding potential voltage set at -70 mV. ASIC1a is known to be activated by a pH-shift between 7.4 and 6.0 [133]. Therefore, the experiment was performed at these pH values: first ASIC1a was activated repeatedly by pH drop from 7.4 to 6.0 in the absence of MS-1 and DS-1, a diaryl mono- and a diaryl bis-compound synthesized and analysed

by our collaborators (Prof. Seneci group). After that, the compounds were pre-applied in extracellular solution at pH 7.4 for 40 seconds, and co-applied in extracellular solution at pH 6.0 for 10 seconds. ASIC1a's peak was measured by following the current amplitude. The experimental IC_{50} calculated for DA and DA-like compounds are reported in Table 2, showing a good correlation between the *in silico* data and the experimental data. Thus, such preliminary findings show the possibility to identify a suitable putative binding site for DA analogs.

3.1.4 Attempts to produce the extracellular domain of ASIC1 in bacteria cells

To validate our *in-silico* studies, the synthesized analogs should be tested *in vitro* on the purified protein and the crystal/cryo-EM structures of ASIC1 in the presence of 1-2 DA analogs should be determine. To this aim the expression of the ASIC1 was undertaken, using different organisms of expression. As a first attempt, the mouse ECD-ASIC1a construct, lacking the inter-membrane portion, was chosen using as host expression system the *E. coli*.

The full-length mouse ASIC1 (UniProtKB: Q6NXK8) was used as template for cloning the extracellular domain protein sequence (see Materials and methods, Figure 50) into three different expression vectors (pET28a, pGEX-T41 and pET32a) that have been transformed in two different bacterial strains (SHuffle® T7 and BL21 (DE3) E. coli cells).

The protein expression was performed under a range of different conditions, mainly modifying the temperature and time (Figure 19).

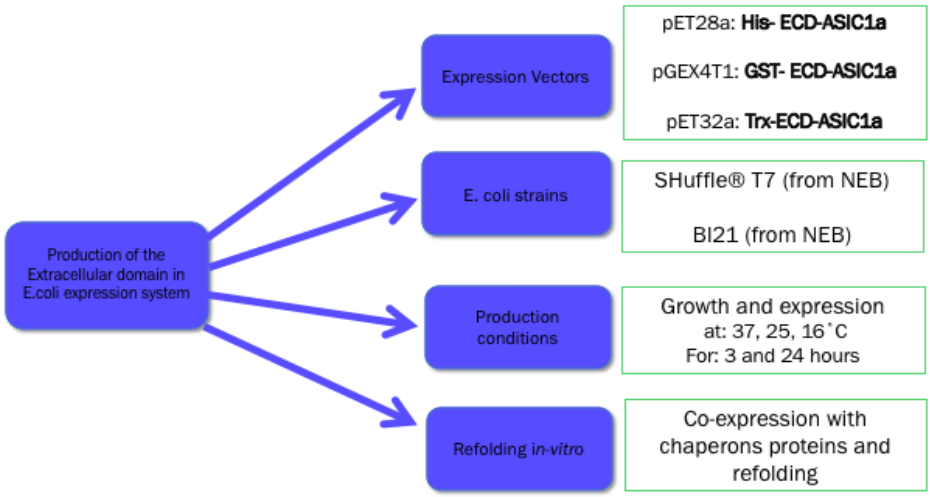

Figure 19: Overview of trials performed on E.coli cells for the production of ECD- ASIC1a

Since mouse ASIC1a (UniProtKB: Q6NXK8) shares about 90% sequence identity with chicken ASIC1, the definition of the soluble domain (from residue 72 to 423) was based on the alignment with the known chicken ASIC1 sequence (PDB: 2QTS). All the designed constructs of ECD-ASIC

were fused at their N-terminus with a tag that simplifies purification steps and possibly improve their solubility. The tags are hexa-Histidine (6XHis), Glutathione S-transferase (GST), and Thioredoxin (Trx), respectively for the aforementioned expression vectors. The cloning trials were successful only for pET28a and pGEX-T41 by traditional cloning approach (Figure 20). The DNA sequencing analysis of selected colonies was done by EUROFIN company.

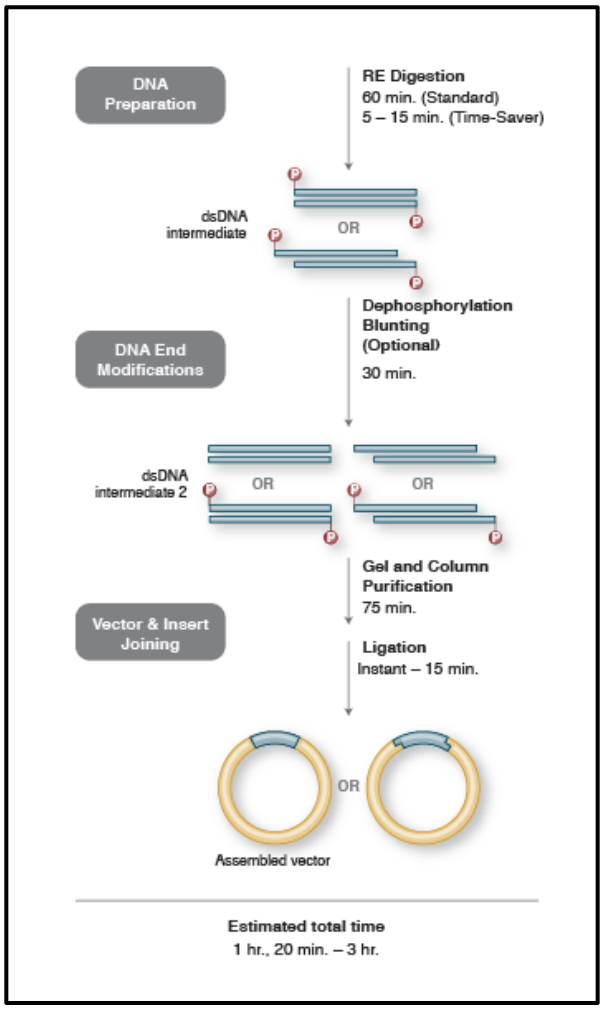

Figure 20: Traditional cloning workflow

Picture obtained from New England BioLabs inc

The expression trials for producing His_6-ECD-ASIC1 in different conditions revealed that the protein was mostly insoluble and accumulated in inclusion bodies. Therefore, unfolding-refolding purification protocols starting from inclusion bodies have been performed, as described in several reviews [134], in order to extract a good yield of the protein. However, refolding of the protein led to a very heterogeneous sample,

most probably due to the presence of 7 cysteine residues, 6 of which are important for structural disulphide bonds formation and thus for a proper protein folding. Therefore, in dilution refolding conditions, ASIC resulted highly aggregated, beside only low refolded protein yields (Figure 21).

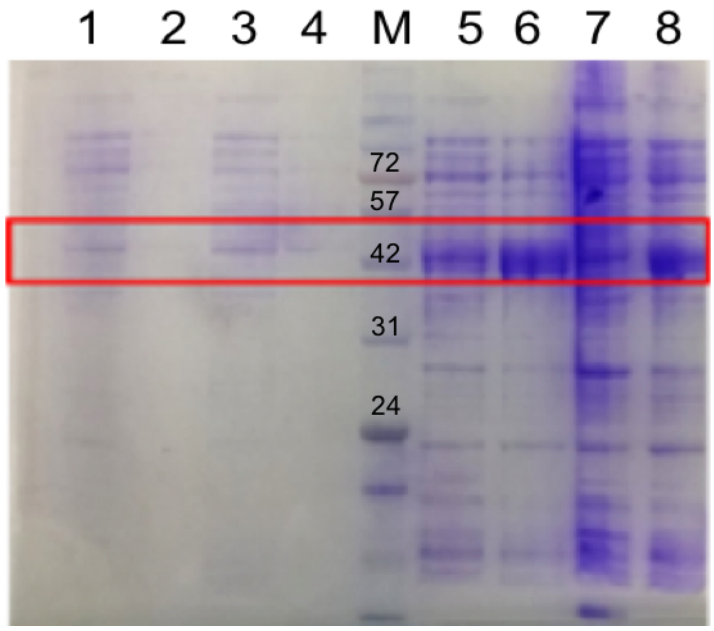

Figure 21: SDS PAGE gel of ECD-ASIC1a

Two types of medium were tested; LB broth (LB) and superior broth (SB) for the growth of Shuffle-His-ECD ASIC1a at different temperatures (16 and 37˚C). The protein seems to be present more in insoluble fractions (pellet) than in soluble fractions (Sol). Lane 1. LB 16 Soluble, 2. LB 37 Sol, 3. SB 16 sol 4. SB 37 Sol, protein marker (M), 5. LB 16 pellet, 6. LB 37 Pellet, 7. SB 16 Pellet, 8. SB 37 Pellet

To overcome this issue, chaperon proteins were used as protein refolding assistance. This approach would guarantee a proper formation of disulphide bonds, prevent protein aggregation and therefore should be useful to achieve sufficient yield of well folded protein. Therefore, ECD-6xHis-ASIC1a was co-expressed in Shuffle cells together with chaperon

proteins (for details see Materials and methods). The eluted and refolded ASIC1a samples were very heterogenous and therefore this approach as well, resulted inefficient.

Last trials of ECD ASIC1a expression in fusion with GST-tag were roughly successful and showed an improvement in the solubility of the protein. However, scaling-up the expression process, yielded only extremely low amount of the recombinant protein. The fact that the protein samples were not highly detectable by SDS-PAGE could be due to an instability of the protein (post-GST cleavage) or to a very low expression level.

Altogether, these extensive trials in bacterial expression system have led to a very limited final yield of such a membrane protein. Therefore, other expression systems were exanimated to overcome this issue.

3.1.5 Expression trials: alternative host systems

3.1.5.1 Baculovirus- infected insect cells: trials at the Weizmann Institute

Although *E. coli* is usually the first organism of choice, the preliminary trials on the production of mouse ECD-ASIC1a were unsuccessful. Therefore, the choice of a different expression system has been mandatory. The baculovirus/insect cell has been shown to provide a good yield of the chicken variant of the protein ASIC1 [52], thus it was the chosen alternative expression system.

The two months spent in the laboratory of Dr. Tamar Unger, at the Weizmann Institute (Israel) via Instruct internship, were necessary to acquire basic knowledge related to eukaryotic cells handling, maintenance and novel methodologies for producing recombinant proteins by using baculovirus-infected insect cells, that have been

transferred back to the home laboratory. The experimental plan was organised in three tasks including cloning, virus amplification for protein expression and protein purification (for details see Materials and methods).

For the expression in baculovirus-infected insect cells, both murine ASIC1a full-length protein and its chicken variant ASIC1, whose structure was published at 1.9 Å resolution [52] were used. By the RF methodology [135] that is based on the QuickChange™ oligonucleotide- directed mutagenesis, 3 constructs have been cloned. In contrast, the RF technique offers several advantages including the specificity and facility to clone precisely ASIC- DNA insert in the desired position (appropriate primers were designed) within a baculovirus transfer plasmid. Briefly, the three constructs that have been designed and used are 2 of mouse ASIC1a full-length (mASIC1a-FL; Δ13mASIC1a-FL and Δ27mASIC1a-FL) and 1 of chicken ASIC1 full-length (cASIC1-FL; Δ13cASIC1). The first step in cloning was achieved successfully by a PCR amplification of ASIC DNA sequence using a set of forward and reverse primers (See supplementary chapter). The cASIC1-FL (provided by professor Gouaux E.) was used too.

The constructs contain 6xHis tag followed by SAG linker and TEV protease recognition sequence.

However, the published protocol for the expression and purification of this construct could not be reproducible. Therefore, a new clone was designed using different viral vectors: pVL1393 (as described for mASIC1a) and pFastBac viral vector (by Bac-to-Bac system).

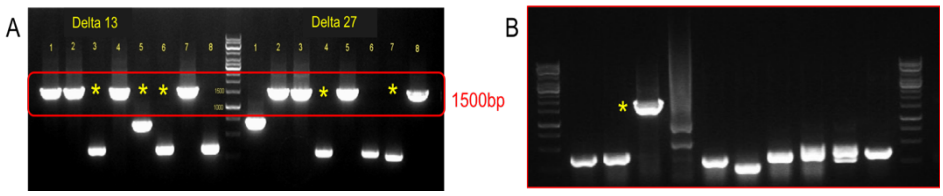

Figure 22: Colony PCR of ASIC1.

The 1% agarose electrophoresis shows the colony-PCR amplification of ASIC1 (mouse (A) and chicken (B) variants) into PvL1393 viral vector through RF cloning technique. Asterisks represent positive colonies at the corresponded size of amplified ASIC1 (1500bp): in A, Lane 1,2,4 and 7: Δ13mASIC1a-FL. Lane 2,3,5 and 8: Δ27mASIC1a-FL. In B, only one picked colony of Δ13cASIC1 was positive. see primers used for colony-PCR in 8.3.2 chapter.

The three constructs were used for preparing baculovirus stocks (first generations: P_0 and P_1), which are needed for the expression in Sf9. Briefly, the viral plasmid DNA and lipid reagent complex (for details see Material and methods) adheres to the Sf9 cell surface and releases, by endocytosis, its DNA into the cell's cytoplasm. The baculovirus genomic vector encodes for the GFP, which allows monitoring of recombinant virus propagation. The amplification of viruses was followed by standard pipeline of baculovirus amplification (see Materials and methods Figure 54).

Viruses of both mouse and chicken have been amplified and tested for expression trials of ASIC1, following the GFP signal. The expression trials were carried out on two constructs: Delta 13 of mASIC1a and cASIC1 (that was cloned in pFastBac vector). The expression performed at small scale (30 mL) was inspired by the published ASIC expression [52]. Infected cells (at $1X10^6$ cells/ mL) were collected after 72 hours (Figure 23). Although the expression levels of cASIC1 seems to be higher than its murine variant, low GFP-signals were observed also for mASIC1a, around the cell membrane, indicating a low expression of a membrane protein. An

optimisation screen has been performed to enhance the infection efficiency and therefore the production yield, by modifying two parameters: 1) the amount of viruses (5, 10 and 50 µL of viruses for 30 mL of Sf9 cell culture); and 2) time of harvesting: cells expressing ASIC were harvested post- 48h instead of 72 hours of infection. Although the expression was performed according to published crystal structures of cASIC1a [136], the results obtained have shown the low expression of both proteins, which are not suitable for biochemical and structural studies.

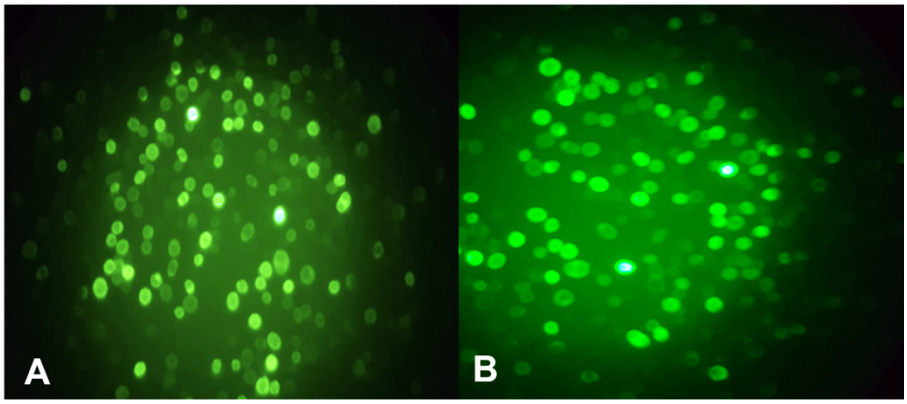

Figure 23: Fluorescence microscopy of Sf9 cell cultures infected with ASIC1 baculoviruses

Images were taken at 72 hours post-infected with first generation of viruses (P_1). There is an abundant GFP expression in bac-to-bac cASIC1 (A) and less in pVL1393-mouse delta 13 (B). However, few GFP signals around the cell membrane were observed.

Although the expression of ASIC1a proteins was low, Sf9 cell cultures were collected for protein purification tests. The purification steps from small scale expression (30 ml) of both mASIC1a and cASIC1 in cell culture, were performed in batch using two kinds of resins: Nickel-beads and TALON resin as described [52] [137]. Even under optimised conditions, the final yield of the recombinant protein constructs was not enough to be

detected in SDS-PAGE by blue-Coomassie staining. The protein was only detected by western blot (using 6XHis tag antibody-Abcam) (Figure 24).

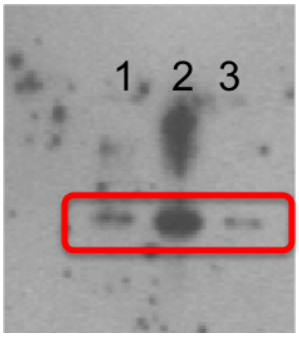

Figure 24: Western blot of ASIC1- anti histidine antibody

Lane 1 and 2 are elution fraction of ASIC1 from affinity chromatography. The protein was detected at the expected theoretical size (56 kDa) lane 3: resin fraction (was used to ensure the presence/absence of the protein yet on the resin).

3.1.5.2 Expression of ASIC1 in mammalian cell culture: trails at the RCaH in Oxford

Mammalian cells are usually the ultimate choice for expressing recombinant membrane proteins of higher eukaryotes, like mammals, as they provide the most native-like cellular environment. Although the protein yields are lower than those required for structural studies, the expression levels could be sufficient for functional characterisations (e.g. ligand-binding assays). The production can be done either by integrating foreign DNA into the host cellular genome or by transient transfection.

During an EMBO practical course (High-throughput protein production and crystallization in Oxford, UK), it was possible to perform production trials on previous constructs (cASIC1 and mASIC1a). The constructs were optimised for the expression into a stable mammalian cell line, HEK 293T. More in detail, the constructs were designed to be cloned into their developed expression vector named pOPINF that assures a versatile-ligation independent cloning method suitable for the expression of

membrane proteins in mammalian, bacterial and insect expression cells (Table 3). The two constructs have been cloned in two different vectors as following: in one case the construct was designed with no specific fluorescence tag (N-6xHis-3C-POI). On the other hand, the recombinant protein was designed with 6xHis and GFP tags fused at its N-terminus to facilitate their identification during infection and purification steps (Table 3). The expression of both was under the control of another later promoter, p10 [138].

Gene name	Vector name	Product	Location	MW no tag (Da)	MW of tag (Da)	MW with tag (Da)	Fluorescence
mASIC1a	pOPINF	His-3C-GFP	Membrane	51,490	2,158	53,648	
mASIC1a	pOPINN-GFP	His-3C-GFP-POI	Membrane	51,490	28,951	80,440	GFP
cASIC1a	pOPINF	His-3C-GFP	Membrane	57,871	2,158	60,029	
cASIC1a	pOPINN-GFP	His-GFP-3C-POI	Membrane	57,871	28,951	86,822	GFP

Table 3: Overview of designed ASIC1a isoform constructs

Mouse (mASIC1) and chicken ASIC1 (cASIC1) for the expression in mammalian cell culture. Protein of interest (POI). Note that the GFP was only expressed in fusion with ASIC (cloned in the pOPINN-GFP vector (Berrow et al., 2009). pOPINF does not encode for GFP.
The GFP in the last column indicates where it has been detected a fluorescent signal of an expression of ASIC. The amounts of viruses used for the transduction was followed based on standard protocols in the facility.

The expression of ASIC1 was detected through GFP signal, 48 hours post-transfection (Figure 25). The HEK293T, mammalian cells, were previously cultured and maintained at 37°C by the facility. Briefly, 1 ml of cells at $1.5x10^5$ cells/ml was added in 24-well plates and incubated for 24h. Transfection reaction (aliquot of the plasmid DNA, serum-free DMEM and

transfection reagent: GeneJuice) is added to the cells and incubated for 3 days at 37°C in a 5% CO_2/95% air environment. An aliquot of the expressing cells has been analysed by following the GFP signal.

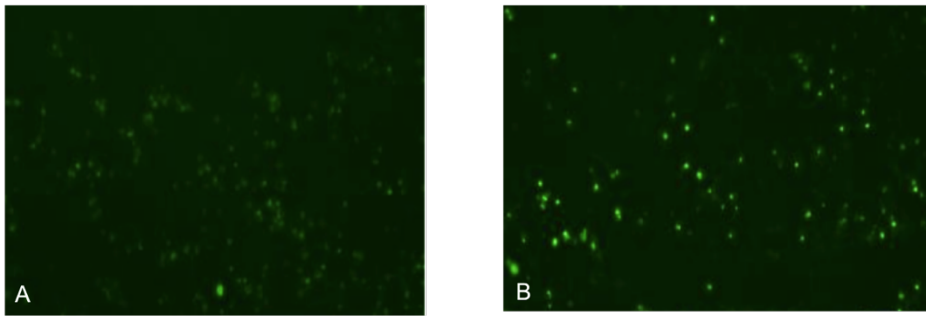

Figure 25: Fluorescence microscopy images of GFP signal

Images taken at 48h post- transfection of HEK293T cell culture with baculoviruses expressing mouse Delta 13 (A) and chicken ASIC1 (B). The expression of both constructs was followed according to the facility's protocols, where the HEK293T were already in culture and got transfected with a "transfection reaction mix". The mix consists of 1 µg of plasmid DNA-insert, see details in the text, 60 µL serum-free DMEM and 2µL of 1.33 mg/ml GeneJuice (transfection reagent). Images are shown after the incubation at 37°C in a 5% CO_2/95% air environment.

These infection results have shown that the expression of cASIC1 is more promising than the mouse variant. Such a result is not surprising as chicken membrane proteins are more stable than other vertebrate variants. However, the expression level of cASIC1 protein seems to be comparable to that obtained with baculovirus-infection system (at the Weizmann institute). A screening for the expression of ASIC1 in HEK293T cells has been performed and assessed by in-gel fluorescence detection (Figure 26), showing poor expression levels of mASIC1a and a degradation of cASIC1, where the presence of high levels of free-GFP signal is an indicator of unstable protein.

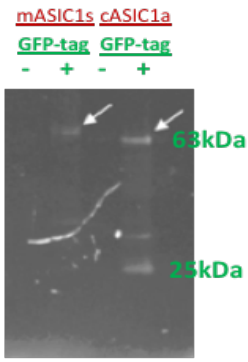

Figure 26: In-gel fluorescence detection of ASIC1 expression

Lysate HEK293T cells expression both mASIC1a and cASIC1 was analysed by SDS-PAGE and imaged by excitation at 488 nm and detection at 512 nm. Here 2 samples of each expressed protein were analysed; with and without the GFP- fusion. Arrows indicate the predictive molecular weight of ASIC1a designed. A lower band was observed at 25kDa, result of incomplete production of ASIC and could be a free GFP.

The GFP signal of mASIC1a is not as strong as the chicken variant, which again suggests that further optimisation of producing such a membrane protein is needed. Both membrane proteins were not detectable for the expression of His-fusion proteins neither by SDS-PAGE stained with blue-Coomassie nor Western blot (anti- histidine tag).

In conclusion, the insect cells and mammalian cell expression systems trials, have shown that there are no significant differences in terms of expression levels of ASIC1 between the two procedures. In both cases the levels of protein expression are definitely low and require optimisation strategy. Indeed, the protein was only detected by a very sensitive detection of GFP, which can indicate that the protein either was partially expressed or expressed but not-well folded during its maturations in the cell. Indeed, the protein was only detected by GFP fluorescence (a very sensitive tool) and Western blot, which can indicate that the protein was either partially expressed or expressed but not correctly folded during its maturation in the cell. Another possibility could come from the design of the constructs, which were probably not suitable for high membrane

protein levels. Associated with the high cost and the complexity of such expression systems, improving the efficiency of the construct and protein design should be improved and one way to do so, is by implementing high-throughput methodology which uses low amount of protein and chemicals, reducing cost and time and obtaining efficient results quickly.

The design of new and more efficient constructs was thus accomplished at MPL-Oxford, as described below.

3.1.5.3 *Main results: production of ASIC1 by high-throughput and insect cells at the MPL, Oxford*

With respect to mammalian cells, baculovirus-insect cells are more suitable for producing ASIC1 in terms of costs, time and final protein yields. At the Membrane Protein Lab (MPL) in Oxford, this is the expression system mainly used to obtain, through their state-of-the-art high-throughput (HTP) equipment, sufficient yield of well-folded and stable membrane proteins for structural and biophysical studies.

Preliminary tests were carried out at HTP small-scale screens, to identify suitable mouse and chicken ASIC1 constructs for further analysis. In following are reported main results of these screens trials that allowed a huge advance in the project

a. Cloning

The molecular and genetic aspects of ASIC1a in literature were studied to identify the best suitable constructs for expressing the protein using baculovirus-infected insect cells system. Accordingly, 16 construct variants of the channel were designed and were tested at a time by representing different orthologs (8 constructs of each; mus musculus and gallus gallus), caboxy-/amino terminal truncation and finally insertion of tag sequences to monitor the protein productions. See the amino- acid alignment of the 16 construct variants (Figure 27)

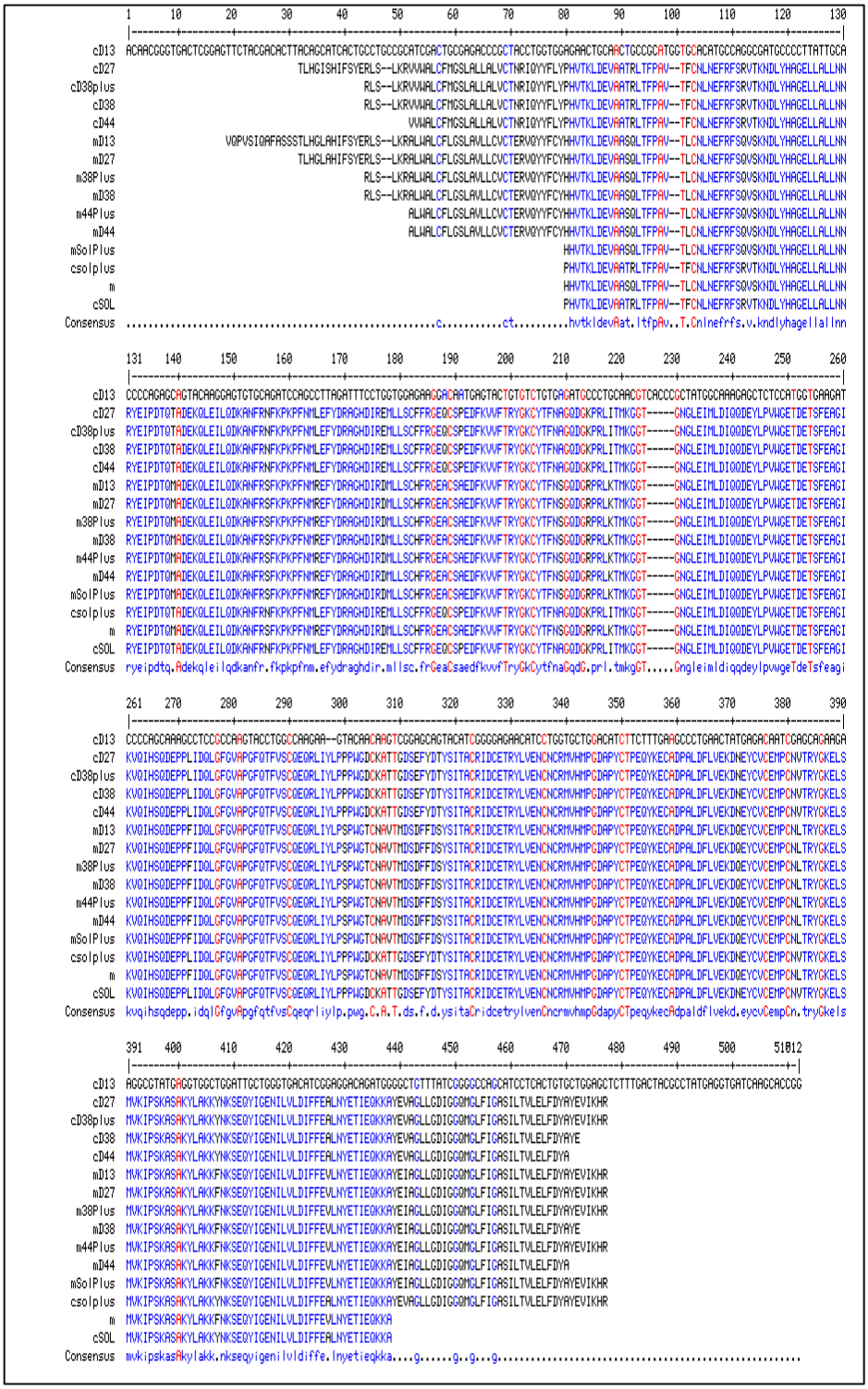

Figure 27: Mlulti- alignment of the 16 designed constructs.

More in detail, a new method of cloning, nam ed in-Fusion® HD Cloning technique [139] has been used. In contrast to what have been done previously, primers were designed in a way that the production of ASIC1 is highly monitored. For instance, the cloning of all the constructs (see Materials and methods chapter) was carried out into a versatile viral vector called pOPINE-neo for the expression of ASIC1 variants in Sf9 cells by designing appropriate primers for each construct. The constructs were designed based, in part, on literature data of the full-length cASIC1 used for structural studies, and in part, based on the rational design for membrane protein production which has been developed from the experience of the MPL.

Indeed, in contrast of previous data, here the recombinant protein was expressed directly in fusion with GFP- and 8xHis (instead of 6xHis sequence) at its C-terminus (see Materials and methods-Figure 52).

The introduction of an octa-Histidine tag-fusion at the C-terminal can affect significantly the properties of proteins expression level, their behaviour in solution and their ability to form suitable samples for structural and biochemical characterisation. In previous trials, the use of a standard N-terminal 6-histidine tag has demonstrated to be not suitable for IMAC purification (both Ni^{2+} or Co^{2+}) as a result a very low protein yield was achieved.

Another important feature of the new designed constructs (Figure 52) is that the expression of the ASIC1-genes is under the control of p10 promoter, which should provide 10-20 times fold more expression level [138]. Furthermore, direct and downstream fusion with fluorescent tag (e.g. GFP) serves as an indicator of a proper folding of the channel. By these

means, one can not only correlate the whole-cell fluorescence count with the expression of correctly integrated membrane proteins, but also examine the size of overexpressed membrane proteins using in-gel fluorescence along with biochemical assays (like western blot assay).

In-Fusion™ cloning was carried out by high-throughput PCR (see primers (Figure 51). Detection on agarose gel of PCR products (Figure 28) and DNA analyses confirmed the success of obtaining 16 constructs cloned into pOPINE-neo vector.

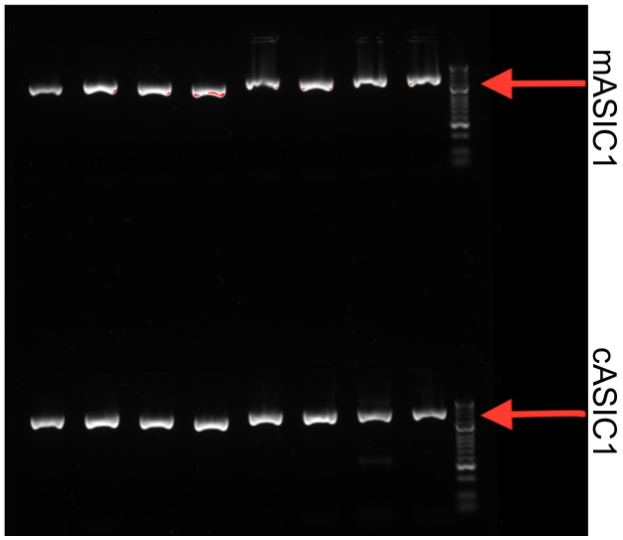

Figure 28: 1% Agarose gel of high-throughput PCR cloning for the 16 constructs

Mouse (mASIC1a) and chicken ASIC1 (cASIC1) into pOPINE- neo viral vector. Red arrows indicate the size of ASIC inserts (1200-1500 bp)

PCR products were purified and transformed, by HTP manner, into stellar competent E. coli cells cultured in deep well-plates. The plasmid-containing cells were selected after 24h at 37°C on LB/Amp multi-well

plates. Picked colonies were further amplified and analysed for DNA sequencing (Table 7). Best clones were used for baculovirus preparation and amplification.

b. Bacmid preparation and virus amplification

After choosing the appropriate production host, it is necessary to examine and optimize the expression conditions. The first step in the pipeline is transfecting insect cells with the transfection mix (containing Sf 900II cell culture mediums, linearised bacmide, vector of Gene of Interest (GOI), Fugene HD). Sf9 cells were cultured into a 24-wells plate and transfected with the viral bacmid containing ASIC-DNA constructs at $1X10^6$ cells/ml density. Transfected cells were detected at the fluorescence microscope for the GFP-signal (Figure 29). The transfection of the eGFP plasmid containing ASIC1a- constructs into insect cells yielded bright and diffuse GFP fluorescence in the cell membrane (Figure 29) indicating the correct membrane protein expression in the cells. Overall, it was possible to generate stocks of viruses for each construct, which was used for protein expression screens successfully.

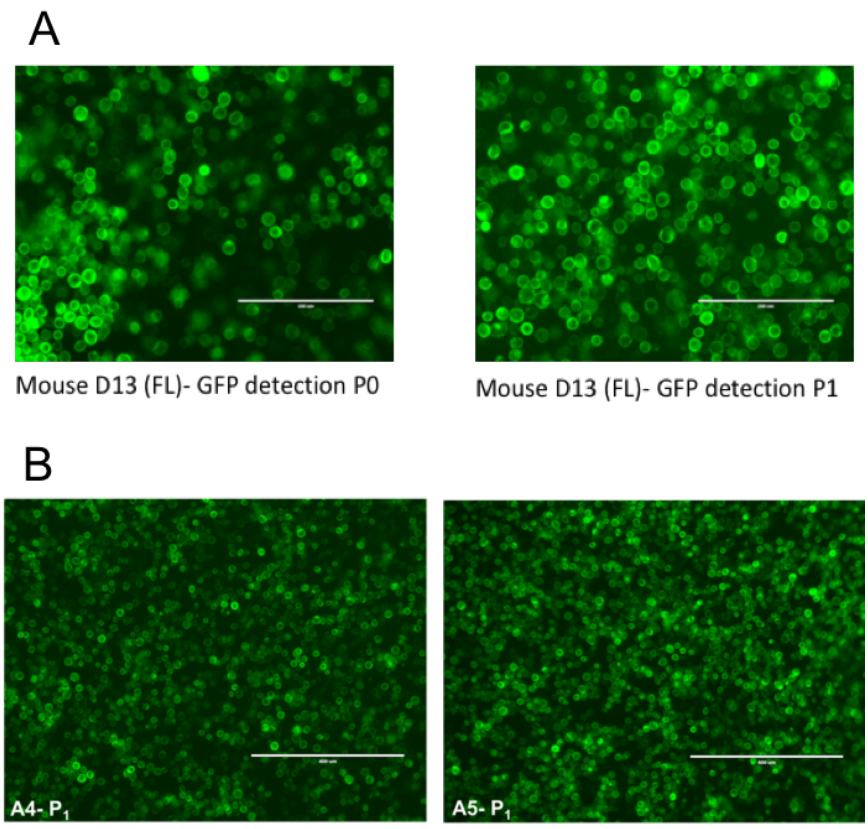

Figure 29: A panel of fluorescence microscope images from insect cells expressing ASIC1

Sf9 expressing full length GFP- ASIC1a protein. The images were taken 7 days after transfection and here are shown only the transfection results of full-length channels; mASIC1a for both generation of viruses P_0 (left image A) and P_1 (right image A). While in Images (B) are showing the differences between the intensity of expressed ASIC1a-GFP-His_8 of the two variants; mASIC1a (left) and cASIC1(right), localisation in Sf9- cell membranes. The images were taken using the first generation of viruses (P_1) for transfecting insect cells in suspension.

c. Expression tests

Although expression screening can be performed using the P_0 virus stock, the most reliable route is to first amplify the P_0 virus and then use the resulting P_1 virus for small or medium scale expression screening. By HTP approach, it was possible to test all the 16 constructs of ASIC1. The screens start with small-scale expression trials (1-3 mL Sf9 cell culture).

Infection of Sf9 ($1X10^6$ cells/mL density and 99% viability) were seeded in 24-wells plates for expression tests in suspension culture (see material and methods chapter). The expression of ASIC1 was detected after 72h of transfection: a band on SDS-PAGE gel was observed at the expected molecular weight for ASIC at the monomeric state of oligomerisation (58-60 kDa) as well as by in-gel fluorescence, by following the GFP expression (Figure 30). The comparison results of mouse and chicken ASIC1 constructs on small-scale tests are reported in Figure 30.

In conclusion, for ASIC1 productions and scaling-up, the best expressing conditions, mainly based on the number of viruses and the time of infection, resulted the following:

1. 3 µL of viruses were sufficient for transfecting 3 mL Sf9 cell culture to guarantee promising expression levels of the recombinant membrane protein.
2. 72 hours post-infection resulted the best time of harvesting for production of ASIC1 (most of the constructs). At this time point ASIC1 appears to be more stable.

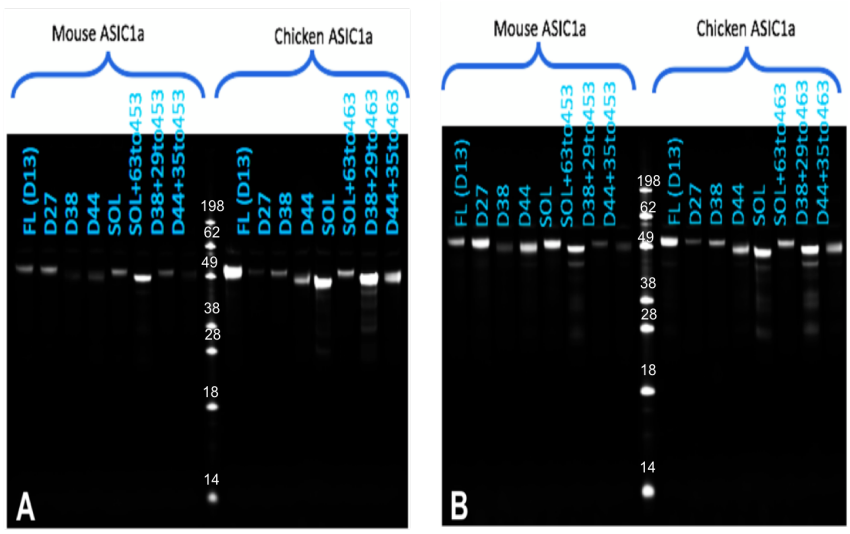

Figure 30: In-gel fluorescence assay. The proteins were analysed 72h post-infection

Isolated and solubilised in 1% DDM and 0.03% CHS from Sf9 membranes. The expression was detected by following their GFP- signal intensity that correspond to the theoretical molecular weight of the protein; 63-70 kDa and comparing different amounts of viruses at the first generation (P_1); 3 µL (A) and 30 µL (B). Overall, l most of the constructs (both mouse (left side of the marker) and chicken (right side of the marker) ASIC1) were well expressed. Nevertheless, some were less detected in-gel which, could be either due to a low expression level or instability of the protein (e.g. the truncated constructs; D38 and D44)

Along with in-gel fluorescence assay, samples were also used for high-throughput fluorescence detection size exclusion chromatography (FSEC) monitoring the GFP fluorescence signal. The 16 constructs were solubilized in standard detergent (1% DDM and 0.03% CHS) and injected onto a Superose 6 10/300 increase column (GE-healthcare) for the assay. It was performed using the Shimadzu UHPLC system equipped with an autosampler and a GFP fluorescence detector (Figure 31). The preliminary FSEC screen has shown that, in comparison with the FSEC traces of the cAISC1, mASIC1a are generally more instable and polydisperse.

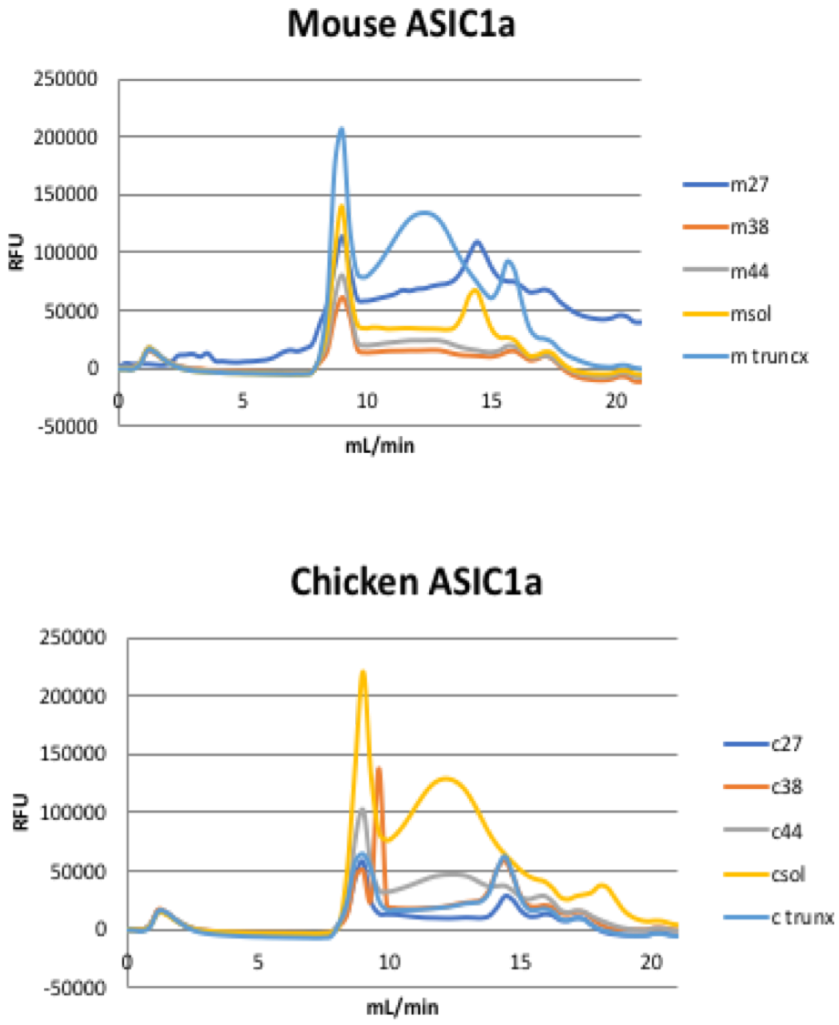

Figure 31: FSEC profiles of solubilised GFP fusion ASIC1 constructs, from baculovirus- infected Sf9 cell culture using P1

Each ASIC construct has been tested for its solubility and monodispersity monitoring the GFP signal on a size exclusion chromatography, using a FPLC system coupled to fluorescence detector (FSEC). This screening is essential as a quality check before the scale up of the protein production. Briefly, each expressed construct (from P1 generation of viruses) was solubilized in 1% w/v DDM supplied with 0.03% w/v CHS detergent, injected onto a column. The FESC traces (each construct is shown with different colour) indicate the dispersity of the protein-detergent complex sample. Fluorescence of GFP was measured at 509 nm by excitation of 488 nm.

Similarly, to P_1, FSEC analysis on crude solubilized membranes was carried out testing the second generation of viruses, P_2, at different amounts. The full length ASIC1 constructs (mouse and chicken D13), were deeply analysed by testing the transfection efficiency, by changing the amounts and generation titter of baculovirus, an improvement in the ASIC1 expression level (Figure 32) has been observed. Results shown by in-gel fluorescence and FSEC profile suggest two important results: 1) the expression level of cASIC1 is higher than the mouse constructs, which means that mASIC1a needs a time-consuming of optimisation trials also at genomic levels; 2) optimal conditions for expressing cASIC1 require the use of a low amount (3 µL) of the first generation of baculoviruses (P_1). These two assays were important in order to determine the best amount of virus's generation titre and the best expressed constructs for scale up.

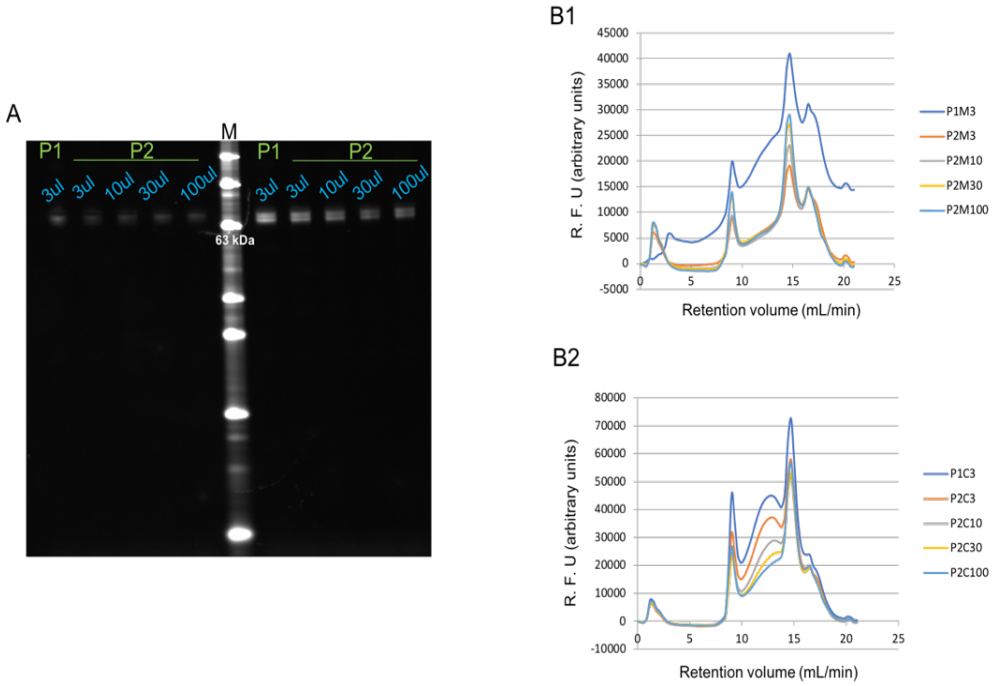

Figure 32: High-throughput screening for ASIC1a expression in sf9 cells (3 mL) by in-gel fluorescence using both P1 and P2

(A) The expression of the protein was followed by monitoring the fluorescent signal from the GFP-ASIC1 constructs (mouse (left side of the gel) and chicken (right side of the gel) variants). Here, the screening was performed comparing 3 µl of primary (P1) and different titration (3, 10, 20 and 100 µl) of secondary (P2) generation of viruses. Samples were detected 72 hours post-transfection of lysed sf9 cell pellet (3ml) with lysis buffer containing 1% DDM solution. (B) fluorescence-detection size-exclusion chromatography (FSEC) of (B1) mouse ASIC1a and (B2) chicken ASIC1, treated under the same condition as described before, loaded into a FSEC column to check the monodispersity of the full length (called D13) ASIC1 variants. Comparing the traces of B1 and B2, it seems that the mouse (B1) are more unstable than the chicken (B2) ASIC1 and therefore, thus mouse constructs are not promising for the scaling up.

d. High-throughput detergent screening

Critical factors, such as buffer components, can affect final yield of solubilised protein. The aggregation of membrane proteins includes detergent choice, salt concentration, and presence of additives. Extraction of membrane proteins from their biological membranes is usually assisted by detergents. The identification of detergents that maintain the protein in a soluble, monodispersed state is one of the critical points in the protocol. The optimization of these parameters is often a time- and protein-consuming process. Therefore, here HTP approaches, that enabled the test of a number of conditions in parallel and save time, have been used. The reason behind using first DDM and then screening other detergents is because some detergents are advantageous during the purification steps but are not recommended for crystallisation or/and Cryo-EM grids preparation. Therefore, once the best construct has been chosen from the preliminary tests in DDM (in this specific case the full-length of chicken ASIC1 (D13)), other categories of detergents are screened. The detergent screening has suggested that for ASIC's solubilisation, it is necessary to add a cholesterol (CHS) together with the detergent of choice (Table 8). For instance, large micelle-forming detergents such as n-dodecyl-b-D-maltoside (DDM) and polyoxyethylene (9)dodecyl ether (C12E9) are more likely to maintain the membrane protein in solution; however, the large size of the micelle denotes a reduced surface of protein molecules exposed to form protein–protein interactions essential for crystal lattice formation.

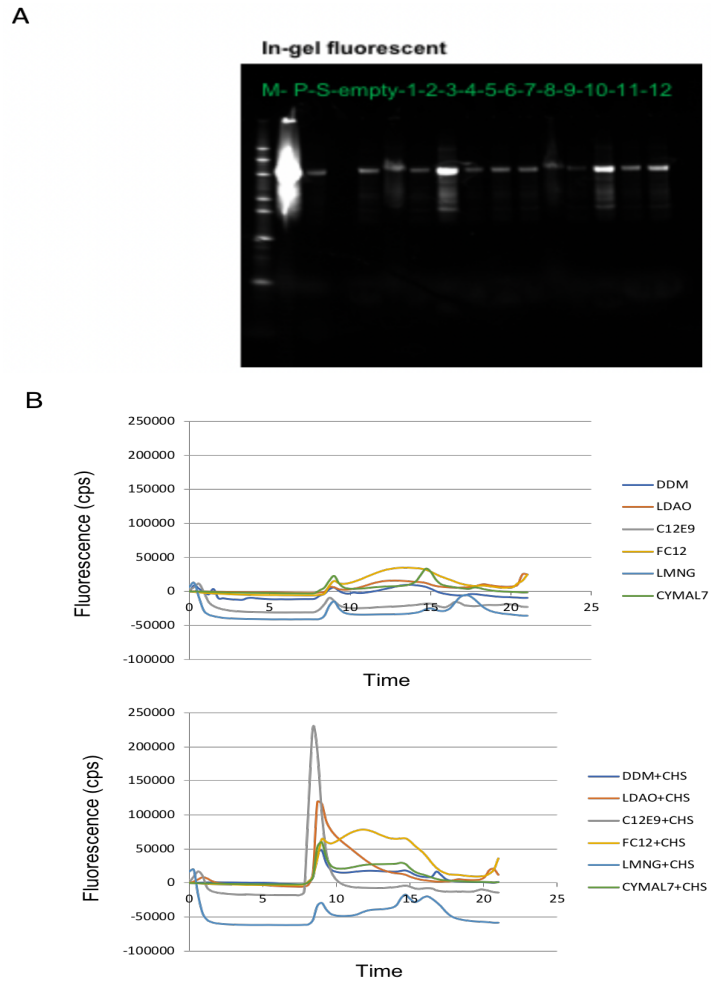

Figure 33: Detergent screening and solubilisation detection

The screen was performed using only the full- length construct of chicken ASIC1 (called D13). (A) In-gel fluorescence of purified full-length chicken ASIC1 that was solubilised with different detergents in presence/absence of cholesteryl hemisuccinate (CHS). (B) the two panels represent the FSEC traces profiles of ASIC solubilised in different detergents without the addition of CSH (upper graph) and in presence of CHS (lower graph). Lane protein marker (M), pellet (P), soluble fraction (S), lane 1 (DDM), lane 2 (LDAO), lane 3 (C12E9), lane 4 (FC12), lane 5 (LMNG), lane 6 (CYMAL), lane 7-12 (the same order of lane 1-6 but, with the addition of CHS).

The addition of CHS was thought to improve the detergent extraction efficiency and monodispersity of cASIC1a–GFP–His_8. Such behaviour was observed mainly in DDM, C12E9-solubilized membranes. The assay was repeated several times as it was not clear which detergent could have been the suitable choice. Thereby, along with literature data, the mix DDM and CHS have been selected as detergent for purifying ASIC1a (Figure 33). Once the detergent is chosen, the best membrane protein: detergent ratio may also be established through solubilisation trials, as described before (see materials and methods).

e. Purification protocol and protein quality test with synthesized DA-like compounds

The best expression condition was achieved by using Sf9 cell culture, infected with ratio 1:1000 viruses P_1: cell culture volume (µL) at $1X10^6$ cells/mL density (as defined in HTP-expression tests). Herein, the production was scaled-up (Figure 35).

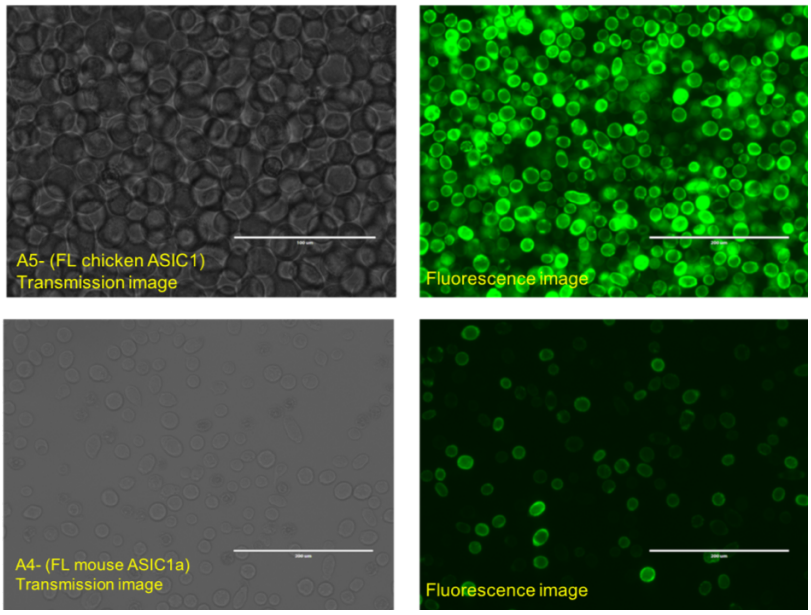

Figure 34: ASIC1a expression and GFP signal detection

Images are taken after 72h transfection of 100mL Sf9- expressing ASIC1a. The cells were grown in suspension at 27°C- 150rpm. A5 represents the chicken ASIC1 and A4 is the mouse variant.

Although the cASIC1 (construct number: A5) expression seems to be greater than that of mouse variant (construct number: A4), both were well detected with high GFP signal on the cell membrane (Figure 35). To identify the best extraction and purification conditions, 2mL of cell culture were used and lysate (see material and methods). Isolated membranes were solubilised by adding 40 mM DDM and 0.006- 0.1% of CHS and the addition of three compounds (DA, DG296 and DG327) were tested during the solubilisation steps in order to try to lock the protein in certain state and increase its solubility. Literature data [128] showed that the addition of $CaCl_2$ could stabilise the solubilised membrane protein, and therefore $CaCl_2$ was used as a control in this test.

Solubilised membrane proteins were incubated with Ni-NTA that binds the His-tagged protein, over-night at +4°C under stirring. This is necessary to ensure protein stability and specificity binding to occur.

After several washing steps using imidazole, His-tagged ASIC1 proteins were eluted with high concentration of imidazole and the eluted fractions were used for SDS-PAGE (Figure 35). A band at the expected molecular weight (between 63-80 kDa) was observed by in-gel fluorescence (Figure 35). The presence of the compounds has shown no significant differences on the stabilisation and/ extraction of cASIC1 (Figure 36). In fact, as revealed by the FSEC profile (for the mouse ASIC1a (construct called A4), the protein aggregates and highly polydisperse in the presence of DA (Figure 36- yellow and orange traces). This is in contrast to what has been achieved with the chicken ASIC1 (construct called A5) and of what Jasti and colleagues [52] has observed since the data (Figure 36- blue trace), has shown a very stable and monodisperse profile on the FSEC. This stabilisation is due to the well expression, extraction and/ solubilisation of the protein.

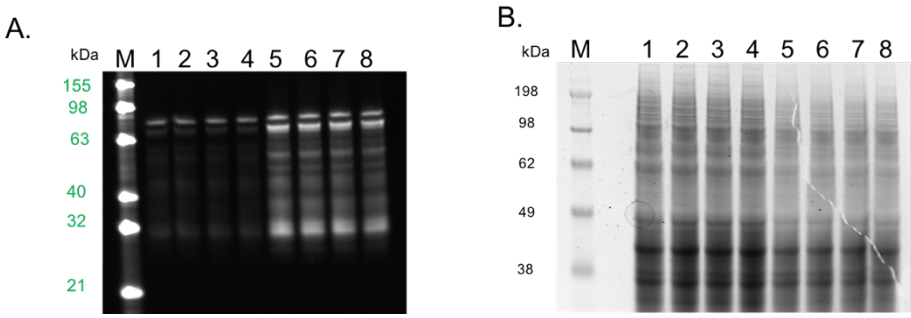

Figure 35: overexpression of mouse and chicken full-length ASIC1 with the different compounds

A. Detection by in-gel fluorescence for both GFP signal (left gel) and for protein denaturation in Coomassie staining (right gel). Interestingly, on the in-gel fluorescence, a double protein bands are observed as well as and the presence of free GFP fraction (low band). Left gel (A); benchmark protein ladder (M), lane 1: mouse ASIC1 (A4 construct) control (in presence of $CaCl_2$), lane 2: A4-DA, lane3: A4- DG296 compound, lane 4: A4-DG327, lane 5: chicken ASIC (A5 construct) control (in presence of $CaCl_2$), lane 6: A5-DA, lane 7: A5-DG296, lane 8: A5-DG327. Right gel (B): Protein ladder (M), lane 1: chicken ASIC (A5 construct) control (in presence of $CaCl_2$), lane 2: A5-DA, lane 3: A5-DG296, lane 4: A5- DG327, lane 5: mouse ASIC1 (A4 construct) control (in presence of $CaCl_2$), lane 6: A4-DA, lane7: A4- DG296 compound, lane 8: A4-DG327

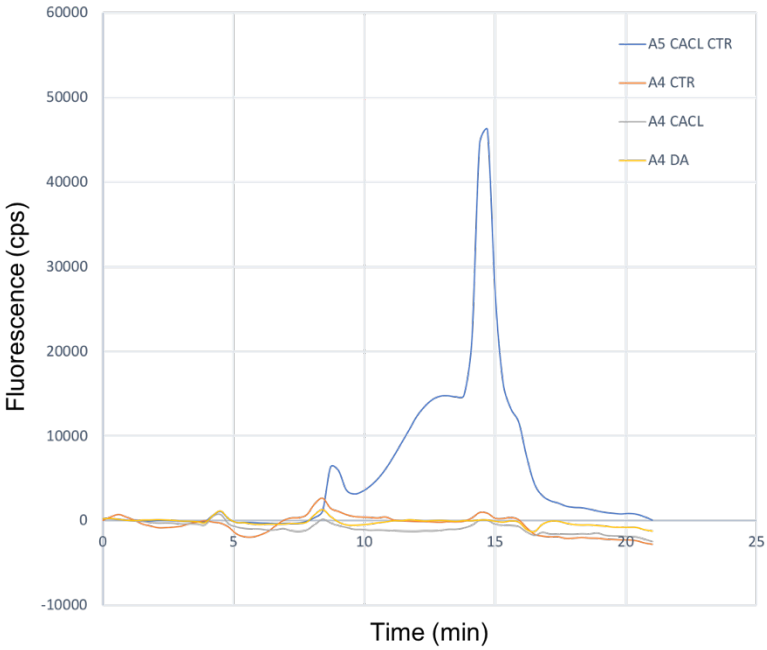

Figure 36: The FSEC traces of solubilised full length ASIC1

Under the same conditions of solubilisation (lysis buffer supplied with 1%DDM and CHS), both mouse and ASIC1a were compared for their monodispersity. In blue is indicated the chicken variant (cASIC1) that was solubilised with the addition of CaCl. In grey, yellow and orange are indicating the monodispersity level the mouse variant (mASIC1a) in CaCl, adding diminazene (DA) and the control (CTR) respectively. The results shown on the graph ndicates that the chicken variant is much stable and monodisperse than the mouse ASIC1.

As observed, no huge differences arise between the control sample (sample without any additional compound) and the sample solubilised in presence of the compounds (DA, DG327, DG296). This implies that these small molecules have relatively no effect on the protein solubility and stability. To ensure this, biophysical characterisation (such as CD, DLS or NanoDSF) and structural characterisation assays should be performed.

Therefore, the beforementioned FSEC was repeated several times for the isolated full-length chicken ASIC1 (cASIC1- construct A5) produced from 500mL of baculovirus-infected Sf9. The FSEC profile as well as the in-gel

fluorescence (Figure 37 A and B) suggest that purified cASIC1 is well expressed and extracted from cell membrane (Figure 37 A- in lanes E1-3: crude membranes). Furthermore, these quality checks of the protein indicate that the selected detergent (at 1mM DDM+CHS) is the best for maintaining ASIC1a full-length in a soluble (Figure 37 A) and stable (Figure 37 B) form, in its trimeric state, since a very low signal of free GFP is present (in contrast with previous trials).

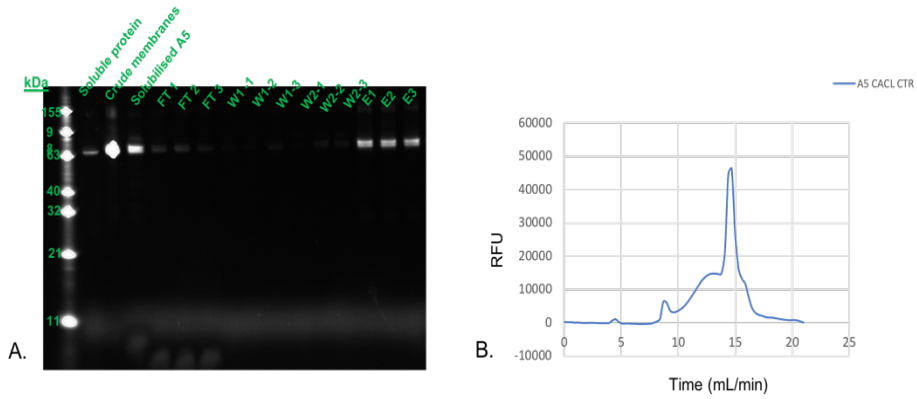

Figure 37: Purification results of performed expression and purification screening on cASIC1 from Nickel resin (Thermofisher)

A) in-gel fluorescence gel of the chicken ASIC1 samples. The samples have been solubilised in buffers supplied with CaCl and 1%DDM+CHS. White bands correspond to the molecular weight of ASIC (monomeric with tags) after the NiNTA purification. (B) Fluorescence-detected size exclusion chromatography (FSEC) that has been performed using the eluted fraction of ASIC to check monodispersity of the membrane protein. The position of the peak (at 15ml/min) corresponding to solubilized GFP fusion protein and the small peak (around 10ml/min) could indicate the void volume.

Abbreviation code; Pre-Nickel, samples of flow through (FT), washing steps (W) and elution fractions (E)

Purified chicken ASIC1 sample from the SEC column (Figure 38) is eluted early almost in the void volume, which is not surprising as the membrane protein is seemed to form the trimer. Nevertheless, the size the protein

on gel indicate a monomeric state of the full-length in denaturated conditions. To confirm the oligomeric state of the purified protein, it would be possible to check it on native gel.

The protein was concentrated using a 100k molecular weight cut-off (MWCO) concentrator and used for biophysical characterisation. In particular, an efficient microscale fluorescent stability molecule, N-[4-(7-diethylamino-4-methyl-3-coumarinyl)phenyl] maleimide (CPM) for stability profiling of membrane proteins was used under different solution and ligand conditions as well as the affinity/ effect of the three compounds (DA and DA-like ligands) with the purified ASIC were tested by microscale thermophoresis technology (MST) (for details see Materials and methods). Both tests were carried out several times, under the same conditions, showing that these compounds could interfere on the stability of the protein. However, these results were very incoherent between each other, suggesting to optimise the conditions of the experiment.

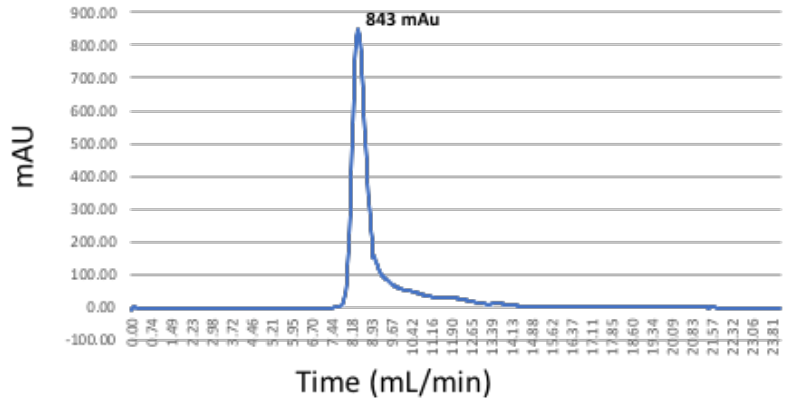

Figure 38: Size-exclusion chromatography elution profile of un-cleaved c ASIC1

The purified protein was injected onto Superdex 200 increase (GE-healthcare) and most of the protein was eluted with the void volume indicating that it could be an aggregation or an oligomeric state (trimer) of ASIC1

The assay aimed at biophysical characterisation of DA-like ligands and their effect on stabilising ASIC1a by quantifying the number of free cysteines of the membrane protein. The more fluorescence, the less stable (unfolding event and cysteine become exposed to solvent) the protein is. The data obtained was unclear since the protein was still carrying the GFP- and HIS_8 tags and therefore, it was not possible to detected the exact effect of these small compounds on the stabilisation of ASIC1a. At the moment this is still under investigation.

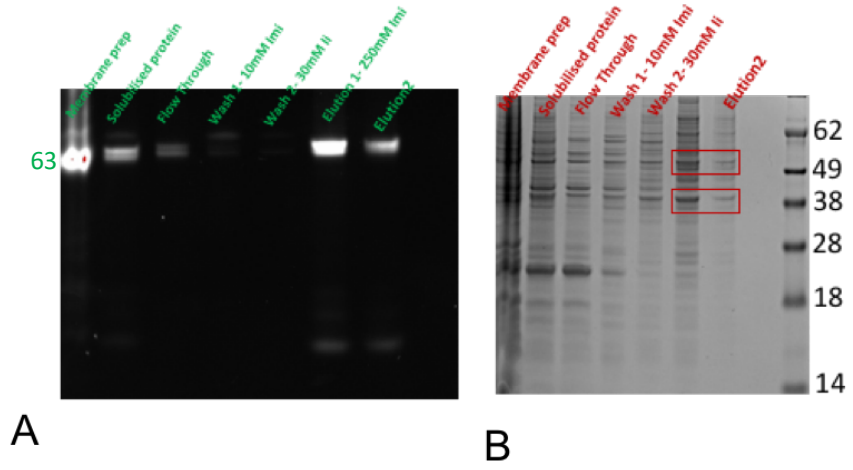

Figure 39: ASIC1 protein detection after an IMAC purification

(A) In-gel fluorescence of cASIC1 (construct A5) of GFP-fused protein and (B) SDS PAGE Coomassie gel indicates moderate expression levels of the membrane protein. This could indicate that the protein either low expressed or need further optimisation.

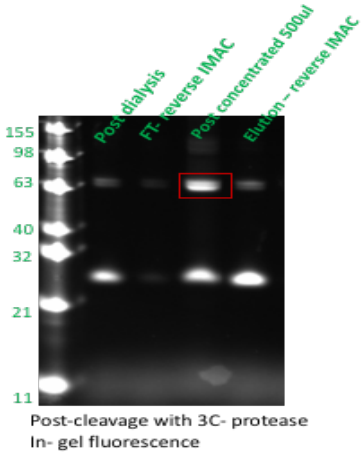

Figure 40: In-gel fluorescent of cleaved chicken ASIC1 (construct A5)

This is a control experiment where the eluted cleaved protein should be not detectable since the GFP-tag is removed

The different tags (GFP and HIS_8) were removed by using a human rhinovirus (HRV 3C) protease after an incubation (Figure 39 and Figure 40). Moreover, a silver stain assay was attempted on purified and cleaved chicken ASIC1 (Figure 41). The Figure 41 shown the observed bands corresponding to the expected molecular weight of cASIC1 in a monomeric state of the full- length protein (53 kDa). While the arrows indicate the possibility of DDM detergent residue or unknow contaminant.

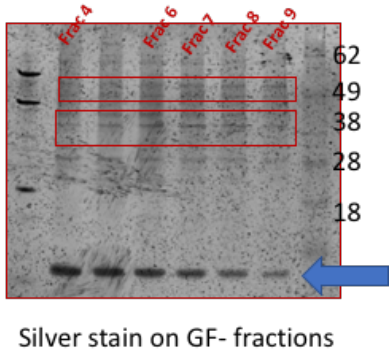

Figure 41: Silver stain gel for sensitive detection of purified proteins

Overall the expression, purification and biochemical characterization of ASIC1 was achieved. However, the amount of achieved membrane protein was not enough to performed structural characterization. Through these two internships via Instruct, I have learned how to express, purify and characterize membrane proteins using HTP techniques. For example, the opportunity given by Instruct at the Weizmann institute was very helpful to start manipulating insect cells and gaining knowledge and practice in the molecular biology of cloning using state-of-the-art methodologies in the field. Such techniques, skills and the expertise of studying a membrane protein using baculovirus- infected insect cells were useful for my career and to transfer back the knowledge into my home-lab for structural and functional characterization

.

3.2 Structure, stability and susceptibility to proteolysis of gelsolin pathological variants probed by a chaperone nanobody

3.2.1 Protein production

The gelsolin pathogenic mutants (as isolated G2 domain) and Nb11 are overexpressed and purified from *E. coli*. Production of the three mutants of the isolated second domain (G2) of gelsolin ($N184K_{G2}$, $D187N_{G2}$ and $G167R_{G2}$) is based on well-established protocols described in [107] and will not be discussed any further.

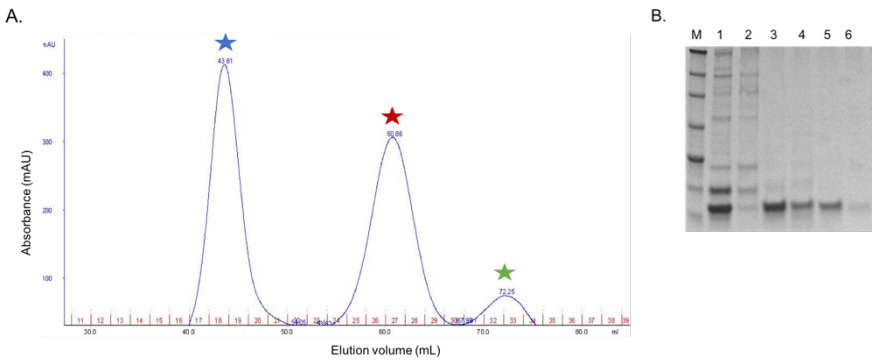

Figure 42: Purification profile of isolated G167RG2. (A) size-exclusion chromatography (superdex 75 of 120 mL) of the $G167R_{G2}$

The protein was eluted and the three peaks were analysed by SDS-PAGE. (B)Lane M, protein marker; Lane 1, cleaved protein with thrombin, Lane 2, elution fraction of the peak with blue star that correspond to contaminants. The monomer/dimer forms of the mutant: lane 3-4 elution fractions indicated with red and green starts respectively. Lane 5-6: are further fractions.

As example, the gel-filtration profile of $G167R_{G2}$ and the SDS-PAGE analysis of the relative fractions were also reported in [108]. Contrary to the other variants, this mutation promotes the dimerization of the protein [108]. During the purification of the G167R protein the two forms, monomer and dimer, can be isolated and studied individually to some extent.

Contrary, the protocol for the production of Nb11 required some optimization. The final yield of Nb11 production is excellent (>20mg/l of culture) and the purity of the protein more than sufficient for structural studies, as can be observed in Figure 43.

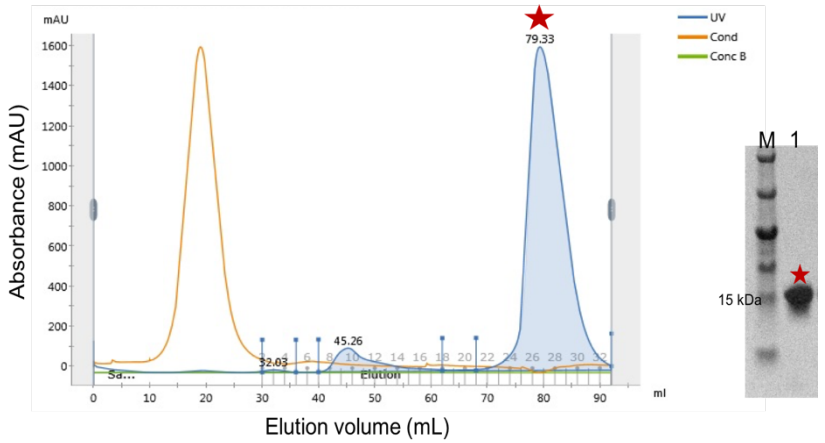

Figure 43: Size exclusion chromatography (SEC) profile of Nb11 purification

Nb11 elutes form Superdex 75 (GE - Healthcare) as a single peak (red star). Pooled fractions corresponding to the peak are analysed by SDS-PAGE (right picture). Lane M, protein marker; Lane 1, purified Nb11

3.2.2 Nb11 protects gelsolin renal mutants from furin proteolysis.

Gelsolin D187N variant is subjected to an aberrant proteolytic cascade which ends with the formation of amyloidogenic fragments. The first protease of this pathway is furin [140], a Ca^{2+}-dependent enzyme of the Golgi apparatus. Nb11 binds the D187N variant and efficiently protects it from aberrant furin proteolysis [85]. Even mutants N184K and G167R are susceptible to furin *in vitro* [141] [108]. Therefore, we investigate the effect of Nb11 on the G2 carrying the kidney mutations, $N184K_{G2}$ and $G167R_{G2}$, and verify whether Nb11 could hamper furin proteolysis.

The assay is performed at 37˚C, pH 6.5 and in the presence of 1 mM $CaCl_2$, conditions that mimic the Golgi environment and required for furin activity. Samples are incubated with 1U of furin protease in the presence (G2:Nb11 molar ratio 1:1) or absence of Nb11, and the reaction is monitored for 24h. Samples are collected periodically and detected at different time points (after 1, 3 and 24 h of incubation) on SDS-PAGE (Figure 44) to define the time-course of the process.

In the absence of Nb11, the three mutants display high susceptibility to furin. Bands corresponding to the larger product of furin proteolysis (10 kDa, marked as G2F* in Figure 44) appear already after 1h incubation, and most of the variants are completely digested after 24 h. Contrary, WT_{G2} is resistant to furin proteolysis under the same conditions (Figure 44 -right panel). If the same assay is repeated in the presence of Nb11, only two bands are visible, corresponding to the theoretical molecular weight of Nb11 and G2s (13 and 14 kDa, respectively), even after 24 h incubation.

This data confirms that Nb11 can bind N184K and G167R variants and protect those mutants from furin proteolysis with an efficiency similar to that observed for the D187N variant.

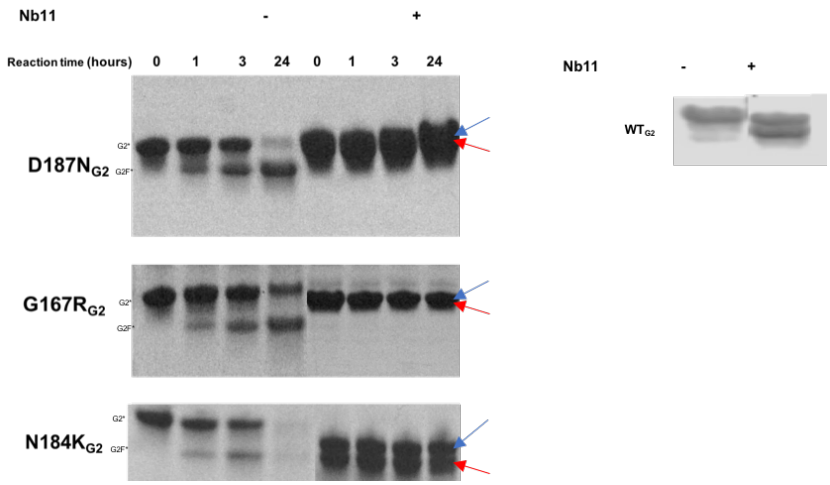

Figure 44: Furin cleavage assay with mutants of the isolated G2 domain in the presence (+) or the absence (-) of Nb11.

Nb11 protects the three G2 mutants from the furin activity. Furin proteolysis is monitored in SDS-PAGE after a 0, 1, 3 and 24 h incubation at 37˚C. Bands marked G2* correspond to the molecular weight of the uncleaved G2 (13kDa). G2F* marks the 10 kDa fragment, larger product of furin cleavage at the 168-RRVV ↓ A-173 site. G2 and Nb11, have similar molecular weight (13 and 14 kDa, respectively). Therefore, once mixed at equal molarity ratio (1:1), they are barely distinguishable as distinct bands, marked by blue (Nb11) and red (G2 proteins) arrows, respectively.

3.2.3 Nb11 stabilizes mutated G2s

Nb11 protects gelsolin pathological variants from furin proteolysis, however, the mechanism behind such protection remains to be elucidated. One hypothesis is that Nb11 affect the thermodynamic stability of the G2 mutants, D187N$_{G2}$ N184K$_{G2}$ and G167R$_{G2}$. To investigate these aspects, thermal stability of WT and mutated G2 is evaluated in the presence/absence of Nb11. In particular, two techniques are used; 1) Thermal denaturation followed by circular dichroism (CD) (Figure 45 A); 2) Thermofluor, where denaturation of the protein is performed in the presence of a fluorogenic probe (Figure 45 B).

For the CD analysis, denaturation of the proteins is induced by a linear temperature gradient and monitored at 218 nm (Figure 45). The CD signal

of Nb11 (Figure 45 A- green curve) decreases over time as the immunoglobulin-like domain lacks alpha-helical structures. On the contrary, the G2s shows a sigmoidal increase in ellipticity (Figure 45 A- blue curve) upon unfolding. As a consequence, the melting curves of the complexes (Nb11: G2s) do not show a standard two-states behaviour. To analyse these results, the denaturation curve of G2:Nb11 complex (red curve) is compared with the calculated sum of the individual denaturation curves of G2 and Nb11 (Figure 45, cyan dashed line). If Nb11 has no stabilisation effect on the G2, the denaturation curve of the complex should superimpose on the curve of the sum because the two proteins unfold independently. Indeed, observing the behaviour of Nb11:WT_{G2} complex, it seems that the nanobody does not have any effect on the stability of the WT protein. Contrary, Nb11 has a significant impact on the stabilisation of the mutants as their denaturation curve is different.

To quantify this stabilisation effect, the thermal stability of each protein is studied by thermofluor experiment and the melting temperature (Tm) calculated (Figure 45 B and Table 4). In the absence of Nb11, Tm values for the mutated G2 are lower than that of the WT_{G2}, ΔTm ranging from 13°C to 17.5 C° (Table 4). Whereas in complex with Nb11, the Tm values of the mutants get close to 60˚C (Table 4) which, is the Tm measured for the WT, indicating a stabilisation of the mutated G2s due to binding of Nb11. This result is quite surprising, Nb11 has no significant effect on the WT protein which means that we are not observing a generic ligand-induced stabilization [142].

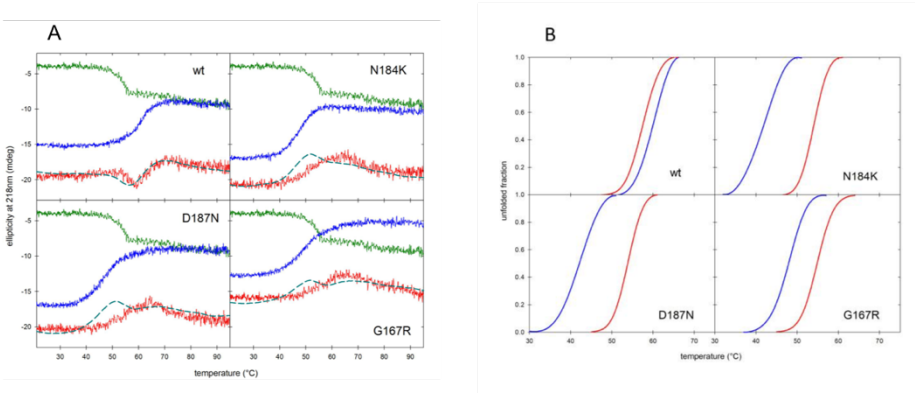

Figure 45: Thermodynamic stabilities of G2- mutants and G2- WT in the presence/absence of Nb11

A) Thermal stabilities, evaluated by CD spectroscopy. Unfolding profiles of WT, D187N, N184K and G167R alone (blue traces) or in complex with Nb11 (red). The curve of the Nb11 alone (green) and the arithmetical sum of Nb11 + individual G2s (dashed cyan traces) is also reported in each panel. (B) thermal stability followed by SYPRO orange fluorescence. In this experiment, the same samples analysed by CD show a standard sigmoidal behaviour, we can therefore calculate Tm values as the minimum of the first derivative of the traces. Denaturation of G2 alone (blue trace) and in complex with Nb11 (G2:Nb11) (red).

		WT	G167R	N184K	D187N
- Nb11	Tm (°C)	60.3	47.5	43.0	44.0
	ΔTm (wt-mut) (°C)	-	13.0	17.5	16.5
+ Nb11	Tm (°C)	58.0	55.0	53.0	54.0
	ΔTm (wt-mut) (°C)	-	2.5	4.5	3.5

Table 4: Tm values (± 1.5 °C) calculate form the thermofluor experiments (figure 47B) in the presence (+ Nb11) or the absence (-) of Nb11. Tm for Nb11 alone is equal to 50 ± 1 °C

3.2.4 Crystal structure of the Nb11- stabilized D187N$_{G2}$

To further investigate the stabilization mechanism of Nb11 on the gelsolin mutants, structural studies are performed.

G2:Nb11 complexes of all three mutants are subjected to extensive crystallisation trials. However, well-diffracting crystals are obtained only for the Nb11:D187N$_{G2}$ complex (Figure 47 and Figure 48) which is structurally analysed and the results are here reported.

To set up crystallisation experiments, the complex is isolated by size-exclusion chromatography (SEC) and concentrated to 12 mg/ml.
Several crystals appeared after 2-6 days at 20˚C (Figure 47) and were tested at the European synchrotron radiation facility (ESRF).

Among all the tested crystals, only two of the D187N:Nb11 complex diffracted to informative resolutions. The first crystal grew in 0.1 M potassium thiocyanate, 30 % PEG 2000 MME and 4.0 M Sodium formate, belonged to the space group $P2_12_12_1$ and diffracted to 1.9 Å resolution. A second crystal belonging to $P4_12_12$ space group diffracted to 2.4 Å and was obtained in 0.1 potassium phosphate, pH 6.2, 10% v/v glycerol and 25% v/v 1,2 propanediol. Data processing and refinement is done using the CCP4 and Phenix suits. The two models presented here will be hereafter referred as the *orthorhombic* and *tetragonal* structures, respectively (Table 5). Due to the difference in quality of the data, only the *orthorhombic* structure will be used to infer the impact of the D187N mutation on the structure of gelsolin.

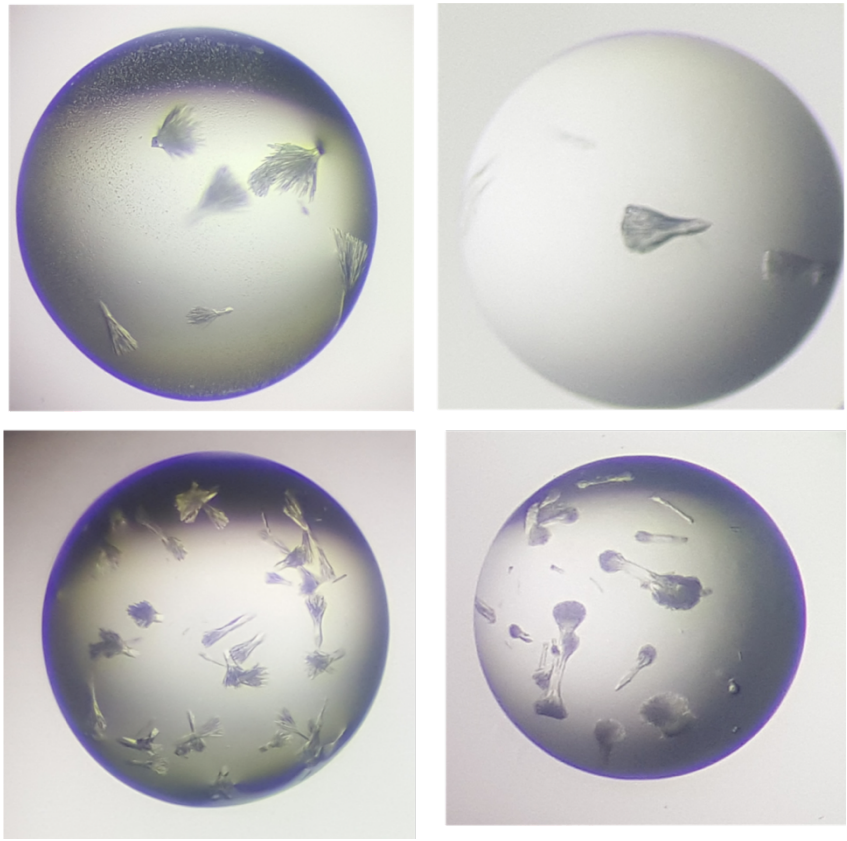

Figure 46: A panel of D187N$_{G2}$:Nb11 crystals shapes

The D187N$_{G2}$:Nb11 complex is compared with the available WT$_{G2}$:Nb11 structure (Figure 49, PDB ID: 4S10). In both structures, Nb11 binding interface is far from the aberrant cleavage site, immediately raising the question of how can the binding of Nb11 in a distal area *shields* the protein from furin proteolysis? the results rule out that the observed interaction is a crystallographic artefact, as it is unlikely that three different crystal packings (WT$_{G2}$:Nb11 crystallized in the triclinic space group) would artificially stabilize exactly the same assembly (Figure 48 and Figure 49).

	Orthorhombic	Tetragonal
PDB ID	6H1F	*Not deposited*
Data collection		
Space group	P 2_1 2_1 2_1	P 4_1 2_1 2
Cell dimensions a, b, c (Å); a, b, g (º)	33.8, 46.8, 132.1; 90.0, 90.0, 90.0	77.0, 77.0, 88.8; 90.0, 90.0, 90.0
Unique reflections	17289	10995
Resolution range (Å)	46.8-1.9 (1.94-1.90)	46.4-2.4 (2.49-2.40)
$CC_{1/2}$	0.990 (0.714)	0.999 (0.800)
Completeness (%)	99.8 (99.9)	100 (100)
Multiplicity	5.1	16.9
Refinement		
Resolution range (Å)	44.1-1.9	46.4-2.4
R_{work} / R_{free} * (%)	19.9/23.3	18.6/26.0
RMSD		
Bonds (Å)	0.006	0.008
Angles (º)	0.786	0.964
Ramachandran plot		
In preferred regions (%)	96	95.7
Outliers (%)	0	0.4
B-factors (Å^2)§	30	66

Table 5: Data collection and refinement statistics of the structures of the complex D187NG2:Nb11

Values in parentheses refer to the highest resolution shell. (*) R-work value = Shkl||Fo| - |Fc||/Shkl|Fo| for all data, except 10%, which were used for R-free calculation. (§) Average temperature factors over the whole structure.

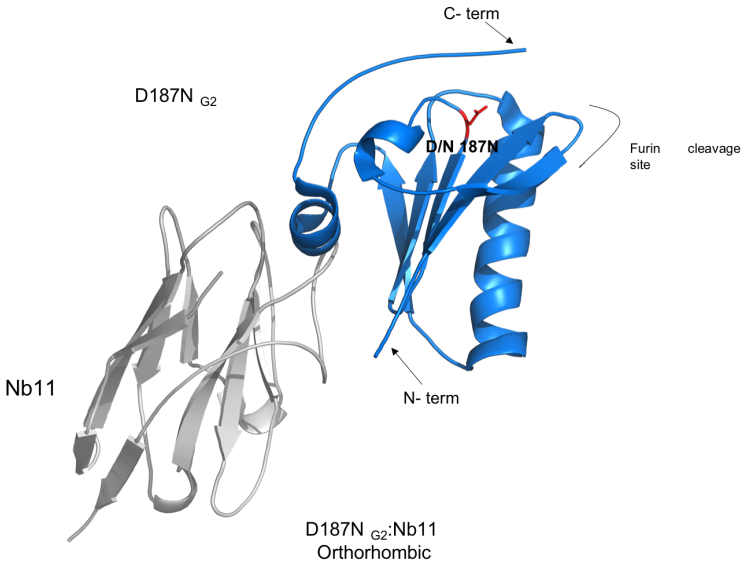

Figure 47: The Crystal Structure of the D187N Gelsolin G2 domain in complex with Nb11 (PDB ID: 6H1F)

The two proteins are represented as cartoon and coloured in blue (D187NG2) or grey (Nb11) The last resolved C-terminal residue (E 256) , N-terminal and mutated residue D187N (red) are indicated in the isolated D187NG2 structure . The aberrant cleavage site of furin is far from the site of interaction between the Nb11 and the second domain.

Overall, the structures of the isolated G2 domain ($D187N_{G2}$ and WT_{G2}) are pretty much superimposable (rmsd=0.25 Å over 90 Cα atoms) (Figure 49). Both the structures obtained confirm that Nb11 binds the G2 domain over an extended area including the β5-loop-α2 region (residues 230-234, 238-245) and the loop-β4 stretch (residues 193-198) as already observed for WT gelsolin (PDB: 4S10). The binding region is opposite from the aberrant cleavage site (residues 168-172), which had previously raised suspicions of a crystallographic artifact. The structures obtained here rule out this

hypothesis, since it is unlikely that three different crystal packings (WT G2: Nb11 belongs to P1 space group) artificially stabilize the same assembly (Figure 48). Thus, the 3D structures of G2:Nb11 appear unable to explain how the binding to Nb11 in a distal area could shield G2 from furin proteolysis without additional data. The second remarkable feature of the WT G2 and D187N G2 assemblies is that the G2 structures are almost identical (root mean squared deviation, RMSD, 0.25 Å over 90 Cα atoms). Besides, two

striking differences were observed: the absence of the coordinated calcium ion, and a shorter stretch of ordered C-terminal segment in D187N G2 (Figure 49).

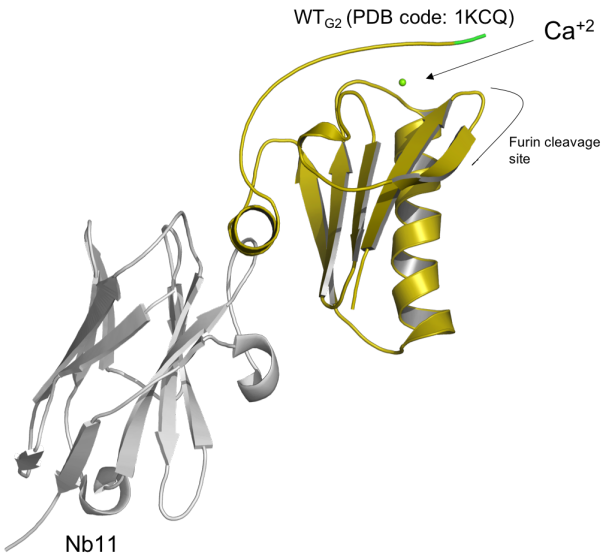

Figure 48: Cartoon presentation of the WTG2 : Nb11 complex

The WT_{G2} (PDB code: 1KCQ) is shown in Olive colour, the Nb11 is presented in grey, $Ca^{2+,}$ which is absent in the structure of the mutant, is shown as a green sphere. The C-terminal residue (E256) is coloured green as well

Nevertheless, few differences are evident. For instance, in the $D187N_{G2}$ structure, electron density for the calcium ion is missing, indicating that the mutant lost the ability to bind the ion, essential for gelsolin activity and stability [90 140 111].

An additional structural feature observed is a shorter resolved C-terminal segment (Figure 49). This might suggest that the remaining stretch of the protein is highly flexible, thus not visible by X-ray crystallography. To further investigate this feature, a disorder prediction algorithm was used. MobiDB-lite indeed indicates the presence of a putative disordered

region between residues 247-285, which might be due to its strongly polar character.

Apart from the described differences, the superimposition of $D187N_{G2}$ (PDB code: 6H1F) on the WT structure (PDB code: 1KCQ) shows neither a major conformational change (as is the case for the renal mutated G2-G167R variant, nor the rearrangement of the hydrogen bond network in the core of the domain, observed in the N184K variant. Aspartate 259 (Figure 49) is already part of the invisible stretch, otherwise the other residues of the calcium coordination sphere (G186, D187 and E209) show a surprising conformational conservation. The secondary structure content is also comparable.

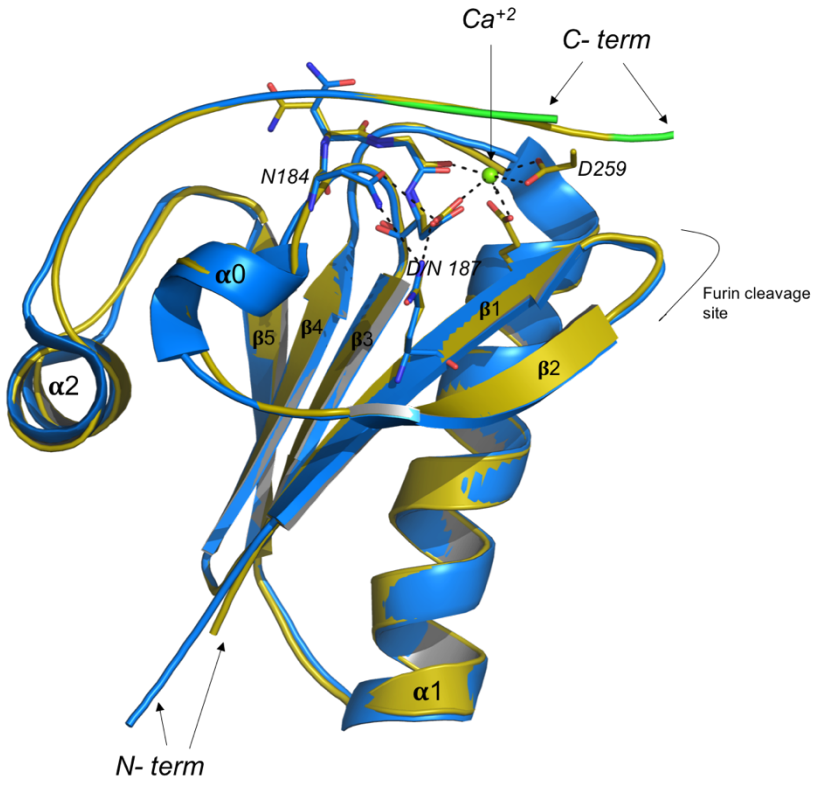

Figure 49: Cartoon representations of the superimpose structures of the WT_{G2} with $D187N_{G2}$

$D187N_{G2}$ (blue), extrapolated from the solved orthorhombic structure of the complex ($D187N_{G2}$:Nb11)-PDB code: 6H1F, and the WT_{G2}- PDB code: 1KCQ (Olive colour). Residues of the calcium (shown in green sphere) cluster and those found altered in the N184K mutant structure are shown as sticks. The two variants share high structural conservation (rmsd=0.25 Å over 90 Cα atoms)

4 Conclusion and future work

The Thesis addressed questions relative to two therapeutically relevant proteins.

Firstly, the characterization of an ion channel: Acid-sensing ion channel 1 (ASIC1). The 3D structure of such protein was used for an *in silico* selection and rational design of DA-analogs small molecules that could potentially and specifically inhibit the activity of the channel (chicken ASIC1). The production of such a membrane protein, both mouse and chicken variants, required extensive trials and expertise. However, this issue has been addressed with a wide spectrum of advanced, novel and high-throughput approaches of cloning, expression host, solubilisation and purification pipeline.

Mouse and chicken ASIC1 were thus produced in small amounts, and functional characterisations of the channel with/without synthesised DA-like small molecules through, for example, microscale thermophoresis (MST), are ongoing. Thus, it is necessary to maintain the protein at a soluble state. Such task was achieved by screening different categories of detergents. DDM seems to be a suitable detergent for solubilisation/extraction of ASIC. However, it could prove as a limiting factor during biophysical or crystallisation experiments. Thus, alternative strategy such as the Nanodisc system, which provides a novel platform for understanding membrane protein function, can be evaluated. MNG could be an alternative detergent, as it has been proven to enhance the stability of membrane proteins during crystallisation trials. Moreover, an

alternative method, to overcome some detergents problems during crystallization, is to use lipidic structure such as lipid cubic phase (LCP).
Recently, the structure of chicken ASIC1 (cASIC1) obtained by cryo-EM has been published [143] at a resolution of 5.4 Å resolution clearly displaying the cASIC1 interactions with peptide ligand. Thus, it could be used along to the crystallization approach, requiring low amounts of the protein and of DA-like synthesised compounds.

In the second project, I have investigated the molecular mechanism underlying the toxicity of mutated gelsolin by using the recently developed Nb11 nanobody as a probe.
I showed that Nb11 works as a *pharmacological chaperone*. These chaperones restore mutated protein function or prevent their misfolding, either stabilizing the native fold or assisting the folding process. Although the pharmacoperone concept has been around for a while, only a limited number of successful examples can be found in literature and very few drugs belonging to this family are available on the market. Nb11 is the first case of a pharmacoperone-like nanobody whose efficacy has been proven *in vivo*.
Interestingly, Nb11 was originally developed to contrast D187N-mutated gelsolin toxicity. Contrary to other previously developed pharmacological chaperones, which are mutation-specific, I showed that Nb11 protects the gelsolin pathological variants identified so far, irrespective of the pathways or mechanisms leading to their degradation and/or aggregation. In collaboration with Dr. Luisa Diomede, efficacy of Nb11 was proved also on a *C. elegans* model of the disease (see attached

manuscript, in the appendix). Wide-spectrum applicability is of pivotal importance in view of the potential application of Nbs in therapy. Disease-causing mutations yield proteins which are at times difficult to express and purify, due to their solubility, instability or toxicity. My data show that pharmacological chaperones can be developed using the WT protein as target, aiming at the stabilization of the native-like conformation, thus increasing the number of diseases that can be potentially tackled with an analogous strategy.

The chaperone property of Nb11 was crucial also to obtain the crystallographic structure of the elusive D187N variant. This structure is the ultimate validation of a pathological mechanism that has been proposed long time ago but that was missing a mechanistic description of the underlying molecular events. Indeed, the D187N substitution impairs calcium binding. As a consequence, the C-terminal tail of the domain becomes extremely flexible, partially exposing the core of the domain. Major conformational changes are likely prevented in the crystal by Nb11. To investigate this aspect, molecular dynamic simulations have been performed in collaboration with Dr. T. Giorgino (see attached manuscript, in the appendix). These data clearly show that mutated G2, in the absence of Nb11, eventually populates a partially unfolded conformation.

This work set the bases for a drug discovery project for the identification or design of novel drugs against AGel amyloidosis. We have, in fact, demonstrated that a molecule that binds and stabilizes the G2 fold has the potential to block the first step of the aberrant proteolytic cascade. Moreover, we have validated a druggable site on the G2 structure that

can be targeted in *in silico* screening for small ligands or to rationally design novel binders.

5 Materials and methods

5.1 Acid- Sensing Ion Channel 1 (ASIC1)

5.1.1 Molecular dynamic simulation and *in-silico* docking

Molecular dynamics simulations were performed using the program GROMACS [144] compiled with the ALMOST and PLUMED, using the chicken ASIC1 trimer structure (PDB code: 4FZ0). Three DA molecules were located ~35 Å from the pH sensor, or from the putative binding domain proposed by Chen et al. The system was simulated by the use of Amber03W force field in explicit TIP4P05 water. The simulation lasted for 80- ns and van der Waals and short-range electrostatic interactions were cut-off at 0.9 nm. However, long range electrostatics were treated with the Particle Mesh Ewald method and a mesh size of 0.12 nm. The canonical ensemble was enforced by keeping the volume fixed and by thermosetting the system with the Nosé-Hoover thermostat at 310K.

In silico docking: The analysis was carried out using the *in silico* docking AutoDock4 [145] for virtual analysis and the Python Molecule Viewer 1.4.5 to analyse the data. New DA-like compounds (see results and discussion chapter) were designed by using Marvinsketch programme (ChemAxon company). In order to perform the docking run, a selected grid box of 26 x 26 x 26 Å was prepared covering the pH sensor site (on the extracellular domain of the ion channel). The docking was computed with 50 independent genetic algorithm runs. During the simulation, the protein was constrained as rigid, whereas the molecules were free to move. The molecules were performed in 3D version as PDB format and docked on

the extracellular domains of chicken ASIC1 (PDB code: 3HGC). Their correct conformation poses were checked by Python molecular viewer.

5.1.2 Trials in Escherichia coli

Briefly about the vectors, cells and materials used during the expression of extracellular domain of mouse ASIC1a (Uniprot Q6NXK8) in E. coli, which is shown in yellow in Figure 50. The cloning was carried out using traditional cloning strategy by restriction enzymes (such as NcoI, SacI from NEB) in different expression bacterial vectors including: pGEX-4T-1 (Glutathione S-transferase -tag), pET28a (6X Histidine tag) and in pET32a (Thioredoxin - tag). All the tags were in fusion with the protein ASIC1a at its N-termini for facilitating the purification steps. Plasmids were obtained from GE Healthcare-Life Sciences.

Moreover, the co-expression of ECD-6XHis-ASIC1a was performed in Shuffle cells (SHuffle® T7 Express Competent E. coli- from NEB) together with chaperon proteins (DnaK, GroEL, members of the heat shock protein Hsp70 and Hsp60 families). The use of engineered Shuffle cells was thought to assist the high level of expression of ASIC with its correct disulphide bonds (at least seven) within its cytoplasm. This strain is based on the trxB gor suppressor strain SMG96 where its cytoplasmic reductive pathways have been diminished, allowing for the formation of disulphide bonds in the cytoplasm.

The experiments were performed in volume of cell culture (2-3 L) of LB broth and the expression was induced by 0.7 mM IPTG. The cell's pellet was lysate with a disrupter at 0.25 kPsi pressure and the purification was carried out, first on affinity column (in this case: Nickel resin from Invitrogen- 2mL resin: 2L cell culture) in a gravity flow column at 4˚C. After several washes of the resin, with water and buffer containing 20 mM NaPO4, 300 mM NaCl pH 7.4. The protein tag was done by using thrombin (20 U/ml) and incubation (for 3h and 24h, sample taking for detection in gel SDS) at 4˚C. Eluted fraction was then applied at size exclusion 200 superdex (AKTA system- GE Healthcare and Life Sciences). The recombinant protein obtained was then applied to *in-vitro* refolding by dialysis and then detected by SDS-PAGE (see results and discussion).

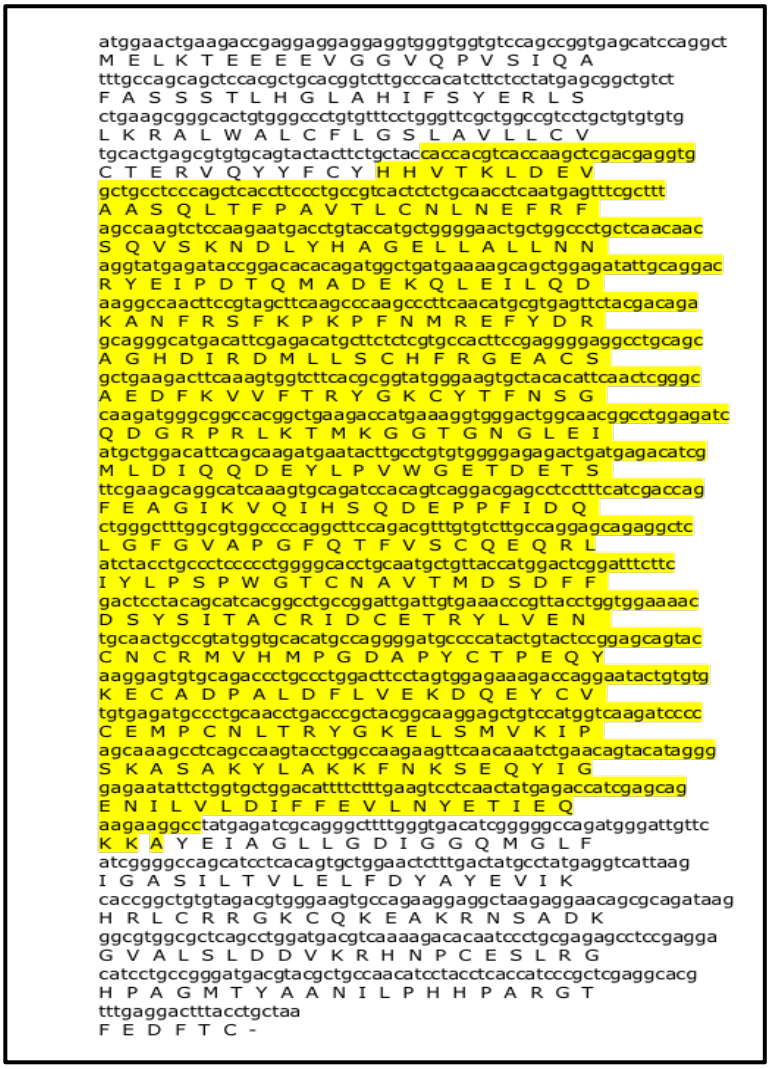

Figure 50: Nucleotide of the full-length Mus musculus acid-sensing ion channel 1a (mASIC1a) and its protein sequence (UniProtKB code: Q6NXK8)

The extracellular domain of the protein (highlighted in yellow) was selected for the cloning in bacterial expression vectors for structural studies with DA- like compounds.

5.1.3 Trials at the home lab to clone the extracellular domain of mouse ASIC1a in viral vector

The same construct (Figure 50) was used for the expression in alternative host system; such as the baculovirus-infected insect cells. Briefly, this construct as well as the full-length of chicken ASIC1 (DNA was kindly provided by Gouaux E. group) were subjected to attempts of cloning into the pFastBac- HTA viral expression vector (from Gibco™, Bac-to-Bac™ HT Vector Kit.). The vector was previously digested with two restriction enzymes (EcoRI-HF, NotI-HF from NEB) for 3 hours at +37˚C. The proteins were supposed to be in fusion with 6XHis-tag at the N-termini to facilitate purification steps.

5.1.4 Trials at the Israel Structural Proteomics Centre (ISPC)- Weizmann Institute for producing ASIC1 using baculovirus system

The expression of beforementioned constructs was performed using new strategies of cloning. Mainly, the plan was based on literature data available on the chicken ASIC1 variant [53] [52])

a. Designing of constructs and cloning

The constructs (mouse UniProtKB: Q6NXK8 and chicken ASIC1 (provided by [52])) were designed in a way that the protein is fused at its N-terminus with 6X histidine-tagged- TEV protease cleavage site. The cloning of three planned full-length (with some truncations) constructs was performed by using a novel methodology called Restriction Free Cloning (RF) [135] :

1. Delta 13 (removing 13 amino acid residues at the N-termini).
2. Delta 27 (removing 26 amino acid residues at the N-termini).
3. Delta 13 chicken ASIC1 (as described in [52]).

The transfer vector, pVL1393, containing the polyhedrin promoter, for the application in the BD BaculoGold™ system for the expression in insect cells (Sf9- from Invitrogen). Briefly for the RF method, the ASIC genes were PCR-amplified using two primers (see 8.3.1); each contains a target-specific sequence and an extension, over-lapping the desired insertion sites at the pVL1393 vector. The double-stranded PCR product was then used as a set of mega-primers for the second amplification reaction. In this step, each of the DNA strands has annealed to the destination vector at a predesigned position and was extended in a linear-amplification reaction. The two new DNA strands form a double stranded nicked-plasmid. Here, the parental DNA was removed by DpnI (from NEB) treatment at +37˚C for 1h. The product of newly plasmid, containing the DNA insert, purified (QIAquick PCR Purification Kit) is introduced into Escherichia coli cells (DH5α cells) where the nicked DNA is sealed by endogenous enzymatic activity.

Purified plasmid DNAs were detected on agarose gel (Figure 22). Positive clones (Figure 22 – marked with yellow star) were then verified by DNA sequencing analysis (see primers sequence 8.3.1 and 8.3.2).

Their concentration was quantified by NanoDrop™ spectrophotometers (Table 6) for further analysis (DNA sequencing and preparation of baculoviruses).

Construct of ASIC	Concentration (ng/µL)
Mouse delta 13	221
Mouse delta 27	68
Chicken delta 13	50

Table 6: List of selected ASIC's colonies, cloned in pVL1393 viral vector, for the expression in insect cells using baculovirus system

b. Virus amplification and protein expression:

The three mentioned constructs (Table1) were used to prepare virus stocks, containing ASIC1 gene, for the infection of insect cells (Sf9- from expression system LLC). The DNA (pVL1393-ASIC gene- 500 ng) of each construct was mixed with an appropriate amount of Sf9 cell culture, clean medium and Escort™ IV Transfection Reagent (Sigma Aldrich). The baculovirus's DNA used is ProGreen™, a linearized viral genome from AB vectors. The first stock of viruses (called P_0) is achieved after 7 days at +27˚C and static incubator, GFP expression signal was identified by fluorescence microscope in order to ensure that the transfection has worked. The viruses were amplified up to third generation (P_3) and then they were used for infecting insect cells at $1X10^6$ cells/mL density. The expression and purification of ASIC proteins (mouse and chicken delta 13) were performed at small scale (up to 30 mL of Sf9 cell culture) as described [136].

Buffers used during the purification of ASIC1:

Ni-agarose beads 50% slurry in EtOH (Adar Biotech). (Beads were washed 3 times in water and then with Ni-binding buffer prior to use). Ni-beads

binding buffer- 50mM Tris (HCl) pH-8.0, 150mM NaCl, 10mM Imidazole. (10-20 mM imidazole can be added to the binding buffer in order to reduce background of non-specific binding to the beads). Washing buffer- 50mM Tris (HCl) pH-8.0, 150mM NaCl, 50mM Imidazole. Ni-beads elution buffer- 50mM Tris (HCl) pH-8.0, 300mM NaCl, 500mM Imidazole, 0.05% (w/v) DDM and protease inhibitor.

5.1.5 Setting up the protocol to produce and characterise ASIC1 at the MPL- OPPF, Oxford

The production of ASIC1 isoform has been achieved through several efforts and multiple-diverse approaches to obtain a stable, functional and monodisperse membrane protein for drug discovery studies.

In particular, this section is summarising the extensive screening trials that have been established and carried out during my internship at the membrane protein lab (MPL) at the Diamond facility (Oxford, United Kingdom) by using high-throughput approaches. The established protocol shown here is based in part on literature data [52] [127] [128] and in part on specific protocols developed for membrane protein production for structural studies at the MPL.

16 constructs were designed for the expression of ASIC1: 8 for the chicken and 8 for the mouse variants by using high-throughput (HTP) screens. This includes adding a fusion protein and amino- and carboxy- terminal truncations. Indeed, starting from the full-length protein (called D13- since it hosts a deletion of 13 amino acid residues at the N-terminal), truncations were designed either at the N-terminal or at the C-terminal, or at both termini, in order to create a library of constructs (Figure 51).

Primer name	Comment	Sequence
Amal_Mm_D13_F	VQP...	aggagatataccatgGTCCAGCCGGTGAGCATCCAGGC
Amal_Mm_D27_F	TLH...	aggagatataccatgACGCTGCACGGTCTTGCCCACATC
Amal_Mm_D38_F	RLS...	aggagatataccatgCGGCTGTCTCTGAAGCGGGCAC
Amal_Mm_D44_F	ALW...	aggagatataccatgGCACTGTGGGCCCTGTGTTTCCTGG
Amal_Mm_Sol_F	HHV...	aggagatataccatgCACCACGTCACCAAGCTCGACGAGG
Amal_Mm_D13_R	...KHR	cagaacttccagtttCCGGTGCTTAATGACCTCATAGGCATAGTC
Amal_Mm_D38_R	...AYE	cagaacttccagtttCTCATAGGCATAGTCAAAGAGTTCCAGCAC
Amal_Mm_D44_R	...DYA	cagaacttccagtttGGCATAGTCAAAGAGTTCCAGCACTGTG
Amal_Mm_Sol_R	...KKA	cagaacttccagtttGGCCTTCTTCTGCTCGATGGTCTC
Amal_Gg_D13_F	GQP...	aggagatataccatgGGGCAGCCGGTGAGCATCCAG
Amal_Gg_D27_F	TLH...	aggagatataccatgACCCTGCACGGGATCTCGC
Amal_Gg_D38_F	RLS...	aggagatataccatgCGGCTGTCGCTGAAGCGCGTGGTC
Amal_Gg_D44_F	VVW...	aggagatataccatgGTGGTCTGGGCGCTCTGCTTCATGG
Amal_Gg_Sol_F	PHV...	aggagatataccatgCCCCACGTCACCAAGCTGGACG
Amal_Gg_D13_R	...KHR	cagaacttccagtttCCGGTGCTTGATCACCTCATAGGCG
Amal_Gg_D38_R	...AYE	cagaacttccagtttCTCATAGGCGTAGTCAAAGAGCTCC
Amal_Gg_D44_R	...DYA	cagaacttccagtttGGCGTAGTCAAAGAGCTCCAGCAC
Amal_Gg_Sol_R	...KKA	cagaacttccagtttCGCCTTCTTCTGCTCGATTGTCTCATAG

Figure 51: List of primers used for cloning each construct in a high throughput PCR reaction

For designing these constructs, the sequence of *Mus musculus* (NCBI reference sequence number: NM_009597.2) and *Gallus gallus* (NCBI reference sequence number: NM_001040467.1) full-length ASIC1 have been used as template; these had been previously used also for cloning into the viral expression vector pVL1393 (see previous paragraph- 5.1.4) by RF-PCR cloning method [135]. Briefly, the constructs were designed in a way that at the 5' end of the gene of interest (for more details see supplementary chapter) of ASIC1a (truncated) is inserted, followed by a human Rhinovirus (HRV) 3C Protease sequence and coupled with two tags; GFP- fluorescent gene and histidine moiety X8- at the 3' end (Figure 52)

Figure 52: An illustration of the designed ASIC1a construct

The 16 constructs were expressed in fusion with GFP- tag and His_8 sequence at their C-terminus

The ASIC1a- constructs contained a His_8 – tag attached to C-terminus to facilitate immobilised metal affinity chromatography (IMAC) purification. In addition, overexpression of all the constructs was coupled with a C-terminal Green Fluorescent Protein (GFP) tag. The GFP- tag at the C-terminus allows to monitor and quantify the membrane-integrated overexpression of ASIC1. In this scenario, the membrane proteins can fold co-translationally; therefore, the GFP will be folded and become fluorescent only once the upstream ASIC1- protein has first integrated into the cell membranes.

5.1.5.1 High-throughput cloning and baculovirus stocks preparation

The designed truncated constructs were cloned in the pOPINEneo-3C-eGFP-8XHis vector, which was developed from the pOPINE (Figure 53), using the HTP PCR cloning approach that offers more versatile, fast and efficient ligation-independent cloning. pOPINEneo-3C-eGFP-8His is the same as pOPINE- except that it has a neo cassette (for selection in mammalian cells) and the affinity tag is 8 instead of 6 His. This will guarantee also a stronger binding to resin for a good purification of membrane proteins.

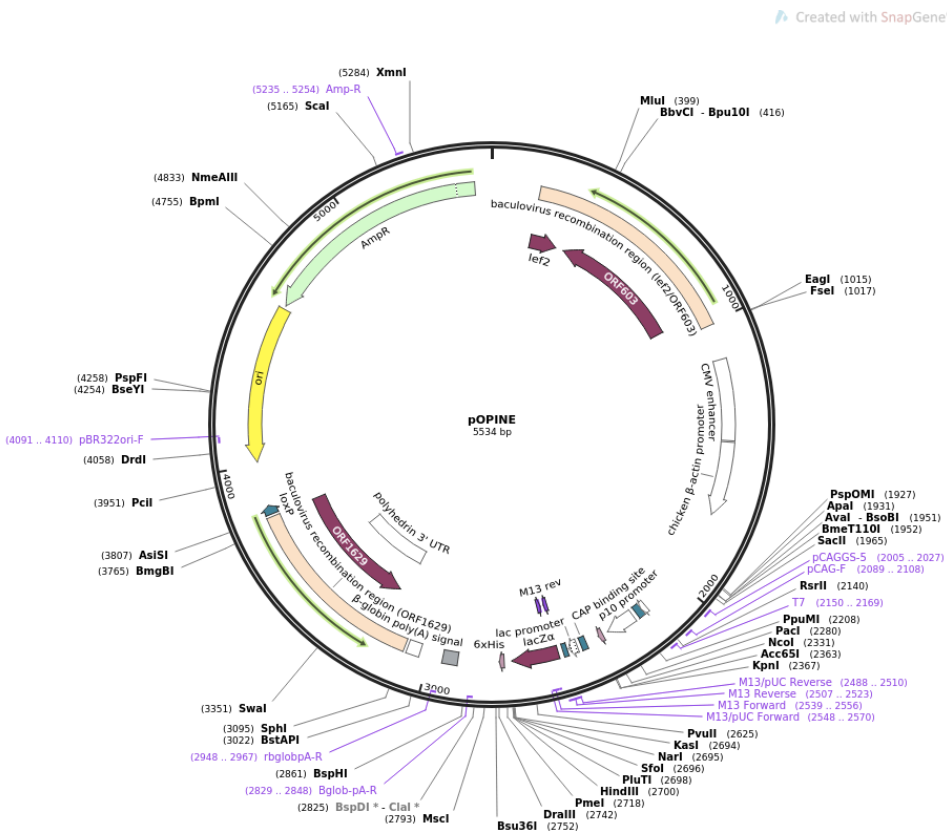

Figure 53: pOPINE vector sequence

The expression of ASIC1a- gene is under the control of the p10 promoter and was obtained through In-fusion kit.

The cloning of the 16 constructs was performed according to protocols from MPL (OPPF- http://www.oppf.rc-harwell.ac.uk/OPPF/) with minor modifications. Briefly, appropriate primers for each ASIC1-construct were designed with Tm $\geq 68^{\circ}$and ordered in a 96- well plate so that the forward primer and reverse primer plate coordinates match each planned construct. Each reaction of HTP-PCR-cloning (into 96-well plate) contains an appropriate amount of Phusion Flash master mix (Thermoscientific F-

548L), template plasmid of DNA, forward and reverse primers. PCR products were then analysed on agarose gel (1.6% Agarose (Sigma Aldrich) solved in 1X, UltraPure™ TBE Buffer (Invitrogen). Purified PCR-products were treated then with DpnI (10U/µL) and incubated at +37˚C for 30 minutes, followed by a quick "freeze-thaw" procedure (incubation at -80˚C for 10 minutes) that help to lyse the cell pellets and therefore may improve the extraction of membrane proteins. Samples were then used for Cloning Enhancer kit (Clontech), treating the PCR products without purification. At this point the cloning was carried out into pOPINEneo-3C-GFP (plus His_8) that was previously purified in the lab and digested with NcoI and BmEI, AmpR (100 ng/µl) and using the In-Fusion HD Cloning Kit (from Takara Bio USA, Inc.). Stellar *E.coli* competent cells were transformed with 3µL of the diluted sample by a standard heat-shock transformation protocol (cultured in a 24-well plate). Picked successfully transformed colonies were then amplified in *E.coli* cells and HTP-mini plasmid purified and verified by DNA-sequencing analysis. The 16 constructs inserted into the viral expression vector were ready to be used for the transfection steps in Sf9-insect cells (Table 7), previously cultured in Sf900II medium (Gibco) at $0.8X10^6$ cells/mL density.

well	construct name	variant DNA	Clone 1 (ng/µl)	Clone 2 (ng/µl)	Used clone
A4	D13	Mouse	174.6	194.1	1
B4	D27	Mouse	193.4	199.7	1
C4	D38	Mouse	179.4	275	1
D4	D44	Mouse	-1.168	174.3	2
E4	SOL	Mouse	218	-0.5851	1
F4	SOL truncation (63 to 453aa)	Mouse	175.9	161.8	1
G4	D38 truncation (29 to 453aa)	Mouse	197	197.4	1
H4	D44 truncation (35 to 453aa)	Mouse	180.4	169.5	1
A5	D13	Chicken	204.2	297.4	1
B5	D27	Chicken	209	265	1
C5	D38	Chicken	191.1	286	1
D5	D44	Chicken	196.9	172.1	1
E5	SOL	Chicken	165.3	233	1
F5	SOL truncation (63 to 463aa)	Chicken	-0.7246	211.9	2
G5	D38 truncation (39 to 463aa)	Chicken	98.82	198	2
H5	D44 truncation (45 to 463aa)	Chicken	190	159.3	1

Table 7: List of efficiently cloned constructs of ASIC1-GFP-His8

The table reports the name of each construct, its correspondent clone concentration and the chosen clone number for preparing the baculoviruses for transfecting Sf9 cells

5.1.5.2 Transfection of Sf9 cells and virus amplification

Bacmid preparation of the 16 constructs and insect cells Sf9 were completed according to OPPF's standard protocols (http://www.oppf.rc-harwell.ac.uk/OPPF/) using 24-well plates. Briefly, the Sf9 cells were cultured in 24 well-plates (final volume of 500 µL) at $1X10^6$ cells/mL. Once the cells are attached, as monolayer, an appropriate amount of each transfection mix (Sf900II medium- free serum, linearized bacmid (prepared in- house), cloned ASIC-vector at 100-500 ng and the transfection reagent FugeneHD) was added. After an incubation for 7 days at 27˚C, transfected cells were verified by checking the GFP signal on a fluorescence microscope. The viral supernatant was collected and stored in a 96-well storage block at +4˚C in the dark. This is what is called the P_0 virus stock. Figure 54 reports a general overview of the baculovirus amplification pipeline with their relative time of amplification. Except for the P_0 stock preparation, which is carried over in static manner, the amplification of the first (P_1) and second generation (P_2) is performed in suspension cell culture. In the case of ASIC1a-constructs, their relative two generations were followed based on standard protocol of HTP-infection in Sf9-insect cells in 24-well suspension protocol (500 µL Sf9- cell culture at $1X10^6$ cells/mL final volume in each well). In parallel, small-scale expression screens were carried out (3 mL Sf9- cell culture at $1X10^6$ cells/mL final volume in each well) using P_1 and the efficiency of infection was verified by monitoring the GFP signal through two approaches: In-gel fluorescence and FSEC.

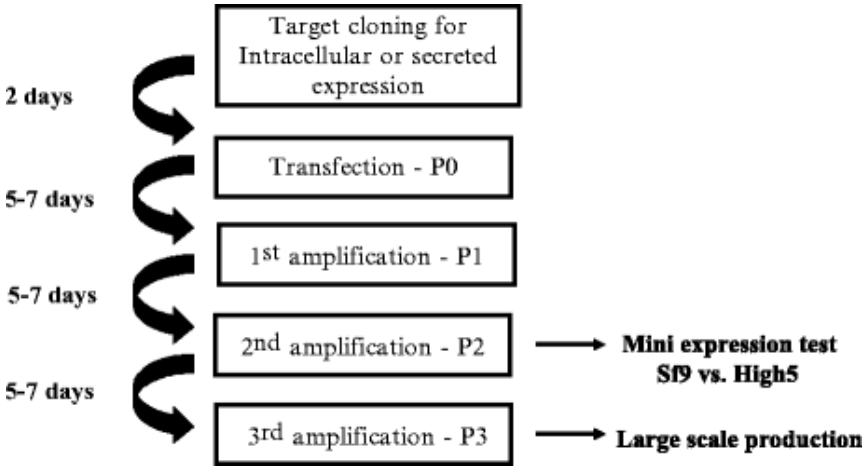

Figure 54: An overview of viral amplification pipeline in insect cells

It requires at least 5-7 days to prepare a viral progeny that contains the gene of interest (image taken from Yoav Peleg and Tamar Unger 2013). Although the most reliable route is to use P2 virus generation for protein expression, in the case of ASIC1a production, P1 viruses were used for optimal expression level

5.1.5.3 Expression in Sf9 using baculovirus- infected insect cells system

Sf9 cells were cultured into a serum-free medium (Sf-900^{TM} III SFM from Gibco^{TM}) in suspension shake flasks. The cells are prepared from low-passage cells (<30 passages) and infected at 1X10^{6} cells/mL density. Through small-scale expression screens of optimisations, different amounts of baculoviruses stocks (3µL of P_1, 3, 10, 30 and 100µL of P2) were tested with 3mL Sf9 cell culture for the production of ASIC1-constructs. Furthermore, the harvesting time was tested in order to verify the time-point to get higher expression level of the membrane protein (48 and 72 post-infection) at 26-27 ˚C.

Once the best conditions were defined by beforementioned trials, a large-scale of expression was carried-out (100 – 500 mL). In fact, the expression of ASIC1 was done in Erlenmeyer shaker flasks (Gibco^{TM}) with Sf9 cells at

$1X10^6$ cells/mL as a density to which it has been added an appropriate amount (1:1000 ratio of viruses: Sf9 cell culture volume) of baculovirus and incubated for 72 hours at 27˚C. After this time of infection, the expression of ASIC1 was checked for the GFP-signal on a fluorescence microscope and collected by centrifuging at 6000*g X* for 30 minutes for further analysis (e.g. by HisPure Ni-NTA resin from Thermoscientific).

5.1.5.4 Detergent screening

Since the structure and dynamics of the membrane protein ASIC1 is highly related to the properties of the surrounding phospholipids in cell membrane, choosing the detergent that should mimic lipid membrane is essential. Thus, a library of eight commercially available detergents families (from Anatrace products) was screened with ASIC1a full length to choose the suitable one (Table 8). Moreover, because ASIC1a is a mammalian membrane protein, the cholesteryl hemisuccinate (CHS 2% stock) was mixed with each detergent as it could significantly improve the stability of the protein [146].

Detergent name	Abbreviation	CMC (mM)
n-Dodecyl-beta-Maltoside	DDM	0.17
Lauryldimethylamine	LDAO	1
Polyoxyethylene(9)dodecyl Ether	C12E9	0.05
FOS-CHOLINE-12	FC12	1.5
Lauryl Maltose Neopentyl Glycol	LMNG	0.01
7-Cyclohexyl-1-Heptyl-β-D-Maltoside	CYMAL-7	0.19

Table 8: List of detergents used for the solubilisation of ASIC1a protein trial

The quality and stability of the solubilized ASIC1a differ considerably with various detergents. Here are reported the employed detergents in the screen and their recommended concentration ranges. The critical micelle concentration (CMC) is an important parameter to consider because it indicates the minimal detergent concentration at which micelles are observed

In order to have equal conditions during the screen, the two generation of baculoviruses (P_1 and P_2) of both full-length constructs (D13) were prepared and used for the assay to compare the solubilisation levels between mouse and chicken ASIC1. 3ml of cultured Sf9 at $1X10^6$ cells/mL in a 24-well shaker plate at 27˚C, were infected with ASIC1- viruses and then collected after 72h. 2ml of expressing cells were taken for the screen. Briefly, cells were harvested at 6000*g* for 15 minutes at +4˚C (Beckman J S5.3 rotor), lysate with PBS (1X) was further clarified by ultracentrifuge (Beckman Coulter ultracentrifuge/rotor system- Rotor 45Ti) at 41,000 rpm for 30 minutes in the same deep well-plate, and extracted membrane protein was isolated by ultracentrifugation at 40,000 rpm at +4˚C for 1h, following standard protocol at MPL (http://www.oppf.rc-harwell.ac.uk/OPPF/) with slight modification.

Indeed, the pellet (containing membranes) was disrupted in PBS buffer supplemented with a tablet of Protease inhibitor cocktail (Sigma Aldrich) and divided in suitable number of aliquots into Ultra-Beckman Eppendorfs and homogenised with a douncer (Life Sciences Kimbl) in the presence of the selected detergents (Table 9) at final detergent concentration of 1% (w/v). Protein-detergent mixture was then incubated at +4˚C with a moderate agitation for 1 hour. After the incubation, the screening samples were centrifuged at 50,000 rpm (in the rotor TLA55-Beckman) for 30 minutes. The supernatant was collected and 10 µl aliquots were taken from each tube for later analysis (e.g. SDS-PAGE and FSEC).

5.1.5.5 Solubilisation and purification of ASIC1

Here is reported in details the solubilisation and purification of ASIC1 (in particular, on chicken ASIC1-full length (D13). Therefore, after 72 hours of expression, Sf9 cell cultures were collected by centrifuge (6000*g* for 15 minutes) and freezed at -80˚C.

Defrosted pellet was resuspended in TBS buffer (150 mM NaCl, 20 mM Tris pH 8.0 (measured and controlled at +4˚C) and supplemented with protease inhibitor cocktail (Sigma Aldrich).

Component	- CHS	+ CHS
DDM	1	7
LDAO	2	8
C12E9	3	9
FC12	4	10
LMNG	5	11
CYMAL	6	12

Table 9: List of detergents used for the screen

Although long carbon chains of detergent are better for membrane proteins, it depends on the type of membrane protein in consideration

Cells were disrupted by sonication (30 seconds on and 10 seconds off for 5 times) and crude membrane fractions were harvested by ultracentrifugation (TLA-55 rotor Beckman) at 41,000 rpm (100,000*g*) at 4°C for 1 hour. The collected pellet (isolated membranes) was further treated to extract ASIC1-membrane protein and maintain in a soluble form. Thus, membranes were homogenized (Kimble™ Kontes ™ Dounce Tissue Grinders, Thermo Fisher Scientific) and solubilized in TBS buffer supplemented with 5 mM $CaCl_2$ and 40mM DDM and 2% CHS detergent. The mixture was then incubated for 1-2h at +4˚C under a modest stirring speed. At this step synthesised small compounds DA, DG296 and DG327 (See supplementary information for stocks preparation) were also mixed with ASIC1 fractions to test their stabilisation effect. After the incubation, solubilised membrane protein was clarified by ultracentrifugation (41,000 rpm at ˚4C for 1h). Collected supernatant (containing the solubilised membrane protein-ASIC1) was incubated with an appropriate amount of

affinity resin, Nickel-metal ion (ProBond™ Nickel-Chelating Resin, Thermofisher) for 24 hours at +4˚C under stirring. The amount of the resin was chosen based on the binding capacity of the resin (following the manufacture indication).

This step was carried out always in batch, so that the mixture of membrane protein-nickel beads was uploaded onto affinity column and subjected to three volumes washes with buffer wash A (300 mM NaCl, 20 mM TRIS pH 8.0, 10 mM Imidazole, 1 mM DDM and 2% CHS and 1 mM CaCl2). Followed by further three washes with buffer wash B (300 mM NaCl, 20 mM TRIS pH 8.0, 30 mM Imidazole, 1 mM DDM and 2% CHS and 1 mM CaCl2). Finally, bound protein was eluted with elution buffer (300 mM NaCl, 20 mM TRIS pH 8.0, 250 mM Imidazole, 1 mM DDM and 2% CHS and 1 mM CaCl2).

The GFP-His_8 moiety was cleaved from ASIC1-sequence by adding the protease HRV3C to the eluted membrane protein fraction. The cleavage was done through dialysis and the protein was uploaded into a dialysis membrane bag with molecular weight cut-off (MWCO) of 6-8000, mixed with an appropriate amount of 3C protease in dialysis buffer (300 mM NaCl, 20 mM TRIS pH 8.0, 5 mM CaCl2, 0.5-1 mM DDM and 2% CHS) and left for overnight under a light stirring. The cleaved protein was separated from the GFP-His-tagged by incubation with Nickel resin (step defined as reverse IMAC); the flowthrough that contains the cleaved protein was collected. Cleaving efficiency of ASIC was analysed by in-gel fluorescence on a 12% SDS PAGE gel. ASIC1-membrane protein was then concentrated up to 3-5 mg/mL in 500 µL (this was the maximum concentration that ASIC can reach) with MWCO 100,000 (Corning® Spin-X® UF 20 mL Centrifugal

Concentrator, life sciences). Moreover, the protein was finally purified by size-exclusion chromatography (SEC), using Superdex 200 increase 10/300 GL (from GE-Healthcare Life). Protein fractions from each step were collected and analysed by biochemical and biophysical techniques.

5.1.5.6 Biochemical and biophysical characterisation

Two analyses, SDS-PAGE with in-gel fluorescence imaging and fluorescence-detection size-exclusion chromatography (FSEC), were used to screen for the overexpression of ASIC1. The effectiveness of various categories of detergents to solubilize and stabilise (in the presence/absence of small compounds DA and DA-like) the protein from isolated membranes was also evaluated using FSEC, as described below.

5.1.5.6.1 SDS-PAGE and In-gel fluorescence

The great utility of having His- and GFP-tag is in being able to keep under control not only the overexpression of ASIC1 but also the monodispersity of the membrane protein samples in detergent solubilisation prior to purification steps or scaling-up by size-exclusion chromatography. SDS is a very fast, simple, and sensitive methods for in-gel visualization of proteins. 10 µL of cleared lysate, solubilised or/and purified ASIC1-samples were transferred to a microtiter plate and mixed with an appropriate amount of SDS-PAGE gel loading buffer (NuPAGE^{TM} LDS sample buffer (4X) and NuPAGE ^{TM} reducing agent, from Invitrogen). Then 10 µL of this sample mixture was loaded onto a SDS-PAGE gel (10% Bis Tris midi gel, Invitrogen) and run at 110-120 at +4˚C for 2-2,5 hours in NuPAGE™ MES SDS Running Buffer (20X). Since ASIC1 is a membrane

protein, it was not boiled before being loaded on gel. Two markers were used; 1) SeeBlue Plus pre-stained standard (Invitrogen) for a staining with Coomassie blue and 2) BenchMark ™ protein ladder (invitrogen) for easy fluorescence visualisation on gel (called in-gel fluorescence). For the second case, the gel was placed onto an imager (e.g. ChemiDoc from BioRad) with a blue light filter to detect the GFP-tag fused with ASIC1 samples. Alternatively, the gel was stained with Coomassie blue.

5.1.5.6.2 Fluorescence- detection size-exclusion chromatograhy

The technique was developed by the group of Eric Gouaux (Kawate and Gouaux, 2006) as a pre-crystallisation screen basing on the fact that detecting a fluorescence in crude extract of membranes can save a lot of time and requires small amounts of sample. Here it was used as alternative functional assay and for the possibility to monitor already the quality of membrane protein and its stability in detergent. Herein, the GFP-tag was used for testing these features by fluorescence- detection size exclusion chromatography (FSEC) using the Shimadzu UHPLC system equipped with an autosampler and a GFP fluorescence detector (excitation at 488 nm and emission at 512 nm). For this high-throughput screening, solubilised and purified ASIC1 was used (this step has been described before in this chapter). 110 µl of sample was loaded into individual vials (Shimadzu lab total vial) on its sample changer and 100 µl of sample was injected onto a Superose 6 10/300 GL gel-filtration column (GE healthcare). The column was pre-equilibrated with running buffer (150 mM NaCl, 20 mM TRIS pH 8.0, 1 mM DDM and CHS, 1 mM CaCl2 supplemented with DNase I (NEB) and 1 mM MgCl2). The set-up and the

procedure were followed according to the manufacture manual (Shimadzu UHPLC system). The run was performed at a flow rate of 0.3 ml/min. Finally, the elution flow volume and the fluorescence intensity data were imported into a spreadsheet program for graphics display (e.g. Excel) and the resulting data were analysed by Shimadzu extractor.

5.1.5.6.3 Microsacale thermophoresis

The affinity between cASIC1-full length and synthesized compounds was measured using Microscale thermophoresis. The protein (cASIC1) was used at its soluble form (un-cleaved) for GFP-signal. The compounds were prepared at 100mM concentration in 100% DMSO and mixed at a final concentration of 0.5uM with 200nM of protein solution. The experiment was done in the presence/absence of the compounds in the protein buffer (300 mM NaCl, 20 mM TRIS pH 8.0, 0.5-1 mM DDM + CHS and 5 mM CaCl2). The samples were loaded into NanoTemper premium coated glass capillaries. Microscale thermophoresis was performed using a Monolith NT.115 MST (NanoTemper® Technologies GmbH) equipped with the Nano BLUE/RED filter combinations. The experimental parameters were: LED power of 100% (for fluorescence excitation) and a laser power of 40% (for creating a temperature gradient) and at 24˚C.

5.1.5.6.4 Microscale Fluorescent Thermal stability using CPM as a dye

The assay utilizes the accessibility of the native cysteine residues to covalent modification as readout for the unfolding process. Cysteine residues are frequently located at helix-helix interaction sites. Therefore, they are ideal sensors for the overall integrity of the membrane protein

structure. Here, they used to test the stability of solubilised chicken ASIC1 (construct A5) in presence/ absence of DA and DA-like compounds in a 96-well microtiter plate.

Firstly, ASIC1 was tested without any compound at different concentration (0.1, 1 and 10 µM) in its buffer (300mM NaCl, 20 mM Tris pH 8.0 and 1mM DDM + 0.06% CHS) to detect the best concentration at which the protein is stable. Then, once the conditions ae defined, the compounds were tested in triplicates in presence of ASIC (ratio of 1 µM protein: 10 µM compound) and the thiol-specific fluorochrome N-[4-(7-diethylamino-4-methyl-3-coumarinyl)phenyl]maleimide (CPM) dye. CPM is practically non-fluorescent in its unbound form [147]. The run was performed by transferring the 96-well plate to the Stratagene Mx3005P fluorimeter instrument. The samples were then subjected to thermal denaturation by heating them with increasing temperatures from 25 °C to 100 °C at a ramp rate of 1°C per 1 or 2 min.

5.2 Gelsolin and nanobody

5.2.1 Protein production

5.2.1.1 Second domain of mutated gelsolin

Constructs and expression conditions for GSN variants as isolated G2 domain were performed as already reported [107] [108]. The here named G2 refers to the shorter G2s construct. Protein purification was described elsewhere but it is here briefly reported. E. coli cell cultures were resuspended in 20 mM Na_2PO_4, pH 7.4, 500 mM NaCl supplemented with Dnase I (Sigma Aldrich), 20 mM $MgCl_2$ and protease inhibitors (cOmplete™ Protease Inhibitor Cocktail- Roch) and lysed by high pressure (25 kPsi) in a Basic Z Bench top (Constant Systems Limited, U.K.). Crude extract was clarified by centrifugation at 18000 RPM, for 40 min at 4°C (Sorvall- Thermo Fisher Scientific). Soluble fraction was loaded onto a 5 ml- His-Trap HP column (GE Healthcare Life Sciences). The column was subjected to three column volume wash steps with 20 mM Na_2PO_4, pH 7.4, 500 mM NaCl and 20 mM Imidazole. Mutated G2-variants were eluted with 20 mM Na_2PO_4, pH 7.4, 500 mM NaCl and 300 mM Imidazole. The 6Xhistidine- tag was removed by thrombin digestion at 20°C under stirring for 2 hours. Cleaved protein was concentrated up to 500 µl by centrifugal filters (Amicon- MWCO 10 kDa) at +4 ˚C and maximum speed (4000 RPM) and passed through a size-exclusion chromatography (SEC); Superdex^{TM} 75 increase 10/300 (GE Healthcare Life Sciences) equilibrated with 20 mM HEPES, pH 7.4, 100 mM NaCl and 1 mM $CaCl_2$. Protein fractions were further concentrated to 10 mg/ml with the previously mentioned centrifugal filters and used for structural and functional assays.

5.2.1.2 Nb11 expression and purification

Synthetic gene coding for Nb11 ([85]) fused to the thrombin cleavage site and 6xHis tag at the C-terminus was purchased by Eurofins genomics (Milan, Italy). Sequence was optimized for *E. coli* codon usage and the gene cloned in a pET11 vector. Tagged Nb11 was produced in *E. coli* shuffle cells grown in LB medium (Sigma-Aldrich) once the cell density reached the value of $O.D_{600\ nm}$=0.6, the expression of the gene was induced with 0.5 mM isopropil-β-D-1-tiogalattopiranoside (IPTG). Cells were harvested by centrifugation (6000 RPM, 15 minutes at +4˚C using JLA-8.1000 Beckman rotor) after 16 h incubation at 20 °C. The cell pellet was resuspended in lysis buffer (20 mM Na_2PO_4, pH 7.4, 500 mM NaCl and 20 mM Imidazole) supplemented with DNase I (Sigma) and cOmplete™ Protease Inhibitor Cocktail and lysed with a cell disruptor operating at 25 kPsi. Lysate cell culture was then clarified by centrifugation at 18000 RPM for 30 minutes at +4˚C (Sorvall- Thermo Fisher Scientific). The clarified crude extract was loaded onto a 5 ml HisTrap (GE- Healthcare comlumn) and Nb11 sample was eluted stepwise with lysis buffer supplemented with 500 mM imidazole. Eluted fractions enriched in Nb11 were further concentrated through the centrifugal filter (as mentioned before) and passed through a Superdex 75^{TM} increase column (GE- Healthcare). The column was previously equilibrated with 20 mM HEPES solution, pH 7.4, containing 100 mM NaCl and Nb11 was eluted with the same buffer.

Note: All the chemicals are from Sigma Aldrich and all the purification steps were carried out on an ÄKTA system enclosed in a 4 °C chromatography chamber.

5.2.2 Thermal denaturation by Circular Dichroism (CD) spectroscopy

CD measurements were performed with a J-810 spectropolarimeter (JASCO Corp., Tokyo, Japan) equipped with a Peltier system for temperature control. All measurements were performed on 15 μM G2, Nb11 or the complex in 20 mM HEPES, 100 mM NaCl and 1 mM $CaCl_2$, pH 7.4. Temperature ramps were recorded from 10°C to 95°C (temperature slope 50 °C/h) in a 0.1 cm path length cuvette and monitored at 218 nm wavelength

5.2.3 Thermofluor

To determine the thermal stability, WT_{G2} and mutated G2 domains were mixed with or without equimolar Nb11. Proteins were diluted at 1 mg/ml concentration in 20 mM HEPES, pH 7.4, 100 mM NaCl and 1 mM $CaCl_2$, and supplemented with 3µl of a 1:500 (v/v) dilution of Sypro Orange dye (Sigma) in a final reaction volume of 15 µl. Each reaction was analysed in triplicates and measured in a MJMiniTM Personal Thermal Cycler (BIO-RAD). The temperature was increased gradually from 10 °C to 100 °C in 0.2 °C steps and fluorescence intensity was measured within the excitation and emission wavelength ranges of 470–505 and 540–700 nm, respectively. Tm values were calculated as the minimum of the first-derivative of the traces using the manufacturer software and the value is reported as the average of triplicate measures.

5.2.4 Furin assay

Furin cleavage assays were performed in a total volume of 30 µl, using 1U of commercial furin enzyme (BioLabs) and 1 mg/ml of WT and mutated G2 in 20 mM 2-(N-morpholino) ethane sulfonic acid, pH 6.5, 100 mM NaCl 1 mM CaCl2, in the presence or the absence of 1 mg/ml of Nb11. To monitor the susceptibility to proteolysis, 12 µl aliquots of the reaction mix were collected right upon addition of furin and at different time points (1, 3 and 24 hours) post-incubation at 37 °C. The reaction was blocked by adding to each sample 4 µl of Sodium Dodecyl Sulphate - PolyAcrylamide Gel Electrophoresis (SDS-PAGE) loading buffer 4X (Bio-Rad) supplemented with 0.7 mM β-mercaptoethanol and by incubation at 90 °C for 3 min. 10 µl of the boiled samples were analysed and detected 12% SDS-PAGE (Gene script) in 1X MES running buffer (180 V for 50 minutes

5.2.5 Crystallisation, data processing and structure analysis

The crystallisation trials of the three mutants were carried out in a similar manner. For simplicity, here is reported the example of the $D187N_{G2}$ one in complex with Nb11. The complex was prepared by mixing equimolar amounts of the individual proteins. The complex was loaded on a Superdex 75^{TM} increase column (GE- Healthcare). equilibrated with 20 mM HEPES solution, pH 7.4, 100 mM NaCl, 1 mM CaCl2. The complex eluted as a single peak, consistent with the complex theoretical molecular weight, that was collected and concentrated to 12 mg/ml in the same buffer, using centrifugal filters (Amicon- MWCO 10 kDa). This sample ($D187N_{G2}$:Nb11) was used for extensive screening of the crystallization

conditions using an Oryx-8 crystallization robot (Douglas Instruments) and several commercial solutions in a sitting-drop set-up (e.g. molecular dimensions - Morpheus®, JCSG-plus™, JCSG 1 and 2, and Hampton) and some early-obtained microcrystals were used for micro-seeding experiments. The purified complex (0.15/0.25 µl) was mixed with 0.25/0.15 µl of the reservoir solutions. Among all the screens, two different conditions yielded crystals within a week of incubation at 20 °C: 1) 0.1 M potassium thiocyanate, 30 % poly (ethylene glycol) methyl ether 2000 and 4.0 M sodium formate; and 2) 0.1 potassium phosphate, pH 6.2, 10% v/v glycerol and 25% v/v 1,2 propandiol. Crystals were soaked with the respective reservoir solution supplemented with 20% glycerol, flash-frozen in liquid N2 and tested/collected on beamline ID23-1 (European Synchrotron Radiation Facility, Grenoble, France).

The datasets were processed with XDS [148], scaled with AIMLESS [149] and the structure solved by molecular replacement using the program PHASER [150] and the pdb ID is 4S10 as searching model. The two aforementioned crystallization conditions resulted in two data sets of different qualities and space groups: One crystal is related to the orthorhombic space group $P2_12_12_1$ and a second crystal belongs to tetragonal $P4_12_12$ space group. Both structures were refined with PHENIX refine [151] and manual model building performed with COOT [152]. The structure of poorer quality (referred as the tetragonal) could be refined only partially. On the contrary, the orthorhombic structure was refined to 1.9 Å and deposited in the pdb database with accession code 6H1F. PyMOL tool (The PyMOL Molecular Graphic System, Version 2.0

Schrödinger) was used to analyse the refined structures and to prepare the figures. All structures used for the B factor analysis were subjected to 3 cycles of refinement with PHENIX refine, B factors for the WT_{G2}:Nb11 and $D187N_{G2}$:Nb11 were averaged between the one molecule in the asymmetric unit, or between the structures refined on different datasets respectively; otherwise the analysis was performed as reported earlier [153].

6 Manuscript / Paper

The manuscript (attached in Pdf – A4 format)

The paper is published on the 6th of January 2019:

Giorgino T, **Hassan A**, Mattioni D Milani M, Mastrangelo E, Barbiroli A, Verhelle A, Gettemans J, Barzago MM, Diomede L, de Rosa M. Nanobody interaction unveils structure, dynamics and proteotoxicity of the Finnish-type amyloidogenic gelsolin variant. Biochim Biophys Acta Mol Basis Dis. 2019 Mar 1;1865(3):648-660. doi: 10.1016/j.bbadis.2019.01.010. Epub 2019 Jan 6.

Following is reported my contribution as a PhD student in the paper

The results reported in the thesis reflect my contributions to the attached paper. I was mainly involved in the production of the proteins and their biochemical/biophysical characterization (thermal stability and furin susceptibility). Moreover, I took part in the crystallization of the complex, collection of diffraction data, data processing and analysis.

7 References

1. Jaskolski, M., Dauter, Z. & Wlodawer, A. A brief history of macromolecular crystallography, illustrated by a family tree and its Nobel fruits. *FEBS J.* 281, 3985–4009 (2014).
2. Thomas, S. E. *et al.* Structural Biology and the Design of New Therapeutics: From HIV and Cancer to Mycobacterial Infections: A Paper Dedicated to John Kendrew. *J. Mol. Biol.* 429, 2677–2693 (2017).
3. Zheng, H. *et al.* X-ray crystallography over the past decade for novel drug discovery - where are we heading next? *Expert Opin Drug Discov* 10, 975–989 (2015).
4. Zhou, S.-F. & Zhong, W.-Z. Drug Design and Discovery: Principles and Applications. *Molecules* 22, 279 (2017).
5. Hillisch, A., Heinrich, N. & Wild, H. Computational Chemistry in the Pharmaceutical Industry: From Childhood to Adolescence. *ChemMedChem* 10, 1958–1962 (2015).
6. Navia, M. A. *et al.* Three-dimensional structure of aspartyl protease from human immunodeficiency virus HIV-1. *Nature* 337, 615–620 (1989).
7. Mahalingam, A. K. *et al.* HIV-1 protease inhibitors with a transition-state mimic comprising a tertiary alcohol: improved antiviral activity in cells. *Journal of Medicinal Chemistry* 53, 607–615 (2010).
8. Kolb, P., Ferreira, R. S., Irwin, J. J. & Shoichet, B. K. Docking and chemoinformatic screens for new ligands and targets. *Curr. Opin. Biotechnol.* 20, 429–436 (2009).
9. Kolb, P. & Irwin, J. Docking Screens: Right for the Right Reasons? *Current Topics in Medicinal Chemistry* 9, 755–770 (2009).
10. Uhlén, M. *et al.* Proteomics. Tissue-based map of the human proteome. *Science* 347, 1260419–1260419 (2015).
11. Overington, J. P., Al-Lazikani, B. & Hopkins, A. L. How many drug targets are there? *Nature Reviews Drug Discovery* 5, 993–996 (2006).
12. Bernaudat, F. *et al.* Heterologous expression of membrane proteins: choosing the appropriate host. *PLoS ONE* 6, e29191 (2011).
13. Sjöstrand, D., Diamanti, R., Lundgren, C. A. K., Wiseman, B. & Högbom, M. A rapid expression and purification condition screening protocol for membrane protein structural biology. *Protein Sci.* 26, 1653–1666 (2017).

14. Burgess-Brown, N. A. *et al.* Codon optimization can improve expression of human genes in Escherichia coli: A multi-gene study. *Protein Expression and Purification* 59, 94–102 (2008).
15. Valderrama-Rincon, J. D. *et al.* An engineered eukaryotic protein glycosylation pathway in Escherichia coli. *Nature Chemical Biology* 8, 434–436 (2012).
16. Service, R. F. Structural genomics. Tapping DNA for structures produces a trickle. *Science* 298, 948–950 (2002).
17. Yamashita, A., Nango, E. & Ashikawa, Y. A large-scale expression strategy for multimeric extracellular protein complexes using Drosophila S2 cells and its application to the recombinant expression of heterodimeric ligand-binding domains of taste receptor. *Protein Sci.* 26, 2291–2301 (2017).
18. Sørensen, H. P. Towards universal systems for recombinant gene expression. *Microb. Cell Fact.* 9, 27 (2010).
19. Karasawa, A. & Kawate, T. Expression and Purification of a Mammalian P2X7 Receptor from Sf9 Insect Cells. *Bio Protoc* 7, (2017).
20. Warne, T. *et al.* Structure of a beta1-adrenergic G-protein-coupled receptor. *Nature* 454, 486–491 (2008).
21. Jarvis, D. L. Recombinant protein expression in baculovirus-infected insect cells. *Meth. Enzymol.* 536, 149–163 (2014).
22. Hopkins, R., Esposito, D. & Gillette, W. Widening the bottleneck: Increasing success in protein expression and purification. *J. Struct. Biol.* 172, 14–20 (2010).
23. Khan, K. H. Gene expression in Mammalian cells and its applications. *Advanced Pharmaceutical Bulletin* 3, 257–263 (2013).
24. Sunley, K. & Butler, M. Strategies for the enhancement of recombinant protein production from mammalian cells by growth arrest. *Biotechnology Advances* 28, 385–394 (2010).
25. Privé, G. G. Detergents for the stabilization and crystallization of membrane proteins. *Methods* 41, 388–397 (2007).
26. Arachea, B. T. *et al.* Detergent selection for enhanced extraction of membrane proteins. *Protein Expression and Purification* 86, 12–20 (2012).
27. Katsura, K., Kristián, T., Smith, M. L. & Siesjö, B. K. Acidosis induced by hypercapnia exaggerates ischemic brain damage. *J. Cereb. Blood Flow Metab.* 14, 243–250 (1994).
28. Chesler, M. & Kaila, K. Modulation of pH by neuronal activity. *Trends Neurosci.* 15, 396–402 (1992).

29. Siesjö, B. K., Katsura, K. I., Kristián, T., Li, P. A. & Siesjö, P. Molecular mechanisms of acidosis-mediated damage. *Acta Neurochir. Suppl.* 66, 8–14 (1996).
30. Waldmann, R., Champigny, G., Bassilana, F., Heurteaux, C. & Lazdunski, M. A proton-gated cation channel involved in acid-sensing. *Nature* 386, 173–177 (1997).
31. Zha, X. M., Wemmie, J. A., Green, S. H. & Welsh, M. J. Acid-sensing ion channel 1a is a postsynaptic proton receptor that affects the density of dendritic spines. *Proceedings of the National Academy of Sciences* 103, 16556–16561 (2006).
32. Kreple, C. J. *et al.* Acid-sensing ion channels contribute to synaptic transmission and inhibit cocaine-evoked plasticity. *Nature Neuroscience* 17, 1083–1091 (2014).
33. Bohlen, C. J. *et al.* A heteromeric Texas coral snake toxin targets acid-sensing ion channels to produce pain. *Nature* 479, 410–414 (2011).
34. Wemmie, J. A. *et al.* Overexpression of acid-sensing ion channel 1a in transgenic mice increases acquired fear-related behavior. *Proceedings of the National Academy of Sciences* 101, 3621–3626 (2004).
35. Ziemann, A. E. *et al.* Seizure termination by acidosis depends on ASIC1a. *Nature Neuroscience* 11, 816–822 (2008).
36. McIlwrath, S. L., Hu, J., Anirudhan, G., Shin, J. B. & Lewin, G. R. The sensory mechanotransduction ion channel ASIC2 (acid sensitive ion channel 2) is regulated by neurotrophin availability. *Neuroscience* 131, 499–511 (2005).
37. Miesenböck, G., De Angelis, D. A. & Rothman, J. E. Visualizing secretion and synaptic transmission with pH-sensitive green fluorescent proteins. *Nature* 394, 192–195 (1998).
38. Gründer, S. & Pusch, M. Biophysical properties of acid-sensing ion channels (ASICs). *Neuropharmacology* 94, 9–18 (2015).
39. Friese, M. A. *et al.* Acid-sensing ion channel-1 contributes to axonal degeneration in autoimmune inflammation of the central nervous system. *Nat. Med.* 13, 1483–1489 (2007).
40. Vergo, S. *et al.* Acid-sensing ion channel 1 is involved in both axonal injury and demyelination in multiple sclerosis and its animal model. *Brain* 134, 571–584 (2011).
41. Liu, S., Cheng, X.-Y., Wang, F. & Liu, C.-F. Acid-sensing ion channels: potential therapeutic targets for neurologic diseases. *Transl Neurodegener* 4, 10 (2015).

42. Wemmie, J. A., Price, M. P. & Welsh, M. J. Acid-sensing ion channels: advances, questions and therapeutic opportunities. *Trends Neurosci.* 29, 578–586 (2006).
43. Li, M.-H. *et al.* Acid-sensing ion channels in mouse olfactory bulb M/T neurons. *The Journal of General Physiology* 143, 719–731 (2014).
44. Ortega-Ramírez, A., Vega, R. & Soto, E. Acid-Sensing Ion Channels as Potential Therapeutic Targets in Neurodegeneration and Neuroinflammation. *Mediators of Inflammation* 2017, 1–18 (2017).
45. Bässler, E. L., Ngo-Anh, T. J., Geisler, H. S., Ruppersberg, J. P. & Gründer, S. Molecular and functional characterization of acid-sensing ion channel (ASIC) 1b. *J. Biol. Chem.* 276, 33782–33787 (2001).
46. van Bemmelen, M. X., Huser, D., Gautschi, I. & Schild, L. The Human Acid-Sensing Ion Channel ASIC1a: Evidence for a Homotetrameric Assembly State at the Cell Surface. *PLoS ONE* 10, e0135191 (2015).
47. Babinski, K., Catarsi, S., Biagini, G. & Séguéla, P. Mammalian ASIC2a and ASIC3 subunits co-assemble into heteromeric proton-gated channels sensitive to Gd3+. *J. Biol. Chem.* 275, 28519–28525 (2000).
48. Bassilana, F. *et al.* The acid-sensitive ionic channel subunit ASIC and the mammalian degenerin MDEG form a heteromultimeric H+-gated Na+ channel with novel properties. *J. Biol. Chem.* 272, 28819–28822 (1997).
49. Benson, C. J. *et al.* Heteromultimers of DEG/ENaC subunits form H+-gated channels in mouse sensory neurons. *Proceedings of the National Academy of Sciences* 99, 2338–2343 (2002).
50. Hoagland, E. N., Sherwood, T. W., Lee, K. G., Walker, C. J. & Askwith, C. C. Identification of a calcium permeable human acid-sensing ion channel 1 transcript variant. *J. Biol. Chem.* 285, 41852–41862 (2010).
51. Sherwood, T. W., Lee, K. G., Gormley, M. G. & Askwith, C. C. Heteromeric acid-sensing ion channels (ASICs) composed of ASIC2b and ASIC1a display novel channel properties and contribute to acidosis-induced neuronal death. *J. Neurosci.* 31, 9723–9734 (2011).
52. Jasti, J., Furukawa, H., Gonzales, E. B. & Gouaux, E. Structure of acid-sensing ion channel 1 at 1.9 A resolution and low pH. *Nature* 449, 316–323 (2007).

53. Gonzales, E. B., Kawate, T. & Gouaux, E. Pore architecture and ion sites in acid-sensing ion channels and P2X receptors. *Nature* 460, 599–604 (2009).
54. Chu, X.-P., Papasian, C. J., Wang, J. Q. & Xiong, Z.-G. Modulation of acid-sensing ion channels: molecular mechanisms and therapeutic potential. *Int J Physiol Pathophysiol Pharmacol* 3, 288–309 (2011).
55. Swain, S. M. & Bera, A. K. Coupling of proton binding in extracellular domain to channel gating in acid-sensing ion channel. *J. Mol. Neurosci.* 51, 199–207 (2013).
56. Sluka, K. A., Winter, O. C. & Wemmie, J. A. Acid-sensing ion channels: A new target for pain and CNS diseases. *Curr Opin Drug Discov Devel* 12, 693–704 (2009).
57. Kellenberger, S. & Schild, L. Epithelial sodium channel/degenerin family of ion channels: a variety of functions for a shared structure. *Physiol. Rev.* 82, 735–767 (2002).
58. Saugstad, J. A., Roberts, J. A., Dong, J., Zeitouni, S. & Evans, R. J. Analysis of the membrane topology of the acid-sensing ion channel 2a. *J. Biol. Chem.* 279, 55514–55519 (2004).
59. Yu, Y. *et al.* A nonproton ligand sensor in the acid-sensing ion channel. *Neuron* 68, 61–72 (2010).
60. Dubé, G. R., Elagoz, A. & Mangat, H. Acid sensing ion channels and acid nociception. *Curr. Pharm. Des.* 15, 1750–1766 (2009).
61. Escoubas, P. *et al.* Isolation of a tarantula toxin specific for a class of proton-gated Na+ channels. *J. Biol. Chem.* 275, 25116–25121 (2000).
62. Chen, X., Kalbacher, H. & Gründer, S. The tarantula toxin psalmotoxin 1 inhibits acid-sensing ion channel (ASIC) 1a by increasing its apparent H+ affinity. *The Journal of General Physiology* 126, 71–79 (2005).
63. Chen, X., Kalbacher, H. & Gründer, S. Interaction of acid-sensing ion channel (ASIC) 1 with the tarantula toxin psalmotoxin 1 is state dependent. *The Journal of General Physiology* 127, 267–276 (2006).
64. Dawson, R. J. P. *et al.* Structure of chicken acid-sensing ion channel 1 AT 3.0 A resolution in complex with psalmotoxin. (2012). doi:10.2210/pdb3s3x/pdb
65. Saez, N. J. *et al.* A dynamic pharmacophore drives the interaction between Psalmotoxin-1 and the putative drug target acid-sensing ion channel 1a. *Mol. Pharmacol.* 80, 796–808 (2011).
66. Sherwood, T. *et al.* Identification of protein domains that control proton and calcium sensitivity of ASIC1a. *J. Biol. Chem.* 284, 27899–27907 (2009).

67. Schild, L., Schneeberger, E., Gautschi, I. & Firsov, D. Identification of amino acid residues in the alpha, beta, and gamma subunits of the epithelial sodium channel (ENaC) involved in amiloride block and ion permeation. *The Journal of General Physiology* 109, 15–26 (1997).
68. Korkushko, A. O., Kryshtal, O. A., Bessonov, B. I. & Klyshta, M. D. [Blocking by amiloride of hydrogen ion-activated sodium permeability of sensory neuron membranes]. *Vrach Delo* 84–87 (1984).
69. Formaker, B. K., Hettinger, T. P., Savoy, L. D. & Frank, M. E. Amiloride-Sensitive and Amiloride-Insensitive Responses to NaCl + Acid Mixtures in Hamster Chorda Tympani Nerve. *Chemical Senses* 37, 603–612 (2012).
70. Kuduk, S. D. *et al.* Synthesis, structure-activity relationship, and pharmacological profile of analogs of the ASIC-3 inhibitor A-317567. *ACS Chem Neurosci* 1, 19–24 (2010).
71. Tomaszewski, A. & Büsselberg, D. Cisplatin modulates voltage gated channel currents of dorsal root ganglion neurons of rats. *NeuroToxicology* 28, 49–58 (2007).
72. Schmidt, A., Rossetti, G., Joussen, S. & Gründer, S. Diminazene Is a Slow Pore Blocker of Acid-Sensing Ion Channel 1a (ASIC1a). *Mol. Pharmacol.* 92, 665–675 (2017).
73. Chen, X. *et al.* Diarylamidines: high potency inhibitors of acid-sensing ion channels. *Neuropharmacology* 58, 1045–1053 (2010).
74. McCarthy, C. A., Rash, L. D., Chassagnon, I. R., King, G. F. & Widdop, R. E. PcTx1 affords neuroprotection in a conscious model of stroke in hypertensive rats via selective inhibition of ASIC1a. *Neuropharmacology* 99, 650–657 (2015).
75. Pignataro, G. *et al.* ASIC1a contributes to neuroprotection elicited by ischemic preconditioning and postconditioning. *Int J Physiol Pathophysiol Pharmacol* 3, 1–8 (2011).
76. Mari, Y., Katnik, C. & Cuevas, J. ASIC1a channels are activated by endogenous protons during ischemia and contribute to synergistic potentiation of intracellular Ca2+ overload during ischemia and acidosis. *Cell Calcium* 48, 70–82 (2010).
77. Pignataro, G., Simon, R. P. & Xiong, Z.-G. Prolonged activation of ASIC1a and the time window for neuroprotection in cerebral ischaemia. *Brain* 130, 151–158 (2007).
78. Lingueglia, E. Acid-sensing ion channels in sensory perception. *J. Biol. Chem.* 282, 17325–17329 (2007).

79. Yin, H. L. & Stossel, T. P. Control of cytoplasmic actin gel-sol transformation by gelsolin, a calcium-dependent regulatory protein. *Nature* 281, 583–586 (1979).
80. Sun, H. Q., Yamamoto, M., Mejillano, M. & Yin, H. L. Gelsolin, a multifunctional actin regulatory protein. *J. Biol. Chem.* 274, 33179–33182 (1999).
81. Li, G. H., Arora, P. D., Chen, Y., McCulloch, C. A. & Liu, P. Multifunctional roles of gelsolin in health and diseases. *Med Res Rev* 32, 999–1025 (2012).
82. Wen, D. *et al.* The plasma and cytoplasmic forms of human gelsolin differ in disulfide structure. *Biochemistry* 35, 9700–9709 (1996).
83. Allen, P. G. Functional consequences of disulfide bond formation in gelsolin. *FEBS Lett.* 401, 89–94 (1997).
84. Wongsantichon, J., Robinson, R. C. & Gettemans, J. Gelsolin nanobody shielding mutant plasma gelsolin from furin proteolysis. (2015). doi:10.2210/pdb4s10/pdb
85. Van Overbeke, W. *et al.* An ER-directed gelsolin nanobody targets the first step in amyloid formation in a gelsolin amyloidosis mouse model. *Hum. Mol. Genet.* 24, 2492–2507 (2015).
86. Nag, S. *et al.* Ca2+ binding by domain 2 plays a critical role in the activation and stabilization of gelsolin. *Proc. Natl. Acad. Sci. U.S.A.* 106, 13713–13718 (2009).
87. Bucki, R., Levental, I., Kulakowska, A. & Janmey, P. A. Plasma gelsolin: function, prognostic value, and potential therapeutic use. *Curr. Protein Pept. Sci.* 9, 541–551 (2008).
88. McLaughlin, P. J., Gooch, J. T., Mannherz, H. G. & Weeds, A. G. Structure of gelsolin segment 1-actin complex and the mechanism of filament severing. *Nature* 364, 685–692 (1993).
89. Wang, H. *et al.* Helix straightening as an activation mechanism in the gelsolin superfamily of actin regulatory proteins. *J. Biol. Chem.* 284, 21265–21269 (2009).
90. Kazmirski, S. L. *et al.* Loss of a metal-binding site in gelsolin leads to familial amyloidosis–Finnish type. *Nature Structural Biology* 9, 112–116 (2002).
91. Pope, B. J., Gooch, J. T. & Weeds, A. G. Probing the effects of calcium on gelsolin. *Biochemistry* 36, 15848–15855 (1997).
92. Ashish *et al.* Global structure changes associated with Ca2+ activation of full-length human plasma gelsolin. *J. Biol. Chem.* 282, 25884–25892 (2007).
93. Kazmirski, S. L., Howard, M. J., Isaacson, R. L. & Fersht, A. R. Elucidating the mechanism of familial amyloidosis- Finnish type:

NMR studies of human gelsolin domain 2. *Proceedings of the National Academy of Sciences* 97, 10706–10711 (2000).

94. Nag, S., Larsson, M., Robinson, R. C. & Burtnick, L. D. Gelsolin: the tail of a molecular gymnast. *Cytoskeleton (Hoboken)* 70, 360–384 (2013).

95. Vouyiouklis, D. A. & Brophy, P. J. A novel gelsolin isoform expressed by oligodendrocytes in the central nervous system. *J. Neurochem.* 69, 995–1005 (1997).

96. Endres, M. *et al.* Neuroprotective effects of gelsolin during murine stroke. *J. Clin. Invest.* 103, 347–354 (1999).

97. Carro, E. Gelsolin as therapeutic target in Alzheimer's disease. *Expert Opin. Ther. Targets* 14, 585–592 (2010).

98. Eke Gungor, H., Sahiner, U. M., Karakukcu, C., Sahiner, N. & Altuner Torun, Y. The plasma gelsolin levels in atopic dermatitis: Effect of atopy and disease severity. *Allergol Immunopathol (Madr)* 44, 221–225 (2016).

99. Silacci, P. *et al.* Gelsolin superfamily proteins: key regulators of cellular functions. *Cellular and Molecular Life Sciences* 61, 2614–2623 (2004).

100. Meretoja, J. Familial systemic paramyloidosis with lattice dystrophy of the cornea, progressive cranial neuropathy, skin changes and various internal symptoms. A previously unrecognized heritable syndrome. *Ann. Clin. Res.* 1, 314–324 (1969).

101. la Chapelle, de, A., Kere, J., Sack, G. H., Tolvanen, R. & Maury, C. P. Familial amyloidosis, Finnish type: G654----a mutation of the gelsolin gene in Finnish families and an unrelated American family. *Genomics* 13, 898–901 (1992).

102. Levy, E. *et al.* Mutation in gelsolin gene in Finnish hereditary amyloidosis. *J. Exp. Med.* 172, 1865–1867 (1990).

103. Carrwik, C. & Stenevi, U. Lattice corneal dystrophy, gelsolin type (Meretoja's syndrome). *Acta Ophthalmol* 87, 813–819 (2009).

104. Sethi, S. *et al.* Clinical, biopsy, and mass spectrometry findings of renal gelsolin amyloidosis. *Kidney Int.* 91, 964–971 (2017).

105. Efebera, Y. A. *et al.* Novel gelsolin variant as the cause of nephrotic syndrome and renal amyloidosis in a large kindred. *Amyloid* 21, 110–112 (2014).

106. Landolt, A. M., Kleihues, P. & Heitz, P. U. Amyloid deposits in pituitary adenomas. Differentiation of two types. *Arch. Pathol. Lab. Med.* 111, 453–458 (1987).

107. Bonì, F. *et al.* Molecular basis of a novel renal amyloidosis due to N184K gelsolin variant. *Sci Rep* 6, 33463 (2016).

108. Bonì, F. *et al.* Gelsolin pathogenic Gly167Arg mutation promotes domain-swap dimerization of the protein. *Hum. Mol. Genet.* 27, 53–65 (2017).
109. Srivastava, A. *et al.* The Gelsolin Pathogenic D187N Mutant Exhibits Altered Conformational Stability and Forms Amyloidogenic Oligomers. *Biochemistry* 57, 2359–2372 (2018).
110. Isaacson, R. L., Weeds, A. G. & Fersht, A. R. Equilibria and kinetics of folding of gelsolin domain 2 and mutants involved in familial amyloidosis-Finnish type. *Proceedings of the National Academy of Sciences* 96, 11247–11252 (1999).
111. Chen, C. D. Furin initiates gelsolin familial amyloidosis in the Golgi through a defect in Ca2+ stabilization. *The EMBO Journal* 20, 6277–6287 (2001).
112. Ratnaswamy, G., Huff, M. E., Su, A. I., Rion, S. & Kelly, J. W. Destabilization of Ca2+-free gelsolin may not be responsible for proteolysis in Familial Amyloidosis of Finnish Type. *Proceedings of the National Academy of Sciences* 98, 2334–2339 (2001).
113. Hamers-Casterman, C. *et al.* Naturally occurring antibodies devoid of light chains. *Nature* 363, 446–448 (1993).
114. Frenken, L. G. *et al.* Isolation of antigen specific llama VHH antibody fragments and their high level secretion by Saccharomyces cerevisiae. *J. Biotechnol.* 78, 11–21 (2000).
115. Muyldermans, S. Single domain camel antibodies: current status. *J. Biotechnol.* 74, 277–302 (2001).
116. Muyldermans, S., Cambillau, C. & Wyns, L. Recognition of antigens by single-domain antibody fragments: the superfluous luxury of paired domains. *Trends Biochem. Sci.* 26, 230–235 (2001).
117. Muyldermans, S. Nanobodies: Natural Single-Domain Antibodies. *Annual Review of Biochemistry* 82, 775–797 (2013).
118. De Genst, E. *et al.* Molecular basis for the preferential cleft recognition by dromedary heavy-chain antibodies. *Proceedings of the National Academy of Sciences* 103, 4586–4591 (2006).
119. Rasmussen, S. G. F. *et al.* Structure of a nanobody-stabilized active state of the β(2) adrenoceptor. *Nature* 469, 175–180 (2011).
120. De Meyer, T., Muyldermans, S. & Depicker, A. Nanobody-based products as research and diagnostic tools. *Trends Biotechnol.* 32, 263–270 (2014).
121. Chakravarty, R., Goel, S. & Cai, W. Nanobody: the 'magic bullet' for molecular imaging? *Theranostics* 4, 386–398 (2014).
122. Kijanka, M., Dorresteijn, B., Oliveira, S. & van Bergen en Henegouwen, P. M. P. Nanobody-based cancer therapy of solid tumors. *Nanomedicine (Lond)* 10, 161–174 (2015).

123. Oliveira, S., Heukers, R., Sornkom, J., Kok, R. J. & van Bergen en Henegouwen, P. M. P. Targeting tumors with nanobodies for cancer imaging and therapy. *J Control Release* 172, 607–617 (2013).
124. Newby, Z. E. R. *et al.* A general protocol for the crystallization of membrane proteins for X-ray structural investigation. *Nat Protoc* 4, 619–637 (2009).
125. Van Overbeke, W. *et al.* Chaperone nanobodies protect gelsolin against MT1-MMP degradation and alleviate amyloid burden in the gelsolin amyloidosis mouse model. *Mol. Ther.* 22, 1768–1778 (2014).
126. Verhelle, A. *et al.* AAV9 delivered bispecific nanobody attenuates amyloid burden in the gelsolin amyloidosis mouse model. *Hum. Mol. Genet.* 26, 3030–3030 (2017).
127. Baconguis, I. & Gouaux, E. Structural plasticity and dynamic selectivity of acid-sensing ion channel-spider toxin complexes. *Nature* 489, 400–405 (2012).
128. Yoder, N., Yoshioka, C. & Gouaux, E. Gating mechanisms of acid-sensing ion channels. *Nature* 555, 397–401 (2018).
129. Liu, S., Cheng, X.-Y., Wang, F. & Liu, C.-F. Acid-sensing ion channels: potential therapeutic targets for neurologic diseases. *Transl Neurodegener* 4, 10 (2015).
130. Baconguis, I., Bohlen, C. J., Goehring, A., Julius, D. & Gouaux, E. X-ray structure of acid-sensing ion channel 1-snake toxin complex reveals open state of a Na(+)-selective channel. *Cell* 156, 717–729 (2014).
131. Jinn-Moon Yang & Cheng-Yan Kao. A family competition evolutionary algorithm for automated docking of flexible ligands to proteins. *IEEE Transactions on Information Technology in Biomedicine* 4, 225–237 (2000).
132. Long, Y. & Li, Z. in *Patch Clamp Technique* (InTech, 2012). doi:10.5772/35069
133. Yokokawa, M., Carnally, S. M., Henderson, R. M., Takeyasu, K. & Edwardson, J. M. Acid-sensing ion channel (ASIC) 1a undergoes a height transition in response to acidification. *FEBS Lett.* 584, 3107–3110 (2010).
134. Yamaguchi, H. & Miyazaki, M. Refolding techniques for recovering biologically active recombinant proteins from inclusion bodies. *Biomolecules* 4, 235–251 (2014).
135. Unger, T., Jacobovitch, Y., Dantes, A., Bernheim, R. & Peleg, Y. Applications of the Restriction Free (RF) cloning procedure for

molecular manipulations and protein expression. *J. Struct. Biol.* 172, 34–44 (2010).

136. Dawson, R. J. P. *et al.* Structure of the acid-sensing ion channel 1 in complex with the gating modifier Psalmotoxin 1. *Nat Commun* 3, 936 (2012).

137. Gonzales, E. B. & Gouaux, E. Crystal structure of a functional acid sensing ion channel in the desensitized state. (2009). doi:10.2210/pdb3hgc/pdb

138. Weyer, U. & Possee, R. D. Functional analysis of the p10 gene 5' leader sequence of the Autographa californica nuclear polyhedrosis virus. *Nucleic Acids Research* 16, 3635–3653 (1988).

139. He, Y., Wang, K. & Yan, N. The recombinant expression systems for structure determination of eukaryotic membrane proteins. *Protein & Cell* 5, 658–672 (2014).

140. Huff, M. E., Page, L. J., Balch, W. E. & Kelly, J. W. Gelsolin Domain 2 Ca2+ Affinity Determines Susceptibility to Furin Proteolysis and Familial Amyloidosis of Finnish Type. *J. Mol. Biol.* 334, 119–127 (2003).

141. Bonì, F. *et al.* Molecular basis of a novel renal amyloidosis due to N184K gelsolin variant. *Sci Rep* 6, 33463 (2016).

142. Wacker, S. A., Bradley, M. J., Marion, J. & Bell, E. Ligand-induced changes in the conformational stability and flexibility of glutamate dehydrogenase and their role in catalysis and regulation. *Protein Science* 19, 1820–1829 (2010).

143. Sun, D. *et al.* Cryo-EM structure of the ASIC1a-mambalgin-1 complex reveals that the peptide toxin mambalgin-1 inhibits acid-sensing ion channels through an unusual allosteric effect. *Cell Discov* 4, 27 (2018).

144. Van Der Spoel, D. *et al.* GROMACS: fast, flexible, and free. *Journal of Computational Chemistry* 26, 1701–1718 (2005).

145. Morris, G. M. *et al.* Automated docking using a Lamarckian genetic algorithm and an empirical binding free energy function. *Journal of Computational Chemistry* 19, 1639–1662 (1998).

146. Alexandrov, A. I., Mileni, M., Chien, E. Y. T., Hanson, M. A. & Stevens, R. C. Microscale fluorescent thermal stability assay for membrane proteins. *Structure* 16, 351–359 (2008).

147. Chesnoy, J. & Fini, L. in *Ultrafast Phenomena V* 46, 14–16 (Springer Berlin Heidelberg, 1986).

148. Kabsch, W. XDS. *Acta Crystallographica Section D Biological Crystallography* 66, 125–132 (2010).

149. Evans, P. R. & Murshudov, G. N. How good are my data and what is the resolution? *Acta Crystallographica Section D Biological Crystallography* 69, 1204–1214 (2013).
150. McCoy, A. J. *et al.* Phaser crystallographic software. *J Appl Crystallogr* 40, 658–674 (2007).
151. Adams, P. D. *et al.* PHENIX: a comprehensive Python-based system for macromolecular structure solution. *Acta Crystallographica Section D Biological Crystallography* 66, 213–221 (2010).
152. Emsley, P., Lohkamp, B., Scott, W. G. & Cowtan, K. Features and development of Coot. *Acta Crystallographica Section D Biological Crystallography* 66, 486–501 (2010).
153. de Rosa, M. *et al.* Decoding the Structural Bases of D76N ß2-Microglobulin High Amyloidogenicity through Crystallography and Asn-Scan Mutagenesis. *PLoS ONE* 10, e0144061 (2015).

8 Supplementary

8.1 Index of figures and tables

Index of figures

Index of tables

8.2 Index of abbreviations

ASIC1	Acid- Sensing Ion Channel 1
BBB	Blood Brain Barrier
cASIC1	Chicken ASIC1
CD	circular dichroism
CHO	Chinese hamster ovarian cells
CHS	Cholesteryl hemisuccinate tris salt
DA	Diminazene Aceturate
dNTPs	deoxyribonucleotidetriphosphates
E. coli	Escherichia coli.
EB	Energy of binding
ECD	Extracellular domain
ECD	Extracellular domain
FL	Full- length
FSEC	Fluorescence-Detection Size-Exclusion Chromatography
G2	Gelsolin-second domain
GFP	Green Fluorescence Protein
GOI	Gene of interest
GPCRs	G protein-coupled receptor
GSN	Gelsolin- Full length protein
HEK	Human Embryonic Kidney cells
HTP	high-throughput
LCP	Lipid-Cubic Phase
mASIC1a	Mouse ASIC1a
MDS	Molecular Dynamics Simulation
MPs	Membrane proteins
NanoDSF	Nano differential scanning fluorimetry
Nb11	Nanobody 11
PCR	Polymerase Chain Reaction
PDB	Protein Data Bank
POI	Protein of interest
RF	Restriction Free
SBDD	Structure- Based Drug Design
Sf9	Spodoptera frugiperda Sf9 cells

8.3 Supplementary material and methods

This appendix will provide a detailed overview of the experimental conditions that are not presented in the material and method chapter of each project.

Buffers

Note: Temperature-sensitive buffers (e.g. Tris-HCl buffers) are adjusted to the needed pH at the temperature that the buffer will be used.

Detergent stocks:

10% DDM + 2% CHS (From Anatrace): dissolve 1gr of DDM in 9,5 mL of MilliQ water**,** 0.2 gr CHS and top-up to 10ml**.** Mixing at +4C for overnight, until it will be dissolved completely. Store at -20C. Note: thaw at RT before the use.

Protein gels:

Sodium dodecyl sulphate poly acrylamide gel electrophoresis (SDS-PAGE):

MES running buffer: 20× MES stock from Invitrogen (50 mM Tris base, 50 mM MES (2-(N-morpholino) ethane sulfonic acid), 1 mM EDTA, 0.1% SDS at pH 7.3).

Coomassie Brilliant Blue staining solution: Coomassie Brilliant Blue R250 (0.25% w/v), methanol (45% v/v), MilliQ H_2O (45% v/v), glacial acetic acid (10% v/v).

Coomassie distain solution: Methanol (45% v/v), MilliQ H2O (45% v/v), glacial acetic acid (10% v/v).

Protein markers:

BenchMark ™ Fluorescence protein standard (Invitrogen™)

SeeBlue Plus2 prestained protein standard (Invitrogen™)

Nickel beads

ProBond™ Nickel-Chelating Resin (Invitrogen™). Binding capacity of 1-5 mg of recombinant protein per 1 ml of resin.

8.3.1 The sequences of the primers used for cloning ASIC1, at the Weizmann Institute of Science

ASIC_mouse delta13_F

CACCATCATCACCACTCCGCGGGTGAAAACCTGTACTTCCAGGGTgtgggtggtgtccagccggt

ASIC_R

CCAGGAAAGGATCAGATCTGCAGCGGCCGCCTAccggtgcttaatgacctcatag

ASIC_mouse delta27_F

CACCATCATCACCACTCCGCGGGTGAAAACCTGTACTTCCAGGGTtccacgctgcacggtcttgc

ASIC1_chicken_F

CACCATCATCACCACTCCGCGGGTGAAAACCTGTACTTCCAGGGTgggcagccggtgagcatccag

ASIC1_chicken_R

CCAGGAAAGGATCAGATCTGCAGCGGCCGCCTAgcaggtgaagtcctcaaaggtg

In the case of cloning the two mouse constructs, two different forward primers have been designed so that it would be possible to generate the truncations at the N-term of the protein with the same reverse primer. No changes have been made at the C-term.

8.3.2 For colony-PCR and DNA analysis, the following sequencing primers were used for sequencing ASIC1 inserts cloned into baculovirus transfer vectors, pVL1393

polyhedrin forward: 5’ -AAATGATAACCATCTCGC-3’ (Invitrogen)

Polyhedrin reverse: 5’- GTCCAAGTTTCCCTG- 3’ (Invitrogen)

8.3.3 The 16 constructs of ASIC1 designed for the high-throughput cloning

Description	Chicken ASIC1a template
Species	Gallus Gallus
Cloning vector	pOPINN-GFP
DNA sequence	ATGGACCTGAAGGTGGACGAGGAGGAGGTGGACAGCGGGCAGCCGGTGAGCATCCAGGCC TTCGCCAGCAGCTCCACCCTGCACGGGATCTCGCACATCTTCTCCTACGAGCGGCTGTCG CTGAAGCGCGTGGTCTGGGCGCTCTGCTTCATGGGTTCGCTGGCGCTGCTCGCCCTGGTC TGCACCAACCGCATCCAGTACTACTTCCTCTACCCCCACGTCACCAAGCTGGACGAGGTG GCCGCCACCAGGCTCACCTTCCCTGCTGTCACCTTCTGCAACCTCAACGAGTTCCGCTTC AGCCGGGTGACCAAGAACGACCTGTACCACGCCGGGGAACTCCTCGCCCTGCTCAATAAC AGATACGAGATCCCGGACACACAGACAGCTGATGAGAAGCAGCTGGAAATCCTACAGGAC AAGGCAAACTTCCGAAACTTCAAGCCCAAACCTTTCAATATGTTGGAGTTTTACGACCGC GCCGGCCACGACATCCGGGAGATGCTGCTCTCCTGCTTCTTCCGTGGGGAGCAGTGCAGC CCTGAAGACTTCAAAGTGGTGTTCACACGCTATGGGAAGTGCTACACGTTCAACGCAGGG CAGGATGGCAAACCCCGGCTCATCACCATGAAGGGGGGCACTGGAAATGGCCTGGAGATC ATGCTGGACATCCAGCAGGACGAGTACCTCCCAGTGTGGGGGGAAACAGATGAGACCTCA TTTGAAGCCGGGATCAAGGTGCAGATCCACAGCCAGGATGAGCCTCCACTCATCGACCAG CTGGGCTTCGGTGTGGCACCCGGCTTCCAGACCTTCGTGTCCTGCCAGGAGCAGCGGCTC ATCTACCTGCCACCTCCCTGGGGCGACTGTAAGGCCACAACGGGTGACTCGGAGTTCTAC GACACTTACAGCATCACTGCCTGCCGCATCGACTGCGAGACCCGCTACCTGGTGGAGAAC TGCAACTGCCGCATGGTGCACATGCCAGGCGATGCCCCTTATTGCACCCCAGAGCAGTAC AAGGAGTGTGCAGATCCAGCCTTAGATTTCCTGGTGGAGAAGGACAATGAGTACTGTGTC TGTGAGATGCCCTGCAACGTCACCCGCTATGGCAAAGAGCTCTCCATGGTGAAGATCCCC AGCAAAGCCTCCGCCAAGTACCTGGCCAAGAAGTACAACAAGTCGGAGCAGTACATCGGG GAGAACATCCTGGTGCTGGACATCTTCTTTGAAGCCCTGAACTATGAGACAATCGAGCAG AAGAAGGCGTATGAGGTGGCTGGATTGCTGGGTGACATCGGAGGACAGATGGGGCTGTTT ATCGGGGCCAGCATCCTCACTGTGCTGGAGCTCTTTGACTACGCCTATGAGGTGATCAAG CACCGGCTGTGCCGGCGGGGCAAATGCCGCAAGAACCACAAGAGGAACAACACGGACAAG GGCGTCGCGCTGAGCATGGATGATGTGAAACGCCACAACCCCTGTGAGAGCCTACGGGGT CACCCGGCTGGCATGACGTACGCA
Amino acid sequence (508 aa)	MDLKVDEEEVDSGQPVSIQAFASSSTLHGISHIFSYERLSLKRVVWALCFMGSLALLALV CTNRIQYYFLYPHVTKLDEVAATRLTFPAVTFCNLNEFRFSRVTKNDLYHAGELLALLNN RYEIPDTQTADEKQLEILQDKANFRNFKPKPFNMLEFYDRAGHDIREMLLSCFFRGEQCS PEDFKVVFTRYGKCYTFNAGQDGKPRLITMKGGTGNGLEIMLDIQQDEYLPVWGETDETS FEAGIKVQIHSQDEPPLIDQLGFGVAPGFQTFVSCQEQRLIYLPPPWGDCKATTGDSEFY DTYSITACRIDCETRYLVENCNCRMVHMPGDAPYCTPEQYKECADPALDFLVEKDNEYCV CEMPCNVTRYGKELSMVKIPSKASAKYLAKKYNKSEQYIGENILVLDIFFEALNYETIEQ KKAYEVAGLLGDIGGQMGLFIGASILTVLELFDYAYEVIKHRLCRRGKCRKNHKRNNTDK GVALSMDDVKRHNPCESLRGHPAGMTYA
Forward primer	aagttctgtttcagggcccgATGGACCTGAAGGTGGACGAGGAG
Reverse primer	atggtctagaaagctttaTGCGTACGTCATGCCAGCCG
Theoretical protein size	57.79 kDa
Description	Chicken ASIC1a – Delta 13 (D13)
Species	Gallus Gallus
Cloning vector	pOPINN-GFP
DNA sequence	GGGCAGCCGGTGAGCATCCAGGCCTTCGCCAGCAGCTCCACCCTGCACGGGATCTCGCAC ATCTTCTCCTACGAGCGGCTGTCGCTGAAGCGCGTGGTCTGGGCGCTCTGCTTCATGGGT TCGCTGGCGCTGCTCGCCCTGGTCTGCACCAACCGCATCCAGTACTACTTCCTCTACCCC CACGTCACCAAGCTGGACGAGGTGGCCGCCACCAGGCTCACCTTCCCTGCTGTCACCTTC TGCAACCTCAACGAGTTCCGCTTCAGCCGGGTGACCAAGAACGACCTGTACCACGCCGGG GAACTCCTCGCCCTGCTCAATAACAGATACGAGATCCCGGACACACAGACAGCTGATGAG

	AAGCAGCTGGAAATCCTACAGGACAAGGCAAACTTCCGAAACTTCAAGCCCAAACCTTTC AATATGTTGGAGTTTTACGACCGCGCCGGCCACGACATCCGGGAGATGCTGCTCTCCTGC TTCTTCCGTGGGGAGCAGTGCAGCCCTGAAGACTTCAAAGTGGTGTTCACACGCTATGGG AAGTGCTACACGTTCAACGCAGGGCAGGATGGCAAACCCCGGCTCATCACCATGAAGGGG GGCACTGGAAATGGCCTGGAGATCATGCTGGACATCCAGCAGGACGAGTACCTCCCAGTG TGGGGGGAAACAGATGAGACCTCATTTGAAGCCGGGATCAAGGTGCAGATCCACAGCCAG GATGAGCCTCCACTCATCGACCAGCTGGGCTTCGGTGTGGCACCCGGCTTCCAGACCTTC GTGTCCTGCCAGGAGCAGCGGCTCATCTACCTGCCACCTCCCTGGGGCGACTGTAAGGCC ACAACGGGTGACTCGGAGTTCTACGACACTTACAGCATCACTGCCTGCCGCATCGACTGC GAGACCCGCTACCTGGTGGAGAACTGCAACTGCCGCATGGTGCACATGCCAGGCGATGCC CCTTATTGCACCCCAGAGCAGTACAAGGAGTGTGCAGATCCAGCCTTAGATTTCCTGGTG GAGAAGGACAATGAGTACTGTGTCTGTGAGATGCCCTGCAACGTCACCCGCTATGGCAAA GAGCTCTCCATGGTGAAGATCCCCAGCAAAGCCTCCGCCAAGTACCTGGCCAAGAAGTAC AACAAGTCGGAGCAGTACATCGGGGAGAACATCCTGGTGCTGGACATCTTCTTTGAAGCC CTGAACTATGAGACAATCGAGCAGAAGAAGGCGTATGAGGTGGCTGGATTGCTGGGTGAC ATCGGAGGACAGATGGGGCTGTTTATCGGGGCCAGCATCCTCACTGTGCTGGAGCTCTTT GACTACGCCTATGAGGTGATCAAGCACCGG
Amino acid sequence (450 aa)	GQPVSIQAFASSSTLHGISHIFSYERLSLKRVVWALCFMGSLALLALVCTNRIQYYFLYP HVTKLDEVAATRLTFPAVTFCNLNEFRFSRVTKNDLYHAGELLALLNNRYEIPDTQTADE KQLEILQDKANFRNFKPKPFNMLEFYDRAGHDIREMLLSCFFRGEQCSPEDFKVVFTRYG KCYTFNAGQDGKPRLITMKGGTGNGLEIMLDIQQDEYLPVWGETDETSFEAGIKVQIHSQ DEPPLIDQLGFGVAPGFQTFVSCQEQRLIYLPPPWGDCKATTGDSEFYDTYSITACRIDC ETRYLVENCNCRMVHMPGDAPYCTPEQYKECADPALDFLVEKDNEYCVCEMPCNVTRYGK ELSMVKIPSKASAKYLAKKYNKSEQYIGENILVLDIFFEALNYETIEQKKAYEVAGLLGD IGGQMGLFIGASILTVLELFDYAYEVIKHR
Forward primer	aggagatataccatgGGGCAGCCGGTGAGCATCCAG
Reverse primer	cagaacttccagtttCCGGTGCTTGATCACCTCATAGGCGTAG
Theoretical protein size	51.20 kDa
Description	Chicken ASIC1a – Delta 27 (D27)
Species	Gallus Gallus
Cloning vector	pOPINN-GFP
DNA sequence	ACCCTGCACGGGATCTCGCACATCTTCTCCTACGAGCGGCTGTCGCTGAAGCGCGTGGTC TGGGCGCTCTGCTTCATGGGTTCGCTGGCGCTGCTCGCCCTGGTCTGCACCAACCGCATC CAGTACTACTTCCTCTACCCCCACGTCACCAAGCTGGACGAGGTGGCCGCCACCAGGCTC ACCTTCCCTGCTGTCACCTTCTGCAACCTCAACGAGTTCCGCTTCAGCCGGGTGACCAAG AACGACCTGTACCACGCCGGGGAACTCCTCGCCCTGCTCAATAACAGATACGAGATCCCG GACACACAGACAGCTGATGAGAAGCAGCTGGAAATCCTACAGGACAAGGCAAACTTCCGA AACTTCAAGCCCAAACCTTTCAATATGTTGGAGTTTTACGACCGCGCCGGCCACGACATC CGGGAGATGCTGCTCTCCTGCTTCTTCCGTGGGGAGCAGTGCAGCCCTGAAGACTTCAAA GTGGTGTTCACACGCTATGGGAAGTGCTACACGTTCAACGCAGGGCAGGATGGCAAACCC CGGCTCATCACCATGAAGGGGGGCACTGGAAATGGCCTGGAGATCATGCTGGACATCCAG CAGGACGAGTACCTCCCAGTGTGGGGGGAAACAGATGAGACCTCATTTGAAGCCGGGATC AAGGTGCAGATCCACAGCCAGGATGAGCCTCCACTCATCGACCAGCTGGGCTTCGGTGTG GCACCCGGCTTCCAGACCTTCGTGTCCTGCCAGGAGCAGCGGCTCATCTACCTGCCACCT CCCTGGGGCGACTGTAAGGCCACAACGGGTGACTCGGAGTTCTACGACACTTACAGCATC ACTGCCTGCCGCATCGACTGCGAGACCCGCTACCTGGTGGAGAACTGCAACTGCCGCATG GTGCACATGCCAGGCGATGCCCCTTATTGCACCCCAGAGCAGTACAAGGAGTGTGCAGAT CCAGCCTTAGATTTCCTGGTGGAGAAGGACAATGAGTACTGTGTCTGTGAGATGCCCTGC AACGTCACCCGCTATGGCAAAGAGCTCTCCATGGTGAAGATCCCCAGCAAAGCCTCCGCC AAGTACCTGGCCAAGAAGTACAACAAGTCGGAGCAGTACATCGGGGAGAACATCCTGGTG CTGGACATCTTCTTTGAAGCCCTGAACTATGAGACAATCGAGCAGAAGAAGGCGTATGAG GTGGCTGGATTGCTGGGTGACATCGGAGGACAGATGGGGCTGTTTATCGGGGCCAGCATC CTCACTGTGCTGGAGCTCTTTGACTACGCCTATGAGGTGATCAAGCACCGG
Amino acid sequence (437 aa)	TLHGISHIFSYERLSLKRVVWALCFMGSLALLALVCTNRIQYYFLYPHVTKLDEVAATRL TFPAVTFCNLNEFRFSRVTKNDLYHAGELLALLNNRYEIPDTQTADEKQLEILQDKANFR NFKPKPFNMLEFYDRAGHDIREMLLSCFFRGEQCSPEDFKVVFTRYGKCYTFNAGQDGKP

	RLITMKGGTGNGLEIMLDIQQDEYLPVWGETDETSFEAGIKVQIHSQDEPPLIDQLGFGV APGFQTFVSCQEQRLIYLPPPWGDCKATTGDSEFYDTYSITACRIDCETRYLVENCNCRM VHMPGDAPYCTPEQYKECADPALDFLVEKDNEYCVCEMPCNVTRYGKELSMVKIPSKASA KYLAKKYNKSEQYIGENILVLDIFFEALNYETIEQKKAYEVAGLLGDIGGQMGLFIGASI LTVLELFDYAYEVIKHR
Forward primer	aggagatataccatgACCCTGCACGGGATCTCGC
Reverse primer	cagaacttccagtttCCGGTGCTTGATCACCTCATAGGCGTAG
Theoretical protein size	49.94 kDa
Description	Chicken ASIC1a – Delta 38 (D38)
Species	Gallus Gallus
Cloning vector	pOPINN-GFP
DNA sequence	CGGCTGTCGCTGAAGCGCGTGGTCTGGGCGCTCTGCTTCATGGGTTCGCTGGCGCTGCTC GCCCTGGTCTGCACCAACCGCATCCAGTACTACTTCCTCTACCCCCACGTCACCAAGCTG GACGAGGTGGCCGCCACCAGGCTCACCTTCCCTGCTGTCACCTTCTGCAACCTCAACGAG TTCCGCTTCAGCCGGGTGACCAAGAACGACCTGTACCACGCCGGGGAACTCCTCGCCCTG CTCAATAACAGATACGAGATCCCGGACACACAGACAGCTGATGAGAAGCAGCTGGAAATC CTACAGGACAAGGCAAACTTCCGAAACTTCAAGCCCAAACCTTTCAATATGTTGGAGTTT TACGACCGCGCCGGCCACGACATCCGGGAGATGCTGCTCTCCTGCTTCTTCCGTGGGGAG CAGTGCAGCCCTGAAGACTTCAAAGTGGTGTTCACACGCTATGGGAAGTGCTACACGTTC AACGCAGGGCAGGATGGCAAACCCCGGCTCATCACCATGAAGGGGGGCACTGGAAATGGC CTGGAGATCATGCTGGACATCCAGCAGGACGAGTACCTCCCAGTGTGGGGGGAAACAGAT GAGACCTCATTTGAAGCCGGGATCAAGGTGCAGATCCACAGCCAGGATGAGCCTCCACTC ATCGACCAGCTGGGCTTCGGTGTGGCACCCGGCTTCCAGACCTTCGTGTCCTGCCAGGAG CAGCGGCTCATCTACCTGCCACCTCCCTGGGGCGACTGTAAGGCCACAACGGGTGACTCG GAGTTCTACGACACTTACAGCATCACTGCCTGCCGCATCGACTGCGAGACCCGCTACCTG GTGGAGAACTGCAACTGCCGCATGGTGCACATGCCAGGCGATGCCCCTTATTGCACCCCA GAGCAGTACAAGGAGTGTGCAGATCCAGCCTTAGATTTCCTGGTGGAGAAGGACAATGAG TACTGTGTCTGTGAGATGCCCTGCAACGTCACCCGCTATGGCAAAGAGCTCTCCATGGTG AAGATCCCCAGCAAAGCCTCCGCCAAGTACCTGGCCAAGAAGTACAACAAGTCGGAGCAG TACATCGGGGAGAACATCCTGGTGCTGGACATCTTCTTTGAAGCCCTGAACTATGAGACA ATCGAGCAGAAGAAGGCGTATGAGGTGGCTGGATTGCTGGGTGACATCGGAGGACAGATG GGGCTGTTTATCGGGGCCAGCATCCTCACTGTGCTGGAGCTCTTTGACTACGCCTATGAG
Amino acid sequence (420 aa)	RLSLKRVVWALCFMGSLALLALVCTNRIQYYFLYPHVTKLDEVAATRLTFPAVTFCNLNE FRFSRVTKNDLYHAGELLALLNNRYEIPDTQTADEKQLEILQDKANFRNFKPKPFNMLEF YDRAGHDIREMLLSCFFRGEQCSPEDFKVVFTRYGKCYTFNAGQDGKPRLITMKGGTGNG LEIMLDIQQDEYLPVWGETDETSFEAGIKVQIHSQDEPPLIDQLGFGVAPGFQTFVSCQE QRLIYLPPPWGDCKATTGDSEFYDTYSITACRIDCETRYLVENCNCRMVHMPGDAPYCTP EQYKECADPALDFLVEKDNEYCVCEMPCNVTRYGKELSMVKIPSKASAKYLAKKYNKSEQ YIGENILVLDIFFEALNYETIEQKKAYEVAGLLGDIGGQMGLFIGASILTVLELFDYAYE
Forward primer	aggagatataccatgCGGCTGTCGCTGAAGCGCG
Reverse primer	cagaacttccagtttCTCATAGGCGTAGTCAAAGAGCTCC
Theoretical protein size	47.92 kDa
Description	Chicken ASIC1a – Delta 44 (D44)
Species	Gallus Gallus
Cloning vector	pOPINN-GFP
DNA sequence	GTGGTCTGGGCGCTCTGCTTCATGGGTTCGCTGGCGCTGCTCGCCCTGGTCTGCACCAAC CGCATCCAGTACTACTTCCTCTACCCCCACGTCACCAAGCTGGACGAGGTGGCCGCCACC AGGCTCACCTTCCCTGCTGTCACCTTCTGCAACCTCAACGAGTTCCGCTTCAGCCGGGTG ACCAAGAACGACCTGTACCACGCCGGGGAACTCCTCGCCCTGCTCAATAACAGATACGAG ATCCCGGACACACAGACAGCTGATGAGAAGCAGCTGGAAATCCTACAGGACAAGGCAAAC TTCCGAAACTTCAAGCCCAAACCTTTCAATATGTTGGAGTTTTACGACCGCGCCGGCCAC GACATCCGGGAGATGCTGCTCTCCTGCTTCTTCCGTGGGGAGCAGTGCAGCCCTGAAGAC TTCAAAGTGGTGTTCACACGCTATGGGAAGTGCTACACGTTCAACGCAGGGCAGGATGGC AAACCCCGGCTCATCACCATGAAGGGGGGCACTGGAAATGGCCTGGAGATCATGCTGGAC

	ATCCAGCAGGACGAGTACCTCCCAGTGTGGGGGGAAACAGATGAGACCTCATTTGAAGCC GGGATCAAGGTGCAGATCCACAGCCAGGATGAGCCTCCACTCATCGACCAGCTGGGCTTC GGTGTGGCACCCGGCTTCCAGACCTTCGTGTCCTGCCAGGAGCAGCGGCTCATCTACCTG CCACCTCCCTGGGGCGACTGTAAGGCCACAACGGGTGACTCGGAGTTCTACGACACTTAC AGCATCACTGCCTGCCGCATCGACTGCGAGACCCGCTACCTGGTGGAGAACTGCAACTGC CGCATGGTGCACATGCCAGGCGATGCCCCTTATTGCACCCCAGAGCAGTACAAGGAGTGT GCAGATCCAGCCTTAGATTTCCTGGTGGAGAAGGACAATGAGTACTGTGTCTGTGAGATG CCCTGCAACGTCACCCGCTATGGCAAAGAGCTCTCCATGGTGAAGATCCCCAGCAAAGCC TCCGCCAAGTACCTGGCCAAGAAGTACAACAAGTCGGAGCAGTACATCGGGGAGAACATC CTGGTGCTGGACATCTTCTTTGAAGCCCTGAACTATGAGACAATCGAGCAGAAGAAGGCG TATGAGGTGGCTGGATTGCTGGGTGACATCGGAGGACAGATGGGGCTGTTTATCGGGGCC AGCATCCTCACTGTGCTGGAGCTCTTTGACTACGCC
Amino acid sequence (400 aa)	VVWALCFMGSLALLALVCTNRIQYYFLYPHVTKLDEVAATRLTFPAVTFCNLNEFRFSRV TKNDLYHAGELLALLNNRYEIPDTQTADEKQLEILQDKANFRNFKPKPFNMLEFYDRAGH DIREMLLSCFFRGEQCSPEDFKVVFTRYGKCYTFNAGQDGKPRLITMKGGTGNGLEIMLD IQQDEYLPVWGETDETSFEAGIKVQIHSQDEPPLIDQLGFGVAPGFQTFVSCQEQRLIYL PPPWGDCKATTGDSEFYDTYSITACRIDCETRYLVENCNCRMVHMPGDAPYCTPEQYKEC ADPALDFLVEKDNEYCVCEMPCNVTRYGKELSMVKIPSKASAKYLAKKYNKSEQYIGENI LVLDIFFEALNYETIEQKKAYEVAGLLGDIGGQMGLFIGASILTVLELFDYA
Forward primer	aggagatataccatgGTGGTCTGGGCGCTCTGCTTC
Reverse primer	cagaacttccagtttGGCGTAGTCAAAGAGCTCCAGCAC
Theoretical protein size	45.51 kDa
Description	Chicken ASIC1a – Extracellular domain (called Sol)
Species	Gallus Gallus
Cloning vector	pOPINN-GFP
DNA sequence	CCCCACGTCACCAAGCTGGACGAGGTGGCCGCCACCAGGCTCACCTTCCCTGCTGTCACC TTCTGCAACCTCAACGAGTTCCGCTTCAGCCGGGTGACCAAGAACGACCTGTACCACGCC GGGGAACTCCTCGCCCTGCTCAATAACAGATACGAGATCCCGGACACACAGACAGCTGAT GAGAAGCAGCTGGAAATCCTACAGGACAAGGCAAACTTCCGAAACTTCAAGCCCAAACCT TTCAATATGTTGGAGTTTTACGACCGCGCCGGCCACGACATCCGGGAGATGCTGCTCTCC TGCTTCTTCCGTGGGGAGCAGTGCAGCCCTGAAGACTTCAAAGTGGTGTTCACACGCTAT GGGAAGTGCTACACGTTCAACGCAGGGCAGGATGGCAAACCCCGGCTCATCACCATGAAG GGGGGCACTGGAAATGGCCTGGAGATCATGCTGGACATCCAGCAGGACGAGTACCTCCCA GTGTGGGGGGAAACAGATGAGACCTCATTTGAAGCCGGGATCAAGGTGCAGATCCACAGC CAGGATGAGCCTCCACTCATCGACCAGCTGGGCTTCGGTGTGGCACCCGGCTTCCAGACC TTCGTGTCCTGCCAGGAGCAGCGGCTCATCTACCTGCCACCTCCCTGGGGCGACTGTAAG GCCACAACGGGTGACTCGGAGTTCTACGACACTTACAGCATCACTGCCTGCCGCATCGAC TGCGAGACCCGCTACCTGGTGGAGAACTGCAACTGCCGCATGGTGCACATGCCAGGCGAT GCCCCTTATTGCACCCCAGAGCAGTACAAGGAGTGTGCAGATCCAGCCTTAGATTTCCTG GTGGAGAAGGACAATGAGTACTGTGTCTGTGAGATGCCCTGCAACGTCACCCGCTATGGC AAAGAGCTCTCCATGGTGAAGATCCCCAGCAAAGCCTCCGCCAAGTACCTGGCCAAGAAG TACAACAAGTCGGAGCAGTACATCGGGGAGAACATCCTGGTGCTGGACATCTTCTTTGAA GCCCTGAACTATGAGACAATCGAGCAGAAGAAGGCG
Amino acid sequence (352 aa)	PHVTKLDEVAATRLTFPAVTFCNLNEFRFSRVTKNDLYHAGELLALLNNRYEIPDTQTAD EKQLEILQDKANFRNFKPKPFNMLEFYDRAGHDIREMLLSCFFRGEQCSPEDFKVVFTRY GKCYTFNAGQDGKPRLITMKGGTGNGLEIMLDIQQDEYLPVWGETDETSFEAGIKVQIHS QDEPPLIDQLGFGVAPGFQTFVSCQEQRLIYLPPPWGDCKATTGDSEFYDTYSITACRID CETRYLVENCNCRMVHMPGDAPYCTPEQYKECADPALDFLVEKDNEYCVCEMPCNVTRYG KELSMVKIPSKASAKYLAKKYNKSEQYIGENILVLDIFFEALNYETIEQKKA
Forward primer	aggagatataccatgCCCCACGTCACCAAGCTGGACG
Reverse primer	cagaacttccagtttCGCCTTCTTCTGCTCGATTGTCTCATAG
Theoretical protein size	40.30 kDa
Description	Chicken ASIC1a – Delta 38 Plus (D38-Plus)
Species	Gallus Gallus

Cloning vector	pOPINN-GFP
DNA sequence	CGGCTGTCGCTGAAGCGCGTGGTCTGGGCGCTCTGCTTCATGGGTTCGCTGGCGCTGCTC GCCCTGGTCTGCACCAACCGCATCCAGTACTACTTCCTCTACCCCCACGTCACCAAGCTG GACGAGGTGGCCGCCACCAGGCTCACCTTCCCTGCTGTCACCTTCTGCAACCTCAACGAG TTCCGCTTCAGCCGGGTGACCAAGAACGACCTGTACCACGCCGGGGAACTCCTCGCCCTG CTCAATAACAGATACGAGATCCCGGACACACAGACAGCTGATGAGAAGCAGCTGGAAATC CTACAGGACAAGGCAAACTTCCGAAACTTCAAGCCCAAACCTTTCAATATGTTGGAGTTT TACGACCGCGCCGGCCACGACATCCGGGAGATGCTGCTCTCCTGCTTCTTCCGTGGGGAG CAGTGCAGCCCTGAAGACTTCAAAGTGGTGTTCACACGCTATGGGAAGTGCTACACGTTC AACGCAGGGCAGGATGGCAAACCCCGGCTCATCACCATGAAGGGGGGCACTGGAAATGGC CTGGAGATCATGCTGGACATCCAGCAGGACGAGTACCTCCCAGTGTGGGGGGAAACAGAT GAGACCTCATTTGAAGCCGGGATCAAGGTGCAGATCCACAGCCAGGATGAGCCTCCACTC ATCGACCAGCTGGGCTTCGGTGTGGCACCCGGCTTCCAGACCTTCGTGTCCTGCCAGGAG CAGCGGCTCATCTACCTGCCACCTCCCTGGGGCGACTGTAAGGCCACAACGGGTGACTCG GAGTTCTACGACACTTACAGCATCACTGCCTGCCGCATCGACTGCGAGACCCGCTACCTG GTGGAGAACTGCAACTGCCGCATGGTGCACATGCCAGGCGATGCCCCTTATTGCACCCCA GAGCAGTACAAGGAGTGTGCAGATCCAGCCTTAGATTTCCTGGTGGAGAAGGACAATGAG TACTGTGTCTGTGAGATGCCCTGCAACGTCACCCGCTATGGCAAAGAGCTCTCCATGGTG AAGATCCCCAGCAAAGCCTCCGCCAAGTACCTGGCCAAGAAGTACAACAAGTCGGAGCAG TACATCGGGGAGAACATCCTGGTGCTGGACATCTTCTTTGAAGCCCTGAACTATGAGACA ATCGAGCAGAAGAAGGCGTATGAGGTGGCTGGATTGCTGGGTGACATCGGAGGACAGATG GGGCTGTTTATCGGGGCCAGCATCCTCACTGTGCTGGAGCTCTTTGACTACGCCTATGAG GTGATCAAGCACCGG
Amino acid sequence (425 aa)	RLSLKRVVWALCFMGSLALLALVCTNRIQYYFLYPHVTKLDEVAATRLTFPAVTFCNLNE FRFSRVTKNDLYHAGELLALLNNRYEIPDTQTADEKQLEILQDKANFRNFKPKPFNMLEF YDRAGHDIREMLLSCFFRGEQCSPEDFKVVFTRYGKCYTFNAGQDGKPRLITMKGGTGNG LEIMLDIQQDEYLPVWGETDETSFEAGIKVQIHSQDEPPLIDQLGFGVAPGFQTFVSCQE QRLIYLPPPWGDCKATTGDSEFYDTYSITACRIDCETRYLVENCNCRMVHMPGDAPYCTP EQYKECADPALDFLVEKDNEYCVCEMPCNVTRYGKELSMVKIPSKASAKYLAKKYNKSEQ YIGENILVLDIFFEALNYETIEQKKAYEVAGLLGDIGGQMGLFIGASILTVLELFDYAYE VIKHR
Forward primer	aggagatataccatgCGGCTGTCGCTGAAGCGCGTGGTC
Reverse primer	cagaacttccagtttCCGGTGCTTGATCACCTCATAGGC
Theoretical protein size	48.56 kDa
Description	Chicken ASIC1a – Delta 44 Plus (D44-Plus)
Species	Gallus Gallus
Cloning vector	pOPINN-GFP
DNA sequence	GTGGTCTGGGCGCTCTGCTTCATGGGTTCGCTGGCGCTGCTCGCCCTGGTCTGCACCAAC CGCATCCAGTACTACTTCCTCTACCCCCACGTCACCAAGCTGGACGAGGTGGCCGCCACC AGGCTCACCTTCCCTGCTGTCACCTTCTGCAACCTCAACGAGTTCCGCTTCAGCCGGGTG ACCAAGAACGACCTGTACCACGCCGGGGAACTCCTCGCCCTGCTCAATAACAGATACGAG ATCCCGGACACACAGACAGCTGATGAGAAGCAGCTGGAAATCCTACAGGACAAGGCAAAC TTCCGAAACTTCAAGCCCAAACCTTTCAATATGTTGGAGTTTTACGACCGCGCCGGCCAC GACATCCGGGAGATGCTGCTCTCCTGCTTCTTCCGTGGGGAGCAGTGCAGCCCTGAAGAC TTCAAAGTGGTGTTCACACGCTATGGGAAGTGCTACACGTTCAACGCAGGGCAGGATGGC AAACCCCGGCTCATCACCATGAAGGGGGGCACTGGAAATGGCCTGGAGATCATGCTGGAC ATCCAGCAGGACGAGTACCTCCCAGTGTGGGGGGAAACAGATGAGACCTCATTTGAAGCC GGGATCAAGGTGCAGATCCACAGCCAGGATGAGCCTCCACTCATCGACCAGCTGGGCTTC GGTGTGGCACCCGGCTTCCAGACCTTCGTGTCCTGCCAGGAGCAGCGGCTCATCTACCTG CCACCTCCCTGGGGCGACTGTAAGGCCACAACGGGTGACTCGGAGTTCTACGACACTTAC AGCATCACTGCCTGCCGCATCGACTGCGAGACCCGCTACCTGGTGGAGAACTGCAACTGC CGCATGGTGCACATGCCAGGCGATGCCCCTTATTGCACCCCAGAGCAGTACAAGGAGTGT GCAGATCCAGCCTTAGATTTCCTGGTGGAGAAGGACAATGAGTACTGTGTCTGTGAGATG CCCTGCAACGTCACCCGCTATGGCAAAGAGCTCTCCATGGTGAAGATCCCCAGCAAAGCC TCCGCCAAGTACCTGGCCAAGAAGTACAACAAGTCGGAGCAGTACATCGGGGAGAACATC CTGGTGCTGGACATCTTCTTTGAAGCCCTGAACTATGAGACAATCGAGCAGAAGAAGGCG

	TATGAGGTGGCTGGATTGCTGGGTGACATCGGAGGACAGATGGGGCTGTTTATCGGGGCC AGCATCCTCACTGTGCTGGAGCTCTTTGACTACGCCTATGAGGTGATCAAGCACCGG
Amino acid sequence (419 aa)	VVWALCFMGSLALLALVCTNRIQYYFLYPHVTKLDEVAATRLTFPAVTFCNLNEFRFSRV TKNDLYHAGELLALLNNRYEIPDTQTADEKQLEILQDKANFRNFKPKPFNMLEFYDRAGH DIREMLLSCFFRGEQCSPEDFKVVFTRYGKCYTFNAGQDGKPRLITMKGGTGNGLEIMLD IQQDEYLPVWGETDETSFEAGIKVQIHSQDEPPLIDQLGFGVAPGFQTFVSCQEQRLIYL PPPWGDCKATTGDSEFYDTYSITACRIDCETRYLVENCNCRMVHMPGDAPYCTPEQYKEC ADPALDFLVEKDNEYCVCEMPCNVTRYGKELSMVKIPSKASAKYLAKKYNKSEQYIGENI LVLDIFFEALNYETIEQKKAYEVAGLLGDIGGQMGLFIGASILTVLELFDYAYEVIKHR
Forward primer	aggagatataccatgGTGGTCTGGGCGCTCTGCTTCATGG
Reverse primer	cagaacttccagtttCCGGTGCTTGATCACCTCATAGG
Theoretical protein size	47.80 kDa
Description	Chicken ASIC1a – Extracellular domain plus (Sol-Plus)
Species	Gallus Gallus
Cloning vector	pOPINN-GFP
DNA sequence	CCCCACGTCACCAAGCTGGACGAGGTGGCCGCCACCAGGCTCACCTTCCCTGCTGTCACC TTCTGCAACCTCAACGAGTTCCGCTTCAGCCGGGTGACCAAGAACGACCTGTACCACGCC GGGGAACTCCTCGCCCTGCTCAATAACAGATACGAGATCCCGGACACACAGACAGCTGAT GAGAAGCAGCTGGAAATCCTACAGGACAAGGCAAACTTCCGAAACTTCAAGCCCAAACCT TTCAATATGTTGGAGTTTTACGACCGCGCCGGCCACGACATCCGGGAGATGCTGCTCTCC TGCTTCTTCCGTGGGGAGCAGTGCAGCCCTGAAGACTTCAAAGTGGTGTTCACACGCTAT GGGAAGTGCTACACGTTCAACGCAGGGCAGGATGGCAAACCCCGGCTCATCACCATGAAG GGGGGCACTGGAAATGGCCTGGAGATCATGCTGGACATCCAGCAGGACGAGTACCTCCCA GTGTGGGGGGAAACAGATGAGACCTCATTTGAAGCCGGGATCAAGGTGCAGATCCACAGC CAGGATGAGCCTCCACTCATCGACCAGCTGGGCTTCGGTGTGGCACCCGGCTTCCAGACC TTCGTGTCCTGCCAGGAGCAGCGGCTCATCTACCTGCCACCTCCCTGGGGCGACTGTAAG GCCACAACGGGTGACTCGGAGTTCTACGACACTTACAGCATCACTGCCTGCCGCATCGAC TGCGAGACCCGCTACCTGGTGGAGAACTGCAACTGCCGCATGGTGCACATGCCAGGCGAT GCCCCTTATTGCACCCCAGAGCAGTACAAGGAGTGTGCAGATCCAGCCTTAGATTTCCTG GTGGAGAAGGACAATGAGTACTGTGTCTGTGAGATGCCCTGCAACGTCACCCGCTATGGC AAAGAGCTCTCCATGGTGAAGATCCCCAGCAAAGCCTCCGCCAAGTACCTGGCCAAGAAG TACAACAAGTCGGAGCAGTACATCGGGGAGAACATCCTGGTGCTGGACATCTTCTTTGAA GCCCTGAACTATGAGACAATCGAGCAGAAGAAGGCGTATGAGGTGGCTGGATTGCTGGGT GACATCGGAGGACAGATGGGGCTGTTTATCGGGGCCAGCATCCTCACTGTGCTGGAGCTC TTTGACTACGCCTATGAGGTGATCAAGCACCGG
Amino acid sequence (391 aa)	PHVTKLDEVAATRLTFPAVTFCNLNEFRFSRVTKNDLYHAGELLALLNNRYEIPDTQTAD EKQLEILQDKANFRNFKPKPFNMLEFYDRAGHDIREMLLSCFFRGEQCSPEDFKVVFTRY GKCYTFNAGQDGKPRLITMKGGTGNGLEIMLDIQQDEYLPVWGETDETSFEAGIKVQIHS QDEPPLIDQLGFGVAPGFQTFVSCQEQRLIYLPPPWGDCKATTGDSEFYDTYSITACRID CETRYLVENCNCRMVHMPGDAPYCTPEQYKECADPALDFLVEKDNEYCVCEMPCNVTRYG KELSMVKIPSKASAKYLAKKYNKSEQYIGENILVLDIFFEALNYETIEQKKAYEVAGLLG DIGGQMGLFIGASILTVLELFDYAYEVIKHR
Forward primer	aggagatataccatgCCCCACGTCACCAAGCTGGACG
Reverse primer	cagaacttccagtttCCGGTGCTTGATCACCTCATAGGCG
Theoretical protein size	44.55 kDa

Supplementary Table 1: Full description of designed constructs of chicken Acid-Sensing Ion Channel 1(cASIC1)

Description	Mouse ASIC1a template
Species	
Cloning vector	pOPINN-GFP
DNA sequence	GTGGGTGGTGTCCAGCCGGTGAGCATCCAGGCTTTTGCCAGCAGCTCCACGCTGCACGGT CTTGCCCACATCTTCTCCTATGAGCGGCTGTCTCTGAAGCGGGCACTGTGGGCCCTGTGT TTCCTGGGTTCGCTGGCCGTCCTGCTGTGTGTGTGCACTGAGCGTGTGCAGTACTACTTC TGCTACCACCACGTCACCAAGCTCGACGAGGTGGCTGCCTCCCAGCTCACCTTCCCTGCC GTCACTCTCTGCAACCTCAATGAGTTTCGCTTTAGCCAAGTCTCCAAGAATGACCTGTAC CATGCTGGGGAACTGCTGGCCCTGCTCAACAACAGGTATGAGATACCGGACACACAGATG GCTGATGAAAAGCAGCTGGAGATATTGCAGGACAAGGCCAACTTCCGTAGCTTCAAGCCC AAGCCCTTCAACATGCGTGAGTTCTACGACAGAGCAGGGCATGACATTCGAGACATGCTT CTCTCGTGCCACTTCCGAGGGGAGGCCTGCAGCGCTGAAGACTTCAAAGTGGTCTTCACG CGGTATGGGAAGTGCTACACATTCAACTCGGGCCAAGATGGGCGGCCACGGCTGAAGACC ATGAAAGGTGGGACTGGCAACGGCCTGGAGATCATGCTGGACATTCAGCAAGATGAATAC TTGCCTGTGTGGGGAGAGACTGATGAGACATCGTTCGAAGCAGGCATCAAAGTGCAGATC CACAGTCAGGACGAGCCTCCTTTCATCGACCAGCTGGGCTTTGGCGTGGCCCCAGGCTTC CAGACGTTTGTGTCTTGCCAGGAGCAGAGGCTCATCTACCTGCCCTCCCCCTGGGGCACC TGCAATGCTGTTACCATGGACTCGGATTTCTTCGACTCCTACAGCATCACGGCCTGCCGG ATTGATTGTGAAACCCGTTACCTGGTGGAAAACTGCAACTGCCGTATGGTGCACATGCCA GGGGATGCCCCATACTGTACTCCGGAGCAGTACAAGGAGTGTGCAGACCCTGCCCTGGAC TTCCTAGTGGAGAAAGACCAGGAATACTGTGTGTGTGAGATGCCCTGCAACCTGACCCGC TACGGCAAGGAGCTGTCCATGGTCAAGATCCCCAGCAAAGCCTCAGCCAAGTACCTGGCC AAGAAGTTCAACAAATCTGAACAGTACATAGGGGAGAATATTCTGGTGCTGGACATTTTC TTTGAAGTCCTCAACTATGAGACCATCGAGCAGAAGAAGGCCTATGAGATCGCAGGGCTT TTGGGTGACATCGGGGGCCAGATGGGATTGTTCATCGGGGCCAGCATCCTCACAGTGCTG GAACTCTTTGACTATGCCTATGAGGTCATTAAGCACCGG
Amino acid sequence (401 aa)	VGGVQPVSIQAFASSSTLHGLAHIFSYERLSLKRALWALCFLGSLAVLLCVCTERVQYYF CYHHVTKLDEVAASQLTFPAVTLCNLNEFRFSQVSKNDLYHAGELLALLNNRYEIPDTQM ADEKQLEILQDKANFRSFKPKPFNMREFYDRAGHDIRDMLLSCHFRGEACSAEDFKVVFT RYGKCYTFNSGQDGRPRLKTMKGGTGNGLEIMLDIQQDEYLPVWGETDETSFEAGIKVQI HSQDEPPFIDQLGFGVAPGFQTFVSCQEQRLIYLPSPWGTCNAVTMDSDFFDSYSITACR IDCETRYLVENCNCRMVHMPGDAPYCTPEQYKECADPALDFLVEKDQEYCVCEMPCNLTR YGKELSMVKIPSKASAKYLAKKFNKSEQYIGENILVLDIFFEVLNYETIEQKKAYEIAGL LGDIGGQMGLFIGASILTVLELFDYAYEVIKHR
Forward primer	aagttctgtttcagggcccgGTGGGTGGTGTCCAGCCGGTG
Reverse primer	atggtctagaaagctttaCCGGTGCTTAATGACCTCATAGGCA
Theoretical protein size	45.46 kDa
Description	Mouse ASIC1a – Delta 13 (D13)
Species	
Cloning vector	pOPINN-GFP
DNA sequence	GTCCAGCCGGTGAGCATCCAGGCTTTTGCCAGCAGCTCCACGCTGCACGGTCTTGCCCAC ATCTTCTCCTATGAGCGGCTGTCTCTGAAGCGGGCACTGTGGGCCCTGTGTTTCCTGGGT TCGCTGGCCGTCCTGCTGTGTGTGTGCACTGAGCGTGTGCAGTACTACTTCTGCTACCAC CACGTCACCAAGCTCGACGAGGTGGCTGCCTCCCAGCTCACCTTCCCTGCCGTCACTCTC TGCAACCTCAATGAGTTTCGCTTTAGCCAAGTCTCCAAGAATGACCTGTACCATGCTGGG GAACTGCTGGCCCTGCTCAACAACAGGTATGAGATACCGGACACACAGATGGCTGATGAA AAGCAGCTGGAGATATTGCAGGACAAGGCCAACTTCCGTAGCTTCAAGCCCAAGCCCTTC AACATGCGTGAGTTCTACGACAGAGCAGGGCATGACATTCGAGACATGCTTCTCTCGTGC CACTTCCGAGGGGAGGCCTGCAGCGCTGAAGACTTCAAAGTGGTCTTCACGCGGTATGGG AAGTGCTACACATTCAACTCGGGCCAAGATGGGCGGCCACGGCTGAAGACCATGAAAGGT GGGACTGGCAACGGCCTGGAGATCATGCTGGACATTCAGCAAGATGAATACTTGCCTGTG TGGGGAGAGACTGATGAGACATCGTTCGAAGCAGGCATCAAAGTGCAGATCCACAGTCAG GACGAGCCTCCTTTCATCGACCAGCTGGGCTTTGGCGTGGCCCCAGGCTTCCAGACGTTT GTGTCTTGCCAGGAGCAGAGGCTCATCTACCTGCCCTCCCCCTGGGGCACCTGCAATGCT GTTACCATGGACTCGGATTTCTTCGACTCCTACAGCATCACGGCCTGCCGGATTGATTGT GAAACCCGTTACCTGGTGGAAAACTGCAACTGCCGTATGGTGCACATGCCAGGGGATGCC

	CCATACTGTACTCCGGAGCAGTACAAGGAGTGTGCAGACCCTGCCCTGGACTTCCTAGTG GAGAAAGACCAGGAATACTGTGTGTGTGAGATGCCCTGCAACCTGACCCGCTACGGCAAG GAGCTGTCCATGGTCAAGATCCCCAGCAAAGCCTCAGCCAAGTACCTGGCCAAGAAGTTC AACAAATCTGAACAGTACATAGGGGAGAATATTCTGGTGCTGGACATTTTCTTTGAAGTC CTCAACTATGAGACCATCGAGCAGAAGAAGGCCTATGAGATCGCAGGGCTTTTGGGTGAC ATCGGGGGCCAGATGGGATTGTTCATCGGGGCCAGCATCCTCACAGTGCTGGAACTCTTT GACTATGCCTATGAGGTCATTAAGCACCGG
Amino acid sequence (450 aa)	VQPVSIQAFASSSTLHGLAHIFSYERLSLKRALWALCFLGSLAVLLCVCTERVQYYFCYH HVTKLDEVAASQLTFPAVTLCNLNEFRFSQVSKNDLYHAGELLALLNNRYEIPDTQMADE KQLEILQDKANFRSFKPKPFNMREFYDRAGHDIRDMLLSCHFRGEACSAEDFKVVFTRYG KCYTFNSGQDGRPRLKTMKGGTGNGLEIMLDIQQDEYLPVWGETDETSFEAGIKVQIHSQ DEPPFIDQLGFGVAPGFQTFVSCQEQRLIYLPSPWGTCNAVTMDSDFFDSYSITACRIDC ETRYLVENCNCRMVHMPGDAPYCTPEQYKECADPALDFLVEKDQEYCVCEMPCNLTRYGK ELSMVKIPSKASAKYLAKKFNKSEQYIGENILVLDIFFEVLNYETIEQKKAYEIAGLLGD IGGQMGLFIGASILTVLELFDYAYEVIKHR
Forward primer	aggagatataccatgGTCCAGCCGGTGAGCATCCAGGC
Reverse primer	cagaacttccagtttCCGGTGCTTAATGACCTCATAGGCATAGTC
Theoretical protein size	51.20 kDa
Description	Mouse ASIC1a – Delta 27 (D27)
Species	
Cloning vector	pOPINN-GFP
DNA sequence	ACCCTGCACGGGATCTCGCACATCTTCTCCTACGAGCGGCTGTCGCTGAAGCGCGTGGTC TGGGCGCTCTGCTTCATGGGTTCGCTGGCGCTGCTCGCCCTGGTCTGCACCAACCGCATC CAGTACTACTTCCTCTACCCCCACGTCACCAAGCTGGACGAGGTGGCCGCCACCAGGCTC ACCTTCCCTGCTGTCACCTTCTGCAACCTCAACGAGTTCCGCTTCAGCCGGGTGACCAAG AACGACCTGTACCACGCCGGGGAACTCCTCGCCCTGCTCAATAACAGATACGAGATCCCG GACACACAGACAGCTGATGAGAAGCAGCTGGAAATCCTACAGGACAAGGCAAACTTCCGA AACTTCAAGCCCAAACCTTTCAATATGTTGGAGTTTTACGACCGCGCCGGCCACGACATC CGGGAGATGCTGCTCTCCTGCTTCTTCCGTGGGGAGCAGTGCAGCCCTGAAGACTTCAAA GTGGTGTTCACACGCTATGGGAAGTGCTACACGTTCAACGCAGGGCAGGATGGCAAACCC CGGCTCATCACCATGAAGGGGGGCACTGGAAATGGCCTGGAGATCATGCTGGACATCCAG CAGGACGAGTACCTCCCAGTGTGGGGGGAAACAGATGAGACCTCATTTGAAGCCGGGATC AAGGTGCAGATCCACAGCCAGGATGAGCCTCCACTCATCGACCAGCTGGGCTTCGGTGTG GCACCCGGCTTCCAGACCTTCGTGTCCTGCCAGGAGCAGCGGCTCATCTACCTGCCACCT CCCTGGGGCGACTGTAAGGCCACAACGGGTGACTCGGAGTTCTACGACACTTACAGCATC ACTGCCTGCCGCATCGACTGCGAGACCCGCTACCTGGTGGAGAACTGCAACTGCCGCATG GTGCACATGCCAGGCGATGCCCCTTATTGCACCCCAGAGCAGTACAAGGAGTGTGCAGAT CCAGCCTTAGATTTCCTGGTGGAGAAGGACAATGAGTACTGTGTCTGTGAGATGCCCTGC AACGTCACCCGCTATGGCAAAGAGCTCTCCATGGTGAAGATCCCCAGCAAAGCCTCCGCC AAGTACCTGGCCAAGAAGTACAACAAGTCGGAGCAGTACATCGGGGAGAACATCCTGGTG CTGGACATCTTCTTTGAAGCCCTGAACTATGAGACAATCGAGCAGAAGAAGGCGTATGAG GTGGCTGGATTGCTGGGTGACATCGGAGGACAGATGGGGCTGTTTATCGGGGCCAGCATC CTCACTGTGCTGGAGCTCTTTGACTACGCCTATGAGGTGATCAAGCACCGG
Amino acid sequence (437 aa)	TLHGLAHIFSYERLSLKRALWALCFLGSLAVLLCVCTERVQYYFCYHHVTKLDEVAASQL TFPAVTLCNLNEFRFSQVSKNDLYHAGELLALLNNRYEIPDTQMADEKQLEILQDKANFR SFKPKPFNMREFYDRAGHDIRDMLLSCHFRGEACSAEDFKVVFTRYGKCYTFNSGQDGRP RLKTMKGGTGNGLEIMLDIQQDEYLPVWGETDETSFEAGIKVQIHSQDEPPFIDQLGFGV APGFQTFVSCQEQRLIYLPSPWGTCNAVTMDSDFFDSYSITACRIDCETRYLVENCNCRM VHMPGDAPYCTPEQYKECADPALDFLVEKDQEYCVCEMPCNLTRYGKELSMVKIPSKASA KYLAKKFNKSEQYIGENILVLDIFFEVLNYETIEQKKAYEIAGLLGDIGGQMGLFIGASI LTVLELFDYAYEVIKHR
Forward primer	aggagatataccatgACGCTGCACGGTCTTGCCCACATC
Reverse primer	cagaacttccagtttCCGGTGCTTAATGACCTCATAGGCATAGTC
Theoretical protein size	49.94 kDa
Description	Mouse ASIC1a – Delta 38 (D38)

Species	
Cloning vector	pOPINN-GFP
DNA sequence	CGGCTGTCGCTGAAGCGCGTGGTCTGGGCGCTCTGCTTCATGGGTTCGCTGGCGCTGCTC GCCCTGGTCTGCACCAACCGCATCCAGTACTACTTCCTCTACCCCCACGTCACCAAGCTG GACGAGGTGGCCGCCACCAGGCTCACCTTCCCTGCTGTCACCTTCTGCAACCTCAACGAG TTCCGCTTCAGCCGGGTGACCAAGAACGACCTGTACCACGCCGGGGAACTCCTCGCCCTG CTCAATAACAGATACGAGATCCCGGACACACAGACAGCTGATGAGAAGCAGCTGGAAATC CTACAGGACAAGGCAAACTTCCGAAACTTCAAGCCCAAACCTTTCAATATGTTGGAGTTT TACGACCGCGCCGGCCACGACATCCGGGAGATGCTGCTCTCCTGCTTCTTCCGTGGGGAG CAGTGCAGCCCTGAAGACTTCAAAGTGGTGTTCACACGCTATGGGAAGTGCTACACGTTC AACGCAGGGCAGGATGGCAAACCCCGGCTCATCACCATGAAGGGGGGCACTGGAAATGGC CTGGAGATCATGCTGGACATCCAGCAGGACGAGTACCTCCCAGTGTGGGGGGAAACAGAT GAGACCTCATTTGAAGCCGGGATCAAGGTGCAGATCCACAGCCAGGATGAGCCTCCACTC ATCGACCAGCTGGGCTTCGGTGTGGCACCCGGCTTCCAGACCTTCGTGTCCTGCCAGGAG CAGCGGCTCATCTACCTGCCACCTCCCTGGGGCGACTGTAAGGCCACAACGGGTGACTCG GAGTTCTACGACACTTACAGCATCACTGCCTGCCGCATCGACTGCGAGACCCGCTACCTG GTGGAGAACTGCAACTGCCGCATGGTGCACATGCCAGGCGATGCCCCTTATTGCACCCCA GAGCAGTACAAGGAGTGTGCAGATCCAGCCTTAGATTTCCTGGTGGAGAAGGACAATGAG TACTGTGTCTGTGAGATGCCCTGCAACGTCACCCGCTATGGCAAAGAGCTCTCCATGGTG AAGATCCCCAGCAAAGCCTCCGCCAAGTACCTGGCCAAGAAGTACAACAAGTCGGAGCAG TACATCGGGGAGAACATCCTGGTGCTGGACATCTTCTTTGAAGCCCTGAACTATGAGACA ATCGAGCAGAAGAAGGCGTATGAGGTGGCTGGATTGCTGGGTGACATCGGAGGACAGATG GGGCTGTTTATCGGGGCCAGCATCCTCACTGTGCTGGAGCTCTTTGACTACGCCTATGAG
Amino acid sequence (420 aa)	RLSLKRALWALCFLGSLAVLLCVCTERVQYYFCYHHVTKLDEVAASQLTFPAVTLCNLNE FRFSQVSKNDLYHAGELLALLNNRYEIPDTQMADEKQLEILQDKANFRSFKPKPFNMREF YDRAGHDIRDMLLSCHFRGEACSAEDFKVVFTRYGKCYTFNSGQDGRPRLKTMKGGTGNG LEIMLDIQQDEYLPVWGETDETSFEAGIKVQIHSQDEPPFIDQLGFGVAPGFQTFVSCQE QRLIYLPSPWGTCNAVTMDSDFFDSYSITACRIDCETRYLVENCNCRMVHMPGDAPYCTP EQYKECADPALDFLVEKDQEYCVCEMPCNLTRYGKELSMVKIPSKASAKYLAKKFNKSEQ YIGENILVLDIFFEVLNYETIEQKKAYEIAGLLGDIGGQMGLFIGASILTVLELFDYAYE
Forward primer	aggagatataccatgCGGCTGTCTCTGAAGCGGGCAC
Reverse primer	cagaacttccagtttCTCATAGGCATAGTCAAAGAGTTCCAGCAC
Theoretical protein size	47.92 kDa
Description	Mouse ASIC1a – Delta 44 (D44)
Species	Gallus Gallus
Cloning vector	pOPINN-GFP
DNA sequence	GCACTGTGGGCCCTGTGTTTCCTGGGTTCGCTGGCCGTCCTGCTGTGTGTGTGCACTGAG CGTGTGCAGTACTACTTCTGCTACCACCACGTCACCAAGCTCGACGAGGTGGCTGCCTCC CAGCTCACCTTCCCTGCCGTCACTCTCTGCAACCTCAATGAGTTTCGCTTTAGCCAAGTC TCCAAGAATGACCTGTACCATGCTGGGGAACTGCTGGCCCTGCTCAACAACAGGTATGAG ATACCGGACACACAGATGGCTGATGAAAAGCAGCTGGAGATATTGCAGGACAAGGCCAAC TTCCGTAGCTTCAAGCCCAAGCCCTTCAACATGCGTGAGTTCTACGACAGAGCAGGGCAT GACATTCGAGACATGCTTCTCTCGTGCCACTTCCGAGGGGAGGCCTGCAGCGCTGAAGAC TTCAAAGTGGTCTTCACGCGGTATGGGAAGTGCTACACATTCAACTCGGGCCAAGATGGG CGGCCACGGCTGAAGACCATGAAAGGTGGGACTGGCAACGGCCTGGAGATCATGCTGGAC ATTCAGCAAGATGAATACTTGCCTGTGTGGGGAGAGACTGATGAGACATCGTTCGAAGCA GGCATCAAAGTGCAGATCCACAGTCAGGACGAGCCTCCTTTCATCGACCAGCTGGGCTTT GGCGTGGCCCCAGGCTTCCAGACGTTTGTGTCTTGCCAGGAGCAGAGGCTCATCTACCTG CCCTCCCCCTGGGGCACCTGCAATGCTGTTACCATGGACTCGGATTTCTTCGACTCCTAC AGCATCACGGCCTGCCGGATTGATTGTGAAACCCGTTACCTGGTGGAAAACTGCAACTGC CGTATGGTGCACATGCCAGGGGATGCCCCATACTGTACTCCGGAGCAGTACAAGGAGTGT GCAGACCCTGCCCTGGACTTCCTAGTGGAGAAAGACCAGGAATACTGTGTGTGTGAGATG CCCTGCAACCTGACCCGCTACGGCAAGGAGCTGTCCATGGTCAAGATCCCCAGCAAAGCC TCAGCCAAGTACCTGGCCAAGAAGTTCAACAAATCTGAACAGTACATAGGGGAGAATATT CTGGTGCTGGACATTTTCTTTGAAGTCCTCAACTATGAGACCATCGAGCAGAAGAAGGCC TATGAGATCGCAGGGCTTTTGGGTGACATCGGGGGCCAGATGGGATTGTTCATCGGGGCC

	AGCATCCTCACAGTGCTGGAACTCTTTGACTATGCC
Amino acid sequence (412 aa)	ALWALCFLGSLAVLLCVCTERVQYYFCYHHVTKLDEVAASQLTFPAVTLCNLNEFRFSQV SKNDLYHAGELLALLNNRYEIPDTQMADEKQLEILQDKANFRSFKPKPFNMREFYDRAGH DIRDMLLSCHFRGEACSAEDFKVVFTRYGKCYTFNSGQDGRPRLKTMKGGTGNGLEIMLD IQQDEYLPVWGETDETSFEAGIKVQIHSQDEPPFIDQLGFGVAPGFQTFVSCQEQRLIYL PSPWGTCNAVTMDSDFFDSYSITACRIDCETRYLVENCNCRMVHMPGDAPYCTPEQYKEC ADPALDFLVEKDQEYCVCEMPCNLTRYGKELSMVKIPSKASAKYLAKKFNKSEQYIGENI LVLDIFFEVLNYETIEQKKAYEIAGLLGDIGGQMGLFIGASILTVLELFDYA
Forward primer	aggagatataccatgGCACTGTGGGCCCTGTGTTTCCTGG
Reverse primer	cagaacttccagtttGGCATAGTCAAAGAGTTCCAGCACTGTG
Theoretical protein size	46.85 kDa
Description	Mouse ASIC1a – Extracellular domain (called Sol)
Species	
Cloning vector	pOPINN-GFP
DNA sequence	CACCACGTCACCAAGCTCGACGAGGTGGCTGCCTCCCAGCTCACCTTCCCTGCCGTCACT CTCTGCAACCTCAATGAGTTTCGCTTTAGCCAAGTCTCCAAGAATGACCTGTACCATGCT GGGGAACTGCTGGCCCTGCTCAACAACAGGTATGAGATACCGGACACACAGATGGCTGAT GAAAAGCAGCTGGAGATATTGCAGGACAAGGCCAACTTCCGTAGCTTCAAGCCCAAGCCC TTCAACATGCGTGAGTTCTACGACAGAGCAGGGCATGACATTCGAGACATGCTTCTCTCG TGCCACTTCCGAGGGGAGGCCTGCAGCGCTGAAGACTTCAAAGTGGTCTTCACGCGGTAT GGGAAGTGCTACACATTCAACTCGGGCCAAGATGGGCGGCCACGGCTGAAGACCATGAAA GGTGGGACTGGCAACGGCCTGGAGATCATGCTGGACATTCAGCAAGATGAATACTTGCCT GTGTGGGGAGAGACTGATGAGACATCGTTCGAAGCAGGCATCAAAGTGCAGATCCACAGT CAGGACGAGCCTCCTTTCATCGACCAGCTGGGCTTTGGCGTGGCCCCAGGCTTCCAGACG TTTGTGTCTTGCCAGGAGCAGAGGCTCATCTACCTGCCCTCCCCCTGGGGCACCTGCAAT GCTGTTACCATGGACTCGGATTTCTTCGACTCCTACAGCATCACGGCCTGCCGGATTGAT TGTGAAACCCGTTACCTGGTGGAAAACTGCAACTGCCGTATGGTGCACATGCCAGGGGAT GCCCCATACTGTACTCCGGAGCAGTACAAGGAGTGTGCAGACCCTGCCCTGGACTTCCTA GTGGAGAAAGACCAGGAATACTGTGTGTGTGAGATGCCCTGCAACCTGACCCGCTACGGC AAGGAGCTGTCCATGGTCAAGATCCCCAGCAAAGCCTCAGCCAAGTACCTGGCCAAGAAG TTCAACAAATCTGAACAGTACATAGGGGAGAATATTCTGGTGCTGGACATTTTCTTTGAA GTCCTCAACTATGAGACCATCGAGCAGAAGAAGGCC
Amino acid sequence (352 aa)	HHVTKLDEVAASQLTFPAVTLCNLNEFRFSQVSKNDLYHAGELLALLNNRYEIPDTQMAD EKQLEILQDKANFRSFKPKPFNMREFYDRAGHDIRDMLLSCHFRGEACSAEDFKVVFTRY GKCYTFNSGQDGRPRLKTMKGGTGNGLEIMLDIQQDEYLPVWGETDETSFEAGIKVQIHS QDEPPFIDQLGFGVAPGFQTFVSCQEQRLIYLPSPWGTCNAVTMDSDFFDSYSITACRID CETRYLVENCNCRMVHMPGDAPYCTPEQYKECADPALDFLVEKDQEYCVCEMPCNLTRYG KELSMVKIPSKASAKYLAKKFNKSEQYIGENILVLDIFFEVLNYETIEQKKA
Forward primer	aggagatataccatgCACCACGTCACCAAGCTCGACGAGG
Reverse primer	aggagatataccatgCACCACGTCACCAAGCTCGACGAGG
Theoretical protein size	40.29 kDa
Description	Mouse ASIC1a – Delta 38 Plus (D38-Plus)
Species	
Cloning vector	pOPINN-GFP
DNA sequence	CGGCTGTCTCTGAAGCGGGCACTGTGGGCCCTGTGTTTCCTGGGTTCGCTGGCCGTCCTG CTGTGTGTGTGCACTGAGCGTGTGCAGTACTACTTCTGCTACCACCACGTCACCAAGCTC GACGAGGTGGCTGCCTCCCAGCTCACCTTCCCTGCCGTCACTCTCTGCAACCTCAATGAG TTTCGCTTTAGCCAAGTCTCCAAGAATGACCTGTACCATGCTGGGGAACTGCTGGCCCTG CTCAACAACAGGTATGAGATACCGGACACACAGATGGCTGATGAAAAGCAGCTGGAGATA TTGCAGGACAAGGCCAACTTCCGTAGCTTCAAGCCCAAGCCCTTCAACATGCGTGAGTTC TACGACAGAGCAGGGCATGACATTCGAGACATGCTTCTCTCGTGCCACTTCCGAGGGGAG GCCTGCAGCGCTGAAGACTTCAAAGTGGTCTTCACGCGGTATGGGAAGTGCTACACATTC AACTCGGGCCAAGATGGGCGGCCACGGCTGAAGACCATGAAAGGTGGGACTGGCAACGGC CTGGAGATCATGCTGGACATTCAGCAAGATGAATACTTGCCTGTGTGGGGAGAGACTGAT GAGACATCGTTCGAAGCAGGCATCAAAGTGCAGATCCACAGTCAGGACGAGCCTCCTTTC

	ATCGACCAGCTGGGCTTTGGCGTGGCCCCAGGCTTCCAGACGTTTGTGTCTTGCCAGGAG CAGAGGCTCATCTACCTGCCCTCCCCCTGGGGCACCTGCAATGCTGTTACCATGGACTCG GATTTCTTCGACTCCTACAGCATCACGGCCTGCCGGATTGATTGTGAAACCCGTTACCTG GTGGAAAACTGCAACTGCCGTATGGTGCACATGCCAGGGGATGCCCCATACTGTACTCCG GAGCAGTACAAGGAGTGTGCAGACCCTGCCCTGGACTTCCTAGTGGAGAAAGACCAGGAA TACTGTGTGTGTGAGATGCCCTGCAACCTGACCCGCTACGGCAAGGAGCTGTCCATGGTC AAGATCCCCAGCAAAGCCTCAGCCAAGTACCTGGCCAAGAAGTTCAACAAATCTGAACAG TACATAGGGGAGAATATTCTGGTGCTGGACATTTTCTTTGAAGTCCTCAACTATGAGACC ATCGAGCAGAAGAAGGCCTATGAGATCGCAGGGCTTTTGGGTGACATCGGGGGCCAGATG GGATTGTTCATCGGGGCCAGCATCCTCACAGTGCTGGAACTCTTTGACTATGCCTATGAG GTCATTAAGCACCGG
Amino acid sequence (425 aa)	RLSLKRALWALCFLGSLAVLLCVCTERVQYYFCYHHVTKLDEVAASQLTFPAVTLCNLNE FRFSQVSKNDLYHAGELLALLNNRYEIPDTQMADEKQLEILQDKANFRSFKPKPFNMREF YDRAGHDIRDMLLSCHFRGEACSAEDFKVVFTRYGKCYTFNSGQDGRPRLKTMKGGTGNG LEIMLDIQQDEYLPVWGETDETSFEAGIKVQIHSQDEPPFIDQLGFGVAPGFQTFVSCQE QRLIYLPSPWGTCNAVTMDSDFFDSYSITACRIDCETRYLVENCNCRMVHMPGDAPYCTP EQYKECADPALDFLVEKDQEYCVCEMPCNLTRYGKELSMVKIPSKASAKYLAKKFNKSEQ YIGENILVLDIFFEVLNYETIEQKKAYEIAGLLGDIGGQMGLFIGASILTVLELFDYAYE VIKHR
Forward primer	aggagatataccatgCGGCTGTCTCTGAAGCGGGCAC
Reverse primer	cagaacttccagtttCCGGTGCTTAATGACCTCATAGGCATAGTC
Theoretical protein size	48.53 kDa
Description	Mouse ASIC1a – Delta 44 Plus (D44-Plus)
Species	
Cloning vector	pOPINN-GFP
DNA sequence	GCACTGTGGGCCCTGTGTTTCCTGGGTTCGCTGGCCGTCCTGCTGTGTGTGTGCACTGAG CGTGTGCAGTACTACTTCTGCTACCACCACGTCACCAAGCTCGACGAGGTGGCTGCCTCC CAGCTCACCTTCCCTGCCGTCACTCTCTGCAACCTCAATGAGTTTCGCTTTAGCCAAGTC TCCAAGAATGACCTGTACCATGCTGGGGAACTGCTGGCCCTGCTCAACAACAGGTATGAG ATACCGGACACACAGATGGCTGATGAAAAGCAGCTGGAGATATTGCAGGACAAGGCCAAC TTCCGTAGCTTCAAGCCCAAGCCCTTCAACATGCGTGAGTTCTACGACAGAGCAGGGCAT GACATTCGAGACATGCTTCTCTCGTGCCACTTCCGAGGGGAGGCCTGCAGCGCTGAAGAC TTCAAAGTGGTCTTCACGCGGTATGGGAAGTGCTACACATTCAACTCGGGCCAAGATGGG CGGCCACGGCTGAAGACCATGAAAGGTGGGACTGGCAACGGCCTGGAGATCATGCTGGAC ATTCAGCAAGATGAATACTTGCCTGTGTGGGGAGAGACTGATGAGACATCGTTCGAAGCA GGCATCAAAGTGCAGATCCACAGTCAGGACGAGCCTCCTTTCATCGACCAGCTGGGCTTT GGCGTGGCCCCAGGCTTCCAGACGTTTGTGTCTTGCCAGGAGCAGAGGCTCATCTACCTG CCCTCCCCCTGGGGCACCTGCAATGCTGTTACCATGGACTCGGATTTCTTCGACTCCTAC AGCATCACGGCCTGCCGGATTGATTGTGAAACCCGTTACCTGGTGGAAAACTGCAACTGC CGTATGGTGCACATGCCAGGGGATGCCCCATACTGTACTCCGGAGCAGTACAAGGAGTGT GCAGACCCTGCCCTGGACTTCCTAGTGGAGAAAGACCAGGAATACTGTGTGTGTGAGATG CCCTGCAACCTGACCCGCTACGGCAAGGAGCTGTCCATGGTCAAGATCCCCAGCAAAGCC TCAGCCAAGTACCTGGCCAAGAAGTTCAACAAATCTGAACAGTACATAGGGGAGAATATT CTGGTGCTGGACATTTTCTTTGAAGTCCTCAACTATGAGACCATCGAGCAGAAGAAGGCC TATGAGATCGCAGGGCTTTTGGGTGACATCGGGGGCCAGATGGGATTGTTCATCGGGGCC AGCATCCTCACAGTGCTGGAACTCTTTGACTATGCCTATGAGGTCATTAAGCACCGG
Amino acid sequence (419 aa)	ALWALCFLGSLAVLLCVCTERVQYYFCYHHVTKLDEVAASQLTFPAVTLCNLNEFRFSQV SKNDLYHAGELLALLNNRYEIPDTQMADEKQLEILQDKANFRSFKPKPFNMREFYDRAGH DIRDMLLSCHFRGEACSAEDFKVVFTRYGKCYTFNSGQDGRPRLKTMKGGTGNGLEIMLD IQQDEYLPVWGETDETSFEAGIKVQIHSQDEPPFIDQLGFGVAPGFQTFVSCQEQRLIYL PSPWGTCNAVTMDSDFFDSYSITACRIDCETRYLVENCNCRMVHMPGDAPYCTPEQYKEC ADPALDFLVEKDQEYCVCEMPCNLTRYGKELSMVKIPSKASAKYLAKKFNKSEQYIGENI LVLDIFFEVLNYETIEQKKAYEIAGLLGDIGGQMGLFIGASILTVLELFDYAYEVIKHR
Forward primer	aggagatataccatgGCACTGTGGGCCCTGTGTTTCCTGG
Reverse primer	cagaacttccagtttCCGGTGCTTAATGACCTCATAGGCATAGTC

Theoretical protein size	47.78 kDa
Description	Mouse ASIC1a – Extracellular domain plus (Sol-Plus)
Species	
Cloning vector	pOPINN-GFP
DNA sequence	CACCACGTCACCAAGCTCGACGAGGTGGCTGCCTCCCAGCTCACCTTCCCTGCCGTCACT CTCTGCAACCTCAATGAGTTTCGCTTTAGCCAAGTCTCCAAGAATGACCTGTACCATGCT GGGGAACTGCTGGCCCTGCTCAACAACAGGTATGAGATACCGGACACACAGATGGCTGAT GAAAAGCAGCTGGAGATATTGCAGGACAAGGCCAACTTCCGTAGCTTCAAGCCCAAGCCC TTCAACATGCGTGAGTTCTACGACAGAGCAGGGCATGACATTCGAGACATGCTTCTCTCG TGCCACTTCCGAGGGGAGGCCTGCAGCGCTGAAGACTTCAAAGTGGTCTTCACGCGGTAT GGGAAGTGCTACACATTCAACTCGGGCCAAGATGGGCGGCCACGGCTGAAGACCATGAAA GGTGGGACTGGCAACGGCCTGGAGATCATGCTGGACATTCAGCAAGATGAATACTTGCCT GTGTGGGGAGAGACTGATGAGACATCGTTCGAAGCAGGCATCAAAGTGCAGATCCACAGT CAGGACGAGCCTCCTTTCATCGACCAGCTGGGCTTTGGCGTGGCCCCAGGCTTCCAGACG TTTGTGTCTTGCCAGGAGCAGAGGCTCATCTACCTGCCCTCCCCCTGGGGCACCTGCAAT GCTGTTACCATGGACTCGGATTTCTTCGACTCCTACAGCATCACGGCCTGCCGGATTGAT TGTGAAACCCGTTACCTGGTGGAAAACTGCAACTGCCGTATGGTGCACATGCCAGGGGAT GCCCCATACTGTACTCCGGAGCAGTACAAGGAGTGTGCAGACCCTGCCCTGGACTTCCTA GTGGAGAAAGACCAGGAATACTGTGTGTGTGAGATGCCCTGCAACCTGACCCGCTACGGC AAGGAGCTGTCCATGGTCAAGATCCCCAGCAAAGCCTCAGCCAAGTACCTGGCCAAGAAG TTCAACAAATCTGAACAGTACATAGGGGAGAATATTCTGGTGCTGGACATTTTCTTTGAA GTCCTCAACTATGAGACCATCGAGCAGAAGAAGGCCTATGAGATCGCAGGGCTTTTGGGT GACATCGGGGGCCAGATGGGATTGTTCATCGGGGCCAGCATCCTCACAGTGCTGGAACTC TTTGACTATGCCTATGAGGTCATTAAGCACCGG
Amino acid sequence (391 aa)	HHVTKLDEVAASQLTFPAVTLCNLNEFRFSQVSKNDLYHAGELLALLNNRYEIPDTQMAD EKQLEILQDKANFRSFKPKPFNMREFYDRAGHDIRDMLLSCHFRGEACSAEDFKVVFTRY GKCYTFNSGQDGRPRLKTMKGGTGNGLEIMLDIQQDEYLPVWGETDETSFEAGIKVQIHS QDEPPFIDQLGFGVAPGFQTFVSCQEQRLIYLPSPWGTCNAVTMDSDFFDSYSITACRID CETRYLVENCNCRMVHMPGDAPYCTPEQYKECADPALDFLVEKDQEYCVCEMPCNLTRYG KELSMVKIPSKASAKYLAKKFNKSEQYIGENILVLDIFFEVLNYETIEQKKAYEIAGLLG DIGGQMGLFIGASILTVLELFDYAYEVIKHR
Forward primer	aggagatataccatgCACCACGTCACCAAGCTCGACGAGG
Reverse primer	cagaacttccagtttCCGGTGCTTAATGACCTCATAGGCATAGTC
Theoretical protein size	44.55 kDa

Supplementary Table 2: Full description of designed constructs of mouse Acid-Sensing Ion Channel 1(mASIC1)